Contribution to the development of autonaumous wake-up radios for the efficient energy in wireless devices

Achille Fumtchum, Florin Doru Hutu

UNIVERSITY OF BUEA

FACULTY OF ENGINEERING AND TECHNOLOGY (FET)

DEPARTMENT OF ELECTRICAL AND ELECTRONIC ENGINEERING

CONTRIBUTION TO THE DEVELOPMENT OF AUTONOMOUS WAKE-UP RADIOS FOR THE EFFICIENT ENERGY IN WIRELESS DEVICES

by

FUMTCHUM Chretien Achille (FE15P063)

M. Eng. in Telecommunications and Networks Engineering

Thesis Submitted to the Faculty of Engineering and Technology of the University of Buea in Partial Fulfilment of the Requirements for the Award of the Degree of Doctor of Philosophy in Telecommunications and Networks Engineering

January, 2023

UNIVERSITY OF BUEA

FACULTY OF ENGINEERING AND TECHNOLOGY (FET)

DEPARTMENT OF ELECTRICAL AND ELECTRONIC ENGINEERING

CERTIFICATION

This thesis of Fumtchum Chretien Achille (FE15P063) entitled: **"Contribution to the development of autonomous wake-up radios for the efficient energy in wireless devices"**, Submitted to the department of Electrical and Electronic Engineering, Faculty of Engineering and Technology of the University of Buea in Partial fulfilment of the requirements for the Award of the degree of doctor of philosophy in Telecommunications and Networks, has been read, examined and approved by the examination panel composed of the following jury :

- Mr Tanyi Emmanuel PhD, Chairman (Professor)
- Mr Bruno Allard PhD, Rapporteur (Professor)
- Mr Moffo Bertrand PhD, Rapporteur (Associate / Professor)
- Mr HUTU Florin-Doru PhD, Thesis supervisor (Associate Professor)
- Mr TSAFACK Pierre PhD, Thesis co-supervisor (Associate Professor)
- Mr Fute Elie T. PhD, Member (Associate / Professor)

Dr Florin HUTU

(Supervisor)

Dr TSAFACK Pierre

(Co-supervisor & Head of Department)

Date: _____

Pr TANYI

Emmanuel (Dean)

Dedication

To my late father who would have been delighted to see his son defending a PhD thesis. To my mother and my wife.

Acknowledgments

I would like to commence by thanking the Dean of the Faculty of Engineering and Technology of the University of Buea, Professor Emmanuel Tanyi, who did not only welcome me to the Faculty, but also kindly considered me over the years. I would like him to find in this my testimony of gratitude for all that I cannot express in a few lines.

I am very grateful to Dr Pierre Tsafack who is the co-supervisor of this work, but who has been my mentor for many years. Sir, thank you for everything. I would like you to know that I have not forgotten a single one of all the kindnesses towards me. I would like you to know that I owe you a huge debt of gratitude.

To Dr Florin Hutu, Associate Professor at INSA Lyon, I say a heartfelt thank you firstly for having accepted to supervise my thesis. Then for all the great good he did for me. Thanks to you I have been in contact with the CITI Laboratory during these years. You have been an excellent trainer for me. I do not forget those promenades in the city of Lyon and its invitations sometimes in the company of your wife whom I thank here for having given me my first map of the city of Lyon to help me to find my way during my stays.

I would like to thank Dr Guillaume Villemaud, Associate Professor at INSA

Lyon, who accompanied me a lot especially at the very beginning of my thesis.

In particular, I would like to express my deep gratitude to the "Service de la Coopération et d'Action Culturelle (SCAC)" of the French Embassy in Cameroon for funding my research stays in France.

I would also like to thank Luca HILTGUN for his availability and his precious help for the printing of multiple cards that allowed me to do the experiments.

I would like to thank Dr Elie Fute and Dr Ngwashi Divine for providing me with valuable advice which help in the course of my work.

I thank my wife Barbara for the love and support over the years.

I give thanks to my mother and my siblings Elisabeth, Robert, Louise, Suzanne and Celestin who have always encouraged me and made themselves available whenever I need any one of them.

I express my gratitude to Professors Fabrice Valois, Florent De Dinechin and Frederic Le Mouel who were respectively director of the Laboratory during my stays and for the administrative documents they signed to facilitate my travels.

I extend my gratitude to Professor Tanguy Risset who was the head of the Socrate team and who also signed an administrative document for me during one of my stays.

Thanks to Caroline Tremeaud and Sandrine Dahan who successively held the

position of administrative assistant and who accompanied me in the procedures.

To all the people I met at the CITI Laboratory, I would like to say thank you for the moments of fun we shared together.

Finally, thanks to all those who have always encouraged me.

Abstract

The work carried out in this thesis focused on the optimization of the energy consumption of connected devices and specifically on their radiofrequency part. The main objective is to propose standby modes with zero energy consumption. More precisely, it is to propose standby modes which are independent on the main energy souce (battery). The work focused amongst others in energy saving mechanisms such as wake-up radio on the one hand, and on the other hand in radio frequency energy harvesting circuits designed to make them autonomous.

To achieve this objective, an exhaustive state of the art of wake-up radio receivers is provided, highlighting their operating frequencies, modulation types, power consumption together with their RF architectures and an assessment of the relationships between these parameters. It is then highlighted some applications ranging from aeronautics to human body communication, including agriculture, security, smart metering, wildlife monitoring, localization and tracking, etc...

A new wake-up radio that was developed at the CITI Laboratory of INSA Lyon is introduced, then by using the block by block analysis technique of a system, we contributed to the improvement of the existing circuit, by changing the matching network with rectifier; thereby increased the gain by about 11 % for all cases of identifiers considered. This gain then allows an improvement in the communication

range of the system by about 13 meters for the 2.45 GHz frequency.

In other places, the radio frequency energy harvesting circuits was investigated as a solution to bring the wake up radio circuit independent on the connected object's main energy source. It is firstly considered the analysis of the main diodes used in these circuits. This diodes include the HSMS 2850, HSMS 2860 and SMS 7630. Here also there is the consideration of all the topologies of the harvesting circuits, and the efficiency domains of each circuit through parametric simulation and determination of the best performing circuits is investigated. This allowed us to establish with precision the circuit that corresponds to our specific application. This was followed by a comparative analysis using classical analysis tools to determine the influence of the frequency on energy harvesting; with the conclusion that the higher the frequency, the less energy is harvested. Finally, an implementation of the energy harvesting circuit was made and we obtained for the input powers 0 dBm and 15 dBm, respectively 8.3 μW and 138.68 μW. These power levels are more than enough to supply any type of WuRx.

Keywords : Wake-up radio; Energy Harvesting; Wireless Power; Internet of Things; Wireless Sensor Nodes.

Contents

List of Figures

List of Tables

List of acronyms and abbreviations

2G The second generation of mobile networks

3G The third generation of mobile networks

5G The fifth generation of wireless technology

ADS Advanced Design System of Keysight's Software Technologies

BCD Bipolar-CMOS-DMOS

Bi-CMOS Bipolar CMOS

BPSK Binary Phase Shift Keying

CERP-IoT Cluster of European Research projects on the Internet of Things

CITI Centre d'Innovation en Télécommunications et Intégration de Services

CMOS Complementary Metal Oxide Semiconductor

DC Direct Current

DMOS Double Diffused Metal Oxide Semiconductor

DTV Digital Television Broadcasting

ECC Electronic Communications Commission

ERP Effective Radiated Power

FCC Federal Communications Commission

FTT Fast Fourier Transform

FSK Frequency Shift Keying

GPS Global Positioning System

HBC Human Body Communications

ICTs Information and Communication Technologies

ID IDentification

ILO Injection-locked Oscillator

IoT Internet of Things

IP Internet Protocol

ISM Industrial Scientific and Medical

IT Information Technology

ITU International Telecommunication Union

LNA Low Noise Amplifier

LSSP Large Signal S-Parameters

MICS Medical Implant Communication Service

OFDM Orthogonal Frequency Division Multiplexing

OOK On-Off Keying

PIR Pyroelectric Infrared

PWUR Passive Wake-Up Radios

RF Radiofrequency

RFID Radiofrequency Identification

SOCRATE Software and Cognitive radio for Telecommunications

SPICE Simulation Program with Integrated Circuit Emphasis

SDR short-range communication devices

SRO Super-Regenerative Oscillator

SRR Super-Regenerative Receiver

SUN Smart Utility Network

UWB Ultra-wideband

WBAN wireless body area network

Wi-Fi Wireless Fidelity : a family of wireless network protocol

WLAN Wireless Local Area Networks

WMTSs Wireless Medical Telemetry Services

WSN Wireless Sensor nodes

WSNs Wireless Sensor Networks

WuR Wake-up Receiver

WuRx Wake-up Radio

WuS Wake-up Signal

WuTx Wake-up Transmitter

Chapter 1

General Introduction

1.1 Introduction

Since the beginning of the Industrial Revolution in the late 18^{th} and early 19^{th} century, the global demand in energy consumption rose exponentially. In the 20^{th} century, this demand further emphasized with the development of mass production of consumer goods, cement factories, metallurgy, the explosion of the automotive industry ...

Briefly all sectors of human activity consume directly or indirectly energy. This growth was supported essentially by the use of non-renewable energy sources. Because of a political crisis between the Western countries and Arab states, an oil embargo has caused energy crisis in the 1970^{s}, with very huge impact on economic and social live of western countries. Because of that crisis, and constantly increasing demand, the researchers focused on the question of energy. It was matter to first develop renewable energy sources, and second to develop ways of effective and efficient use of energy. This research goal is still a topical issue, and the subject of

intense activities in research laboratories.

Over the last 20 years, digital technologies have undergone tremendous growth, resulting in the development of the concept of the digital economy, which today overlaps extraordinarily with almost all areas of human activity. One of the new pillars of the digital economy is undeniably the IoT (Internet of Things). In recent years, it has experienced a spectacular boom, and its use today makes everyday life easier in several aspects. Thus, IoT applies to health, agriculture, transport in all forms, industry, business, smart cities and everything else that can be imagined as human activities.

This impressive development of the IoT has taken place in complementarity with the evolution of mobile communication technologies, which has gone from the first generation (1G) towards the end of the last century to the fifth generation (5G) nowadays. This development implies great changes both from the user point of view and from the point of view of the telecommunications operators; since these changes take place through obvious transformations on the communications speed, the network access methods, the types of modulation, the applications developed around them, etc., these changes have a significant impact on the quality of the services offered by the IoTs.

Considering all these changes both in the communication networks that sustain the IoT, and in the development of the IoT itself, it becomes immediately apparent that this implies a large number of challenges that scientists are working and collaborating on in dynamic ways to address. Among these many challenges is the energy consumption of connected devices, now numbering in the tens of billions; but also the issue of pollution resulting from the use of batteries to supply these connected

devices.

The management of energy resources is nowadays more than ever a priority, especially in view of the predictions made concerning climate change. This energetic issue, which at once arose for heavy industry, has spread to almost all economic and human activities. The development of information technology has enabled the development of the digital economy, which today has transformed the way we produce, exchange and consume. Its applications can be found in tourism, transportation, education, health, agriculture, etc.

From the point of view of scientific and technical research and innovation, the digital economy is based on artificial intelligence, digital processing and transmission of information (telecommunications), and most recently the Internet of Things (IoT). Nevertheless, the field of telecommunications (IT in general), has become more and more polluting, especially if we take into account the use of batteries which ensure continuity of service in the case of an interruption of the electricity network. However, with the COVID-19 crisis, considering the service provided by telecommunications, we can globally recognize a reduction in energy usage. With the lockdowns that have led to a reduction in transportation and human displacements in general, the use of telecommunication supports have allowed a wide development of teleconferences, teleworking, tele-education...

The definition of IoT is evolutionary and depends on paradigm and vision. It has evolved a lot since its inception. It refers to a set of homogeneous things (which can be used in thier environment for sensing and / or actuating) such that one can move from one to another and uniquely addressable, communicating together in a dynamic worldwide network [1]. In this definition, Thing refers to any physical

object (such as Radio-Frequency IDentification (RFID) tags, sensors, actuators, mobile phones, smart items etc.), but also virtual uniquely addressable entity that can moves in space and time. In the early 2000s, an MIT working group defined IoT as: ***"an intelligent infrastructure linking objects, information and people through the computer networks, and where the RFID technology found the basis for its realization"*** [2]. The International Telecommunication Union (ITU) published for the first time in 2005 a report on IoT, which expressed a vision of its omnipresence in Information and Communication Technologies in these terms: ***"a new dimension has been added to the world of information and communication technologies (ICTs): from anytime, anyplace connectivity for anyone, we will now have connectivity for anything. Connections will multiply and create an entirely new dynamic network of networks – an Internet of Things"*** [3]. In 2009 Cluster of European Research projects on the Internet of Things (CERP-IoT) proposed the definition of IoT as ***"a dynamic global network infrastructure with self-capabilities based on standard and interoperable communication protocols where physical and virtual "things" have identities, physical attributes, virtual personalities and use intelligent interfaces, and are seamlessly integrated into the information network"*** [4]. The extension of the latest definition which underlines the interaction between Things and users, is found in [5], and expressed another vision of IoT as : ***"Internet of Things links uniquely identifiable things to their virtual representations in the Internet containing or linking to additional information on their identity, status, location or any other business, social or privately relevant information at a financial or non-financial***

pay-off that exceeds the efforts of information provisioning and offers information access to non-predefined participants. The provided accurate and appropriate information may be accessed in the right quantity and condition, at the right time and place at the right price. The Internet of Things is not synonymous with ubiquitous/pervasive computing, the Internet Protocol (IP), communication technology, embedded devices, its applications, the Internet of People or the Intranet/Extranet of Things, yet it combines aspects and technologies of all of these approaches". The dynamics of the IoT's evolving definition also reflects its impact on the digital and global economy.

The study presented in [6], which is recent and relevant today, showed that there are many applications of IoT in various fields. In that work, it is shown an exponential growth of connected devices. According to the data contained in that paper, the number of connected objects will increase from 20 billion in 2015 to 80 billion in 2030 (cf. Figure 1.1). In other words, a fourfold increase in a 15-year period. It also shows that for the same period, the average number of connected objects per person will rise from 6.4 to 20.4. This ultra-fast growth reflects not only a great interest in the IoT, but also its multiple applications which can be grouped into 5 main areas presented in Figure 1.2: Smart Cities, Smart Homes, Smart Transportation, E-Health and Smart Factories.

.

.

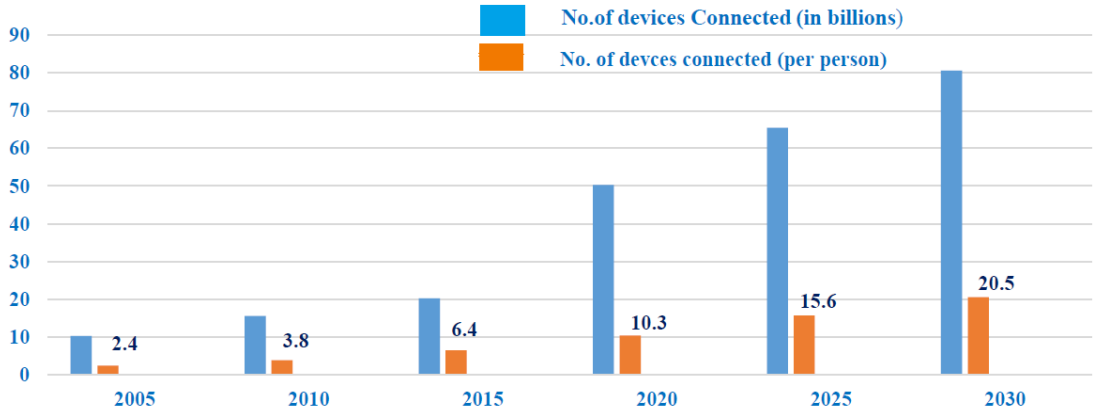

Figure 1.1: 5G IoT Vision from 2005 (3G) to 2030 (5G)[6]

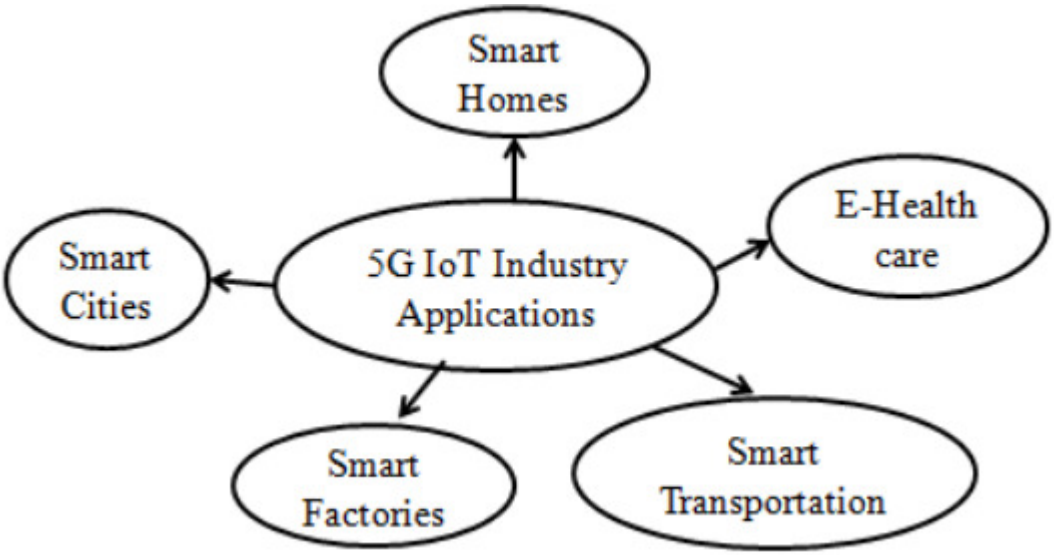

Figure 1.2: Applications of 5G IoT [6]

1.2 Main objective

The SOCRATE team of the CITI laboratory has proposed a new wake-up radio architecture based on the principle of using an identifier integrated to the OFDM (Orthogonal Frequency Division Multiplexing) signal. That wake-up radio (WuRx) device consists in a quasi-passive circuit which is thoroughly explained in the following chapters. The aim of the thesis is to propose a "wake-up" radio receiver architecture which is completely autonomous in terms of energy, i.e. which harvests radio-frequency energy to compensate for the requirement of the WuRx.

Several theoretical as well as technological obstacles will have to be overcome. On the system part, we are going to make a theoretical study. This study will then take into account the technological constraints on the radio-frequency part of the wake-up receiver. On the circuit aspects, it will be necessary to review the impedance matching system of the RF/DC converter block, in order to improve the sensitivity of the receiver. In addition, compared to the first proposed architecture, an energy harvesting system will be added, making the system completely autonomous. The pathway highlighted is the design and use of an ambient or transmitted RF energy harvesting system. Finally, a study of the consumption will allow to evaluate the best approach between permanently maintaining the power supply to the active circuits of the main radio interface or activating them at the appropriate time.

Several application frameworks could be envisaged, from the most practical such as information collection systems or vehicular networks to a higher level of abstraction: wireless sensor networks in the broadest sense. It will indeed be particularly interesting from a scientific point of view to define a general theoretical boundary for energy autonomy, the maximum range of such a system.

1.3 Background of the study

1.3.1 Origin of the problem and context

The growth of the number of connected objects invites two main challenges on the things themselves that are, longevity and energy efficiency. These objects are essentially Sensor Network (WSN) nodes. Sensor nodes have several applications ranging from smart cities [7], to the military domain for tracking enemy positions

[8], through health domain [9], the environment monitoring [10], as well as industrial applications [11], [12]. For all these applications, each node needs a battery for its power supply. However, the small size of some nodes and the accessibility due to a harsh environment at times, does not allow these batteries to be replaced or their replacement is very time and resources consuming. As a result, some nodes are deployed only once and their lifetime depends on the depletion of the battery that supplies them. A node that stops running is said to be dead. If the number of dead nodes increases beyond a certain amount, the network becomes inoperative since the information collected does not reflect the full state of the operating environment.

The most energy consuming part of the connected devices is the radio part. It has been demonstrated that the radio consumes 90% of the energy in standby mode [13]. Therefore, it is necessary to find a way to limit this energy waste so that they have a battery that lasts a longtime to increase the lifetime of a connected device. The low energy consumption systems follow some constraints according to the application and the scenario of usage. So we have the constraint of size which requires objects to have small sizes; the constraint of sensitivity (which is the ability of a radio receiver to provide a signal of acceptable strength and quality at the output with the lowest level input signal), energy consumption, the robustness which is directly linked to the longevity of the object and data rate.

The power efficiency and reliability of communications are often contradictory requirements in WSNs and IoT. It is in this context that was born the development of communicating systems with very low energy consumption. Initially researchers have developed duty cycle systems and subsequently wake-up radio systems.

1.3.2 Duty cycle receiver

Duty cycle based protocol is a technique widely applied to wireless sensor nodes to save energy consumption. It has been shown that a typical node communicates very rarely, and spends most of its time monitoring the channel [14]; which implies that, the main radio remains active and consume a lot of power for nothing. The channel monitoring activity for a node is almost as energy consuming as the communication activity of the node under consideration. In this scenario, a cycling strategy directly reduces energy consumption.

A cycling strategy consists in that the radio interface is active during one cycle, and is switched off during the next cycle while the rest of the system is in standby to resume the active cycle. In order to properly characterize this cycling strategy, it is necessary to take into account the energy consumed by the transmitter that transmits the synchronization signal to initiate communication between the node and the device that gathers the information to be sensed.

Figure 1.3 shows the time diagram of the duty cycling protocol. In this figure, three different periods can be observed. The active period (T_{active}), the standby period (T_{sleep}) and the transition period from standby to active mode (T_{s2a}).

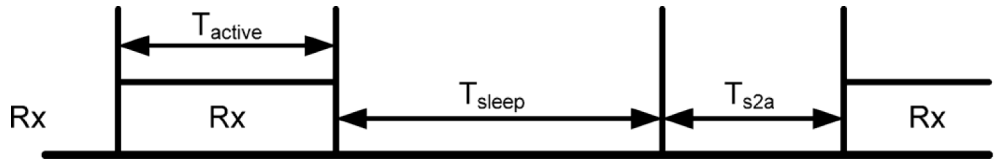

Figure 1.3: Timing sequence of the protocol based duty-cycling [15]

Considering here an ideal operation, i.e. there is no packet collision and in the absence of any interference, the synchronization packets are considered to be

successfully transmitted. The following analysis can be made: in a node based on a duty cycle operation protocol, when a node that is most frequently in sleep mode receives a wake-up message during the active period, it switches to the active state. Thus the data transmission and reception begins. Otherwise, it continues to transmit the synchronization packets until it receives a data packet, or until the time for the connection establishment attempt expires if there is no data. If this happens successfully, the information is transmitted until the end and the node switches to the standby mode. The average power consumed by the node is evaluated by the following equations:

$$P_{avg,Rx} = \eta P_{Rx} + (\frac{T_{sleep}}{T_{sleep} + T_{s2a} + T_{active}})P_{sleep} + (\frac{T_{s2a}}{T_{sleep} + T_{s2a} + T_{active}})P_{s2a} \quad (1.1)$$

$$\eta = \frac{T_{active}}{T_{sleep} + T_{s2a} + T_{active}} \quad (1.2)$$

where η is the duty-cycle and P_{Rx} , P_{sleep} and P_{s2a} are amounts of power consumption respectively in active mode, sleep mode and sleep to active mode respectively. In general, since P_{sleep} is much smaller than P_{Rx} and T_{sleep} is much longer than T_{s2a}, the first term in equation (1.1) denominates the average power consumption. The minimum T_{active} is limited by the wake-up packet size, and hence T_{sleep} can be increased to reduce the average power consumption.

Figure 1.4 illustrates the two extreme scenarios when this strategy is used [15]. The first scenario in Figure 1.4 (a) is the case where the synchronization packet arrives at the moment of the transition of the node from standby to active mode. This is the ideal case and the latency here is only the one related to the sending of

the acknowledgment and the start of the data transfer. This minimum latency case also corresponds to the minimum power consumption by the node, which is parallel to the minimum power consumption by the transmitter. In contrast to this ideal case, Figure 1.4 (b) shows the longest latency. The synchronization message arrives just slightly behind schedule to be ignored. In this case, the power consumption is maximum at the device initiating the communication (generally the gateway) as well as at the connected device. Latency is maximum and the communication is delayed.

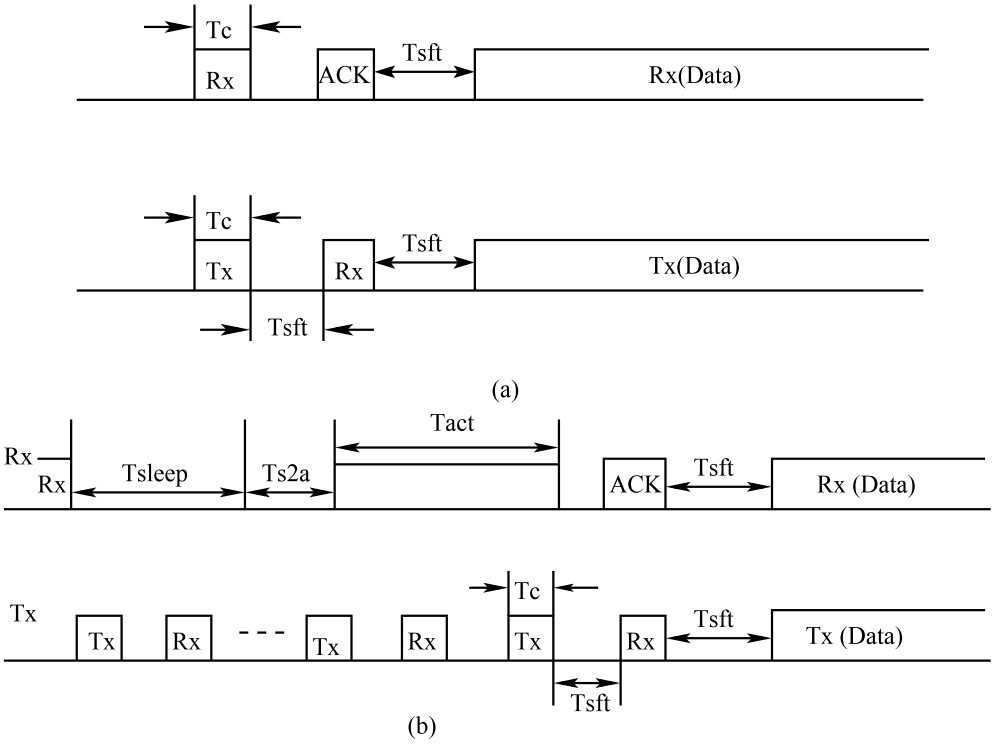

Figure 1.4: Timing sequence of the (a) minimum and (b) maximum sequence of wake-up latency in duty cycling scheme [15]

The following equations are used to determine the average energy consumption

(E_{avg}) and the average latency (L_{avg}) for the transmitter and the receiver.

$$E_{avg,Rx} = \frac{1}{2}\left(E_{Rx,max} + E_{Rx,min}\right) = \frac{1}{2}\left(T_{slp}P_{slp} + T_{s2a}P_{s2a} + T_{act}P_{Rx} + T_C P_{Rx}\right) \tag{1.3}$$

$$E_{avg,Tx} = \frac{1}{2}\left(E_{Tx,max} + E_{Tx,min}\right) = \frac{1}{2}\left(T_{slp} + T_{s2a} + T_{act} + T_C\right) P_{Tx} \tag{1.4}$$

$$L_{avg} = \frac{1}{2}\left(L_{max} + L_{min}\right) = \frac{1}{2}\left(T_{slp} + T_{s2a} + T_{act} + T_C\right) \tag{1.5}$$

1.3.3 Wake-up Radio Receiver

Wake-up mechanism enables the main radio to go to deep sleep as long as there is no transmission intended for it. It is an on-demand approach where the connected device of interest is woken up by a radio signal, namely wake-up signal (WuS). A WuS triggers a node to wake up from the sleep mode to active (reception) mode. This eliminates idle listening and achieves more energy saving, while accelerating packet forwarding by eliminating waiting time at each hop. Furthermore, this alternative is asynchronous and does not require time synchronization. Moreover, overhearing is reduced, and even eliminated with the addressing capability of current wake-up radio systems where only nodes concerned by the communication are awaken.

The use of a wake-up radio reduces collisions between data and wake-up messages and allows simultaneous exchange of these messages (since they are transmitted in different channels). Wake-up radio principle is illustrated in Figure 1.5.

Wake-up radio (WuRx) is a very low power consumption secondary radio, whose unique role is to turn on a primary radio on demand to perform data transfer. In that scheme, the WuRx has a very low energy consumption (10^3 to 10^5 lower than

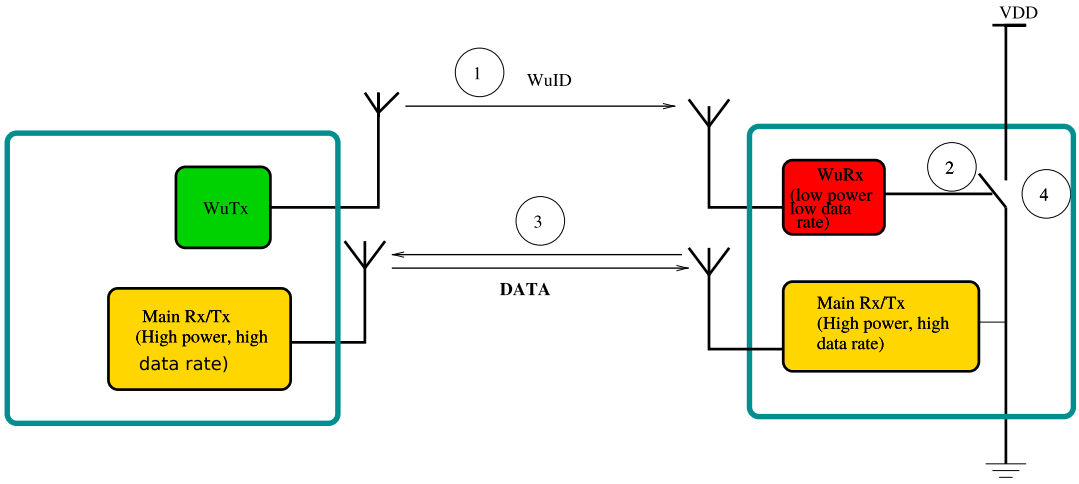

Figure 1.5: Wake-up radio principle

the energy consumption of a typical radio front end), the sum of which preferably ranges from a few nanowatts to a few microwatts. In this type of secondary radio, there is always a trade-off between the sensitivity of the receiver, on which the communication distance depends, and the energy consumption. Figure 1.5 shows the operating principle of WuRx. In that figure, this principle has been illustrated in four steps:

- In the first step, the wake-up transmitter (WuTx) sends a wake-up signal to the wake-up receiver. If the WuS corresponds to the identifier of the node or is simply the appropriate signal, the next step is taken. Otherwise the signal is ignored and nothing happens.
- When the ID signal is the appropriate signal, WuRx radio turns on the main radio and the system moves on to the next step.
- When the main radio is switched on, an ACK message is sent and a data exchange follows.
- At the end of the transmission, the main radio is switched off and the rest of

the system is on standby to await any further transmission. Meanwhile, the secondary wake-up radio remains active for channel monitoring and reactivation of the main radio front-end if the event occurs.

A more complete study of WuRx, which is an important aspect of this thesis, can be found in the next chapter.

1.4 Plan of the manuscript

The writing of this thesis is organised in four chapters. In the first chapter, we situate the thesis project in its context, which allows us to come back on the methods formerly employed to save the energy of the connected devices; then we define the WuRx and its operating principle before identifying the problem to be solved by this thesis.

In chapter 2, we make a deeper review of wake-up radio receivers. In the first articulation, we define their specifications; then we make a classification according to their energy consumption, their architecture, their implementation technology and their identification mode. This is followed by a statistical analysis and finally we present some well-known applications of these wake-up receivers.

Chapter 3 is dedicated to the improvement of quasi-passive radio wake-up; here, the study of each block leads us to improve the RF/DC converter block and subsequently the range of the wake-up radio itself.

In chapter 4, we make a quick study of the RF energy harvesting systems, then we make a description of the analysis methods as well as the tools that will allow us to analyse our circuit. Finally, we design and implement the circuitry that will allow to obtain the WuRx as a battery less system. At this stage, we go to the conclusion

to describe the different perspectives that are offered to this work.

Chapter 2

State of the art of Wake-Up Radios

2.1 Introduction

The Internet of Things (IoT) vision aims to develop smart objects which are not only manageable via the Internet but can also provide information on demand about the environment in which they operate. This information may be used for purposes, including control and supervision, but also for weather forecasting.

The information being the key element of IoT, to be collected, things embedded sensors, which in practice are unfolded like sensor nodes. The IoT as it stands today has a wide range of applications from the field of health care to agriculture, through smart cities, the control of telecommunications facilities as well as nuclear and many others installations, home automation and largely industries field. For use in a particular field such as aeronautics, more than 1000 sensors nodes are deployed [16].

IoT can be made possible in most cases if and only if operating with low power devices that have the capabilities of actuating and sensing. These objects, in the classical scenario are equipped with a battery; their usage sometimes makes them inaccessible for a battery replacement. In [17] we have some use cases of IoT in health that present intra-body and extra-body communication. An example of device usage inside human body is a pacemaker. This type of application obviously does not allow easy battery replacement. It becomes mandatory for such applications to find a battery of very large capacity and reasonable size, which will not be possible to implant in the human body because of the size or to find a way to use energy efficiently. To achieve this goal, duty-cycling was used with the limitations that we presented in the previous chapter. To correct these limitations a novel concept of Wake-Up Radio (WuRx) has been developed and its implementation gives wide satisfaction in terms of energy consumption, which for some cases is around just a few tens to few hundreds of nanowatts [18], [19].

The research advancement in CMOS technology has contributed greatly to the energy consumption performance of wake-up receivers, which take in addition the advantage of integration. The rest of this chapter is organized as follows: Section 2.2 describes requirements and taxonomy, Section 2.3 discusses classifications, Section 2.4 shows statistical analysis of low-power receivers, some applications are depicted in Section 2.5 and conclusion is in Section 2.6.

2.2 Requirements and Taxonomy

The concept of Wake-Up Radio receivers has very large numbers of requirements that are mostly dependable on the application targeted by specific device. Depend-

ing on the operating environment, WuRx must fulfills some design constraints:

- (a) Energy consumption: Energy consumption of Wake-Up receivers is one of the key characteristics of the design of low-power devices. This energy should always be much less (few hundred nanowatts to few microwatts) than the consumption of the main radio. In literature, we have passive and active Wake-Up Radios. Passive WuRs are those that rely only on Wake-up signal (WuS) to supply themselves. In this case, there is no use of classical source of energy (battery). For instance, in [20], a battery-less totally passive Wake-Up Radio is designed and implemented in CMOS technology, working in 915 MHz ISM band for a biomedical implant, takes the advantage of On-Off Keying (OOK) Wake-Up Signal for itself supply. Moreover, another example of fully passive WuRx is described in [21], operating in 2.4 GHz band. Active WuRs as far as they are concerned use battery for their supply. Some practical designs of active WuR are presented in [18],[22], they have advantages of better performance (high robustness, sensitivity, communication range etc.) as compared to passive radios.

- (b) Sensitivity: The sensitivity of a radio receiver is in dBm the lowest power level of information that can be received and interpreted. The lower this quantity, the more sensitive the receiver. In general, high sensitive receivers need high power consumption to operate. Some of the high sensitive low-power receivers can be found in [23], [24], [25] where we have a sensitivity of – 87 dBm for power consumption of 320 μW, – 92.5 dBm sensitivity for 470 μW power consumption and very high sensitivity of – 97 dBm for power consumption of 40 μW respectively.

- (c) Communication range: The range in radio communication is directly linked with the receiver's sensitivity. The design range of WuRx mostly depends on the targeted application and implicitly on the propagation environments. Generally, those distances vary from few centimeters for Body Area Network (BAN) to a few tens of meters for industrial applications as depicted in [16].

- (d) Wake-Up delay: WuR should have low latency so that the global time response of the sensor node should be reduced. Moreover, some application in industry are time critical and require the Wake-Up receiver to act with minimum delay tolerance. H. Milosiu et al. presented in [26] design of a very low-latency system of 60 milliseconds, which can be suitable for many applications in 868 MHz ISM band.

- (e) Frequency: The designers have work on a large range of frequencies in the design of low-power receivers depending on the applications and frequency regulation in corresponding countries. The US Federal Communications Commission (FCC) defined the ISM bands around 915 MHz and 2.45 GHz, while in European Union low-power wireless devices are generally referred to as short-range communication devices (SRD); Electronic Communications Commission (ECC) recommends bands around 433 MHz, 868 MHz and 2450 MHz as ISM bands. Fig 2.11 and Table 2.1 present some designs with their frequency. Many WuRx are principally designed in Industrial Scientific and Medical bands. In Africa and especially in Cameroon, the European standards apply in telecommunications.

- (f) Robustness: The robustness of Wake-Up Receivers is a part of their saving energy strategy. It is defined as the ability to prevent false wake-up. False

wake-up happens when the Wake-Up Transmitter (WuTx) tries to enable specific node and hazardous enables another one instead or many ones. This causes a lot of energy loss resulting in discharging the battery. False wake-up also happens when the addressing scheme is not well designed: the simple presence of signal in the corresponding band in this case can cause it. To solve this problem of robustness, WuRx often uses a coding strategy that attributes a specific code to each node. This may add complexity to the system with the consequence of increased energy consumption [27]. Modulation techniques can also help to prevent false wake-up. When complex modulation schemes are employed, the WuRx architecture complexity increases but on the contrary reduce the false wake-up. Simple modulation technique like On-Off Keying (OOK) that is largely used in WuRx is subject to sensitive wake-up. It is important to specify that the latter type of modulation is used because it causes a very low energy consumption compared to the others.

- (g) Cost and size: WuRx should be cost-effective since sometimes thousands of sensor nodes integrating WuR are used for a given system. In addition, it is obvious that the size should be as small as possible especially those used inside the human body.

2.3 Wake-Up Radio classifications

There are many bases on which WuRs can be classified. In this part, we will classify according to their energy supply, implementation architectures, identification methods and implementation technologies.

2.3.1 Classification based on energy supply

According to such a classification, they are Active WuRs, Passive WuRs and Semi-active WuRs.

Passive wake-up radios (PWUR) are those build around passive components and does not require any power source. In other cases of PWUR, although it is battery free, use the wake-up signal (WuS) as a source of energy which activates main radio generally by triggering from a standby state to an active state. PWUR technology is developed in [21], [28] and the architecture generally deployed is presented in Figure 2.1. It is based on simple envelope detector generally made of series diode with parallel capacitor. In spite of the fact that this completely passive technology is the goal for wake-up receivers, the fact remains that current implementations have a great limitation in sensitivity and consequently in terms of the range of communication.

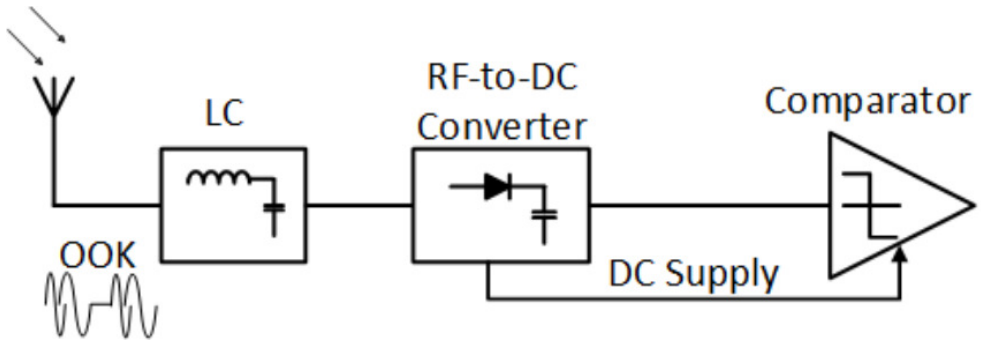

Figure 2.1: Passive Wake-up Radio architecture

Some designs resort to energy harvesting to covert the need of WuRx [29] in terms of power supply. Active WuRs use the battery of communication devices for their supply. The majority of WuRx are actives and are continuously supply.

Semi Passive Wake-Up Radio some components of the device are supplied with the continuous source while the front end remains passive like those in [30], [31].

2.3.2 Classification based on radio architectures

Low-power receivers are implemented using many architectures such as super-heterodyne, injection-locked local oscillator, super-regenerative and non coherent receiver.

a) Super-heterodyne Wake-up Receiver

Reginald Fessenden invented the heterodyning in 1901, which consists in applying a frequency created locally by an oscillator to one of the mixer input and RF frequency to the other input, the mixing of the two frequencies results in the extraction of the modulated signal. The system created in 1901 finds its most important application in super-heterodyne receiver (Figure 2.2) invented in 1918 by E. H. Amstrong. The idea behind super-heterodyne is to filter mixed frequency so that the noise is reduced and the selectivity of the system is increased. The filtered signal is easier to obtain in super-heterodyne receiver. This principle is used in [32] for ultra-low-power receiver (7 μW), high sensitivity (-80 dBm) and low latency (30 ms) duty cycled receiver.

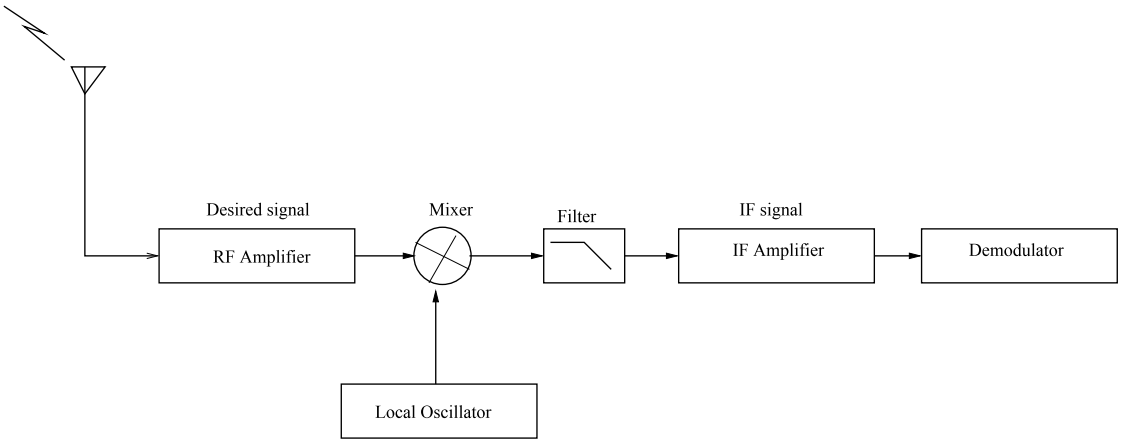

Figure 2.2: Principle of super-heterodyne receiver

b) Injection-locked Local Oscillator (ILO) receiver

This injection circuit is used to provide an external periodic locking signal to the oscillator (injection signal). Under some conditions, the oscillator locks on the injection signal so that the oscillation frequency becomes dependent on frequency of the injected signal. ILOs have properties to lock on one of the fundamental harmonics, or sub-harmonics of the injection signal. A simple representation of the injection oscillator principle is given in Figure 2.3 and Figure 2.4.

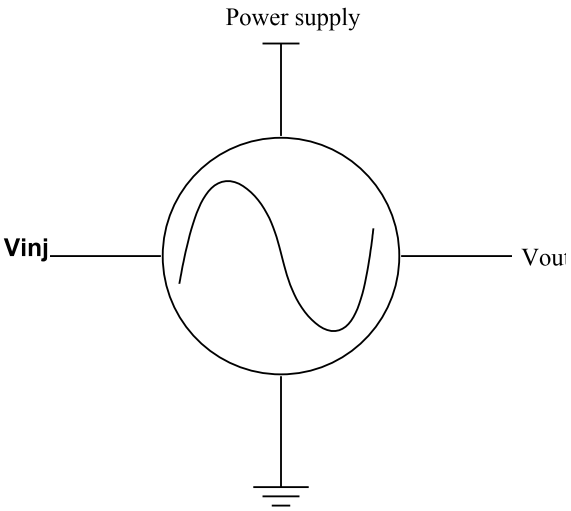

Figure 2.3: Injection-Locked Local oscillator principle.

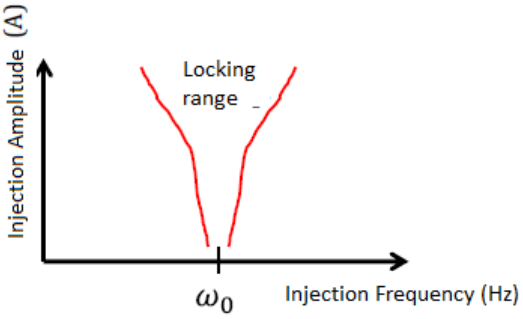

Figure 2.4: Locking range

Locking range is a couple of parameters (power level of injection signal, and frequency of injection signal) that guarantees the oscillator's locking. It is the sensitivity of oscillator, also called locking range with the example of Figure 2.4. The curve in Figure 2.5 shows that for high power, we have a large locking range.

Locking highlights the fact that the oscillator deviates from the free oscillation frequency to oscillate on a nearby frequency, which is the resultant of the free oscillation frequency and the frequency of the injected signal. It is also important to say that oscillator has the property to lock on the multiple or submultiple of the funda-

mental frequency. Under the injection locking conditions, the frequency of injected signal is closed to the resonance of an LC tank. Assuming that the amplitude of the injected voltage V_{inj} is much lower than the amplitude of the free-running oscillator voltage V_{osc}, the locking range can be given by equation 2.1 [28]. The concept ILO is used for the design in [33], [34], and [35] for low-power receiver.

$$\omega_L = \frac{\omega_0}{2Q}\frac{V_{inj}}{V_{osc}} \tag{2.1}$$

Were ω_L is the locking bandwidth around the operating frequency ω_0. Q the quality factor V_{inj} is the peak voltage of the injected signal V_{osc} is the peak voltage of oscillation output signal

The ILO is used for low power receiver as a Frequency Shift Keying (FSK) to On-Off Keying (OOK) converter [36]. The conversion is based on the fact that the input FSK signal presented at the ILO's output can be differentiated by the amplitude variation of the ILO's output, which leads to the frequency-to-amplitude conversion. The conceptual diagram of ILO with LC tank that oscillates at ω_0 and presents a quality factor of Q is shown in Figure 2.5.

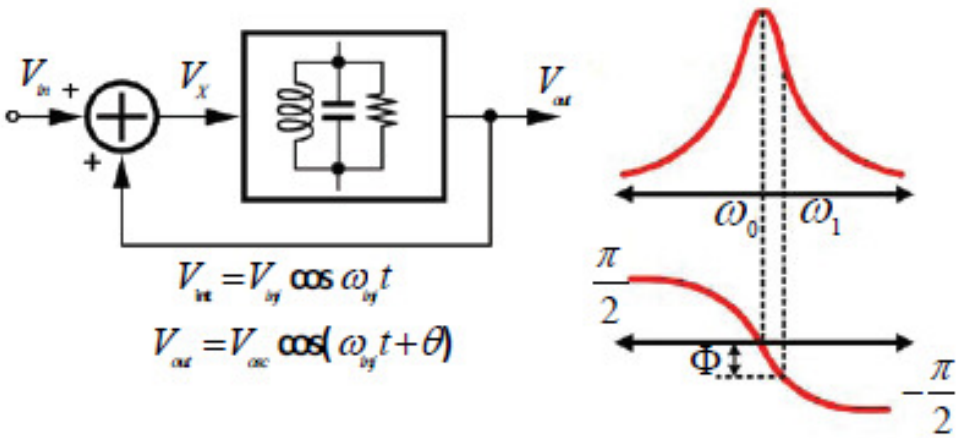

Figure 2.5: Frequency-to-amplitude conversion of ILO based on tank [37]

$$V_{out} \approx V_{osc} \cos\left(\omega_{inj} + \theta\right) \tag{2.2}$$

The output voltage of ILO is given by equation 2.2 [37]. It shows that, the frequency of the output voltage is related to the frequency of injected signal and the proper use of ILO by playing with the locking range of equation 2.1, allows to get a conversion with an envelope detection demodulation as the representation given in Figure 2.6.

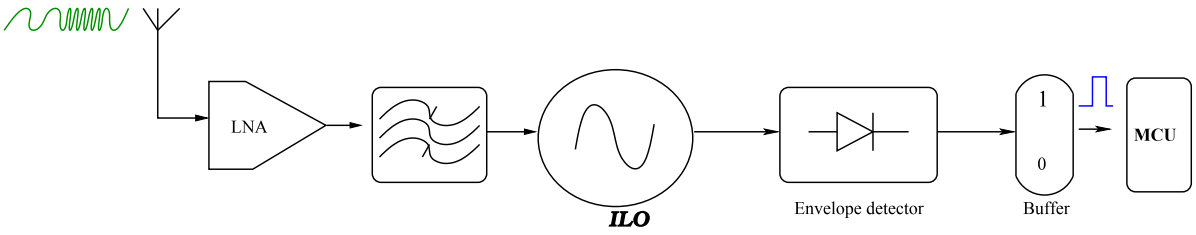

Figure 2.6: FSK envelope detector design

c) Super-Regenerative receiver

A super-regenerative principle is used in the receiver for low power solution based on super-regenerative oscillator (SRO). E.H. Armstrong invented the first Super-regenerative receiver (SRR) in 1922. The works based on the start-up transient characteristic of an oscillator, which is used to achieve filtering and amplification.

In SRR the oscillator is controlled by the quench generator that generates low frequency periodic signal, causes the RF oscillations to rise from starting transient close to the stable point and die out time after time. The RF oscillator can be

modelled as a frequency selective network fed back through a variable gain amplifier. This gain is modified by the damping oscillator, making the closed-loop alternatively unstable and stable. In this way, the signal generated in the oscillator is composed of a series of RF pulses separated by the quench period T_q, and the periodic build-up of the oscillations is determined by the input signal v(t) (see Figure 2.7 and Figure 2.8) [38].

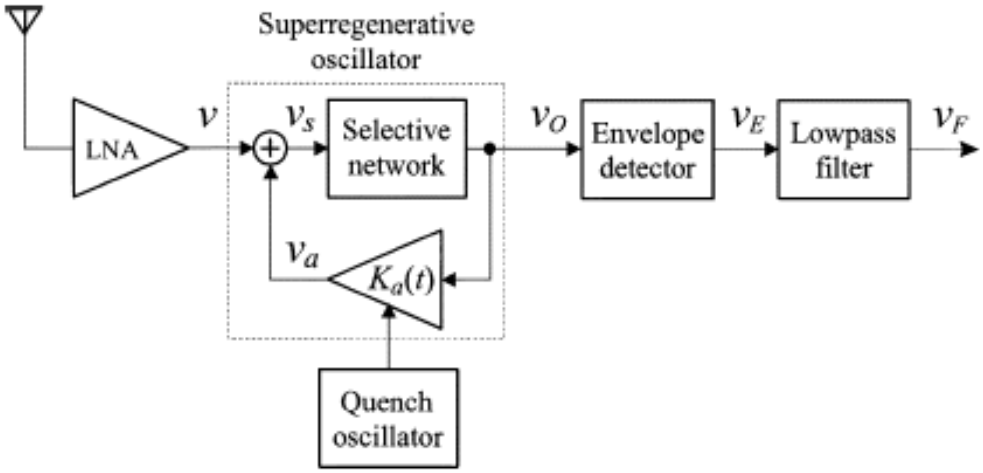

Figure 2.7: Detailed block diagram of the super-regenerative receiver [38]

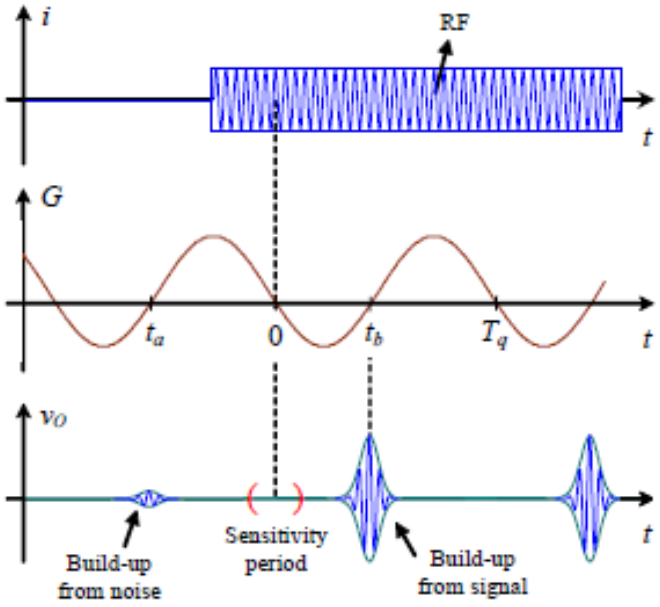

Figure 2.8: Input signal and output voltage of SRR

d) Envelope detector receiver

Envelope detector architecture is suitable for passive Wake-Up Radio as mention earlier. This structure is developed and commented in section (2.3.1).

2.3.3 Classification based on implementation technology

All the designed (see Table 2.1) Wake-Up Receivers known are using mainly four technologies for their implementation. The review of literature informs that those technologies are namely CMOS, Bi-CMOS, BCD, and usage of discrete components.

The CMOS technology takes the advantages of very low-power consumption and high capacity of integration, making small size devices which are the target for many applications.

Bi-CMOS is the combination of two transistor technologies in a single integrated circuit, which are Bipolar and CMOS. This combination brings together the advantages of both technologies. Bipolar junction transistor offers high gain, high speed and low output resistance whereas CMOS offers high input resistance and low power consumption. The drawbacks of the Bi-CMOS integrated circuit are relatively high global power consumption and high complexity procedure of fabrication.

BCD stands for Bipolar-CMOS-DMOS (Double Diffused Metal Oxide Semiconductor): it merges the three technologies and their advantages onto a single IC, resulting in improvement of reliability, robustness to electromagnetic interference, and surface area of devices. BCD technology offers a very high density integration of many complex functions on a same chip and guarantees high reliability to all

applications built on the chip. The representation of BCD technology is shown in Figure 2.9.

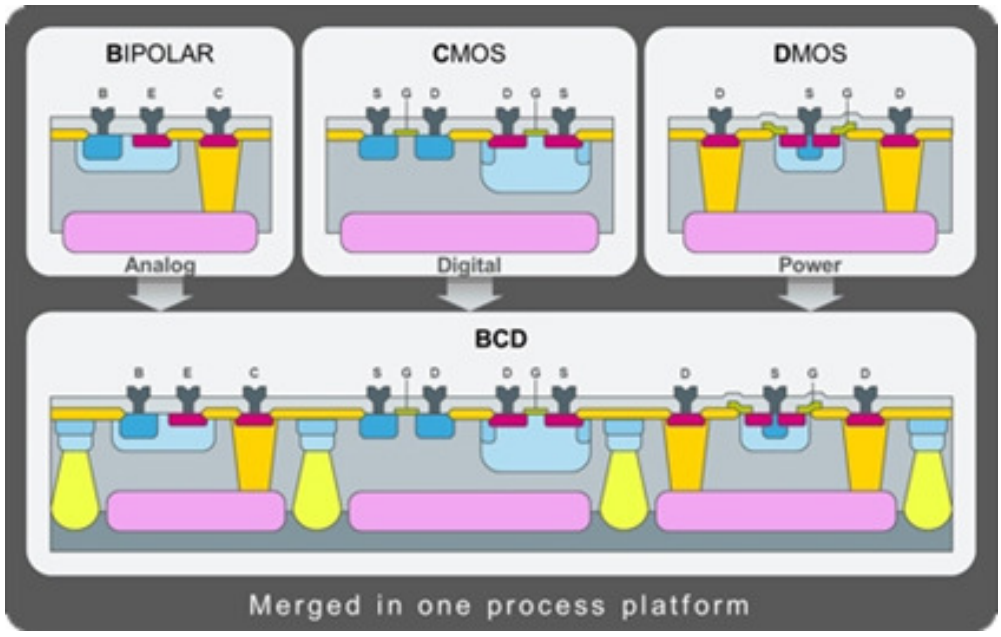

Figure 2.9: Representation of BCD technology

RFID stands for Radio Frequency Identification, which are wireless devices that can be used for identification. RFID system is made up of passive transponder call tag and its reader; the principle is shown in Figure 2.10. In specific case of Wake-Up Radio used, the tag aimed to be attached to a sensor node, with the advantage of identifying uniquely the concerned node. A designed case of WuR using RFID is simulated in [39]; RFID Impulse that is low-power Wake-Up radio for sensor nodes uses an RFID reader as Wake-Up Radio transmitter and a tag as the trigger to enable the node, achieving a distance of 30 meters for a power consumption of 80 μW. The tag of the RFID technology which is here the wake-up radio is made up of chip based on transistors.

Figure 2.10: RFID Wake-Up Radio based prototype [45]

2.3.4 Classification based on Identification Methods

This classification focuses on the way that the wake-up signal (WuS) is formed. The classification is based on the frequency on which the ID is transmitted and the number of WuRx which are addressed.

a) ID-based receiver:

This type of system has a specific address to wake-up only a unique node. In this case, there is avoidance of false wake-up and overall waste of energy (at WSN level). This technique adds more complexity to the system with the advantage of more precision but has high energy consumption.

b) Broadcasting based receiver:

In this case, the WuS enables all nodes in its neighborhood. This implementation is relatively easier than the ID-based one. The main drawback is that a given node can wake-up when there is no need and, in this case, there is some useless energy consumption.

2.4 Statistical analysis of low power system receivers

A review of Wake-Up Radio Receivers leads us to a listing provided in Table 2.1. As it will be shown, there are many correlations between characteristics of WuRs. The choice of those characteristics for a WuR to be designed will be directly linked to the requirements of the targeted application. In this part, we are analysing and comparing different features of wake-up devices regarding their communication range, sensitivity, power consumption, modulation scheme and frequency.

2.4.1 Modulation Technique vs. Power consumption

In Table 2.1, the state of the art of Wake-Up Radio Receivers is summarized, where we make an inventory of 31 designs of the most representative among the available works on the topic; although they are other inventories. From there, we can deduce that the majority of WuRs uses the OOK modulation scheme.

The choice of OOK is directly linked to the power consumption. The implementation of OOK non-coherent receiver is less complex than any other demodulation scheme in receiver design. It requires passive rectifier architectures based on diodes and capacitors as in [20]. We can find from the state of the art that, apart from the case in [19] using PWM, all the other WuRs with less than 1 μW use OOK modulation [18, 20, 21, 40, 41, 42]. Although the OOK modulation scheme provides good power consumption, it is sensitive to interference. Other modulation schemes require sometime more complexity with the consequence of more power consumption like in [35] and [43] that use respectively Binary Phase Shift Keying (BPSK)

and Frequency Shift Keying (FSK). The latter two types of modulation transmit information by modifying the frequency of the carrier signal, so the modulation is robust to additive noise (amplitude noise).

In Figure 2.11, we have the representation of Wake-Up Radio Receivers of Table 2.1, with their modulation scheme and power consumption. As already mentioned, the OOK modulation scheme is the one that dominates in it number, that scheme has been in used so far and continue to be the most present for the recent designs. Each point of the figure matched with the corresponding reference publication.

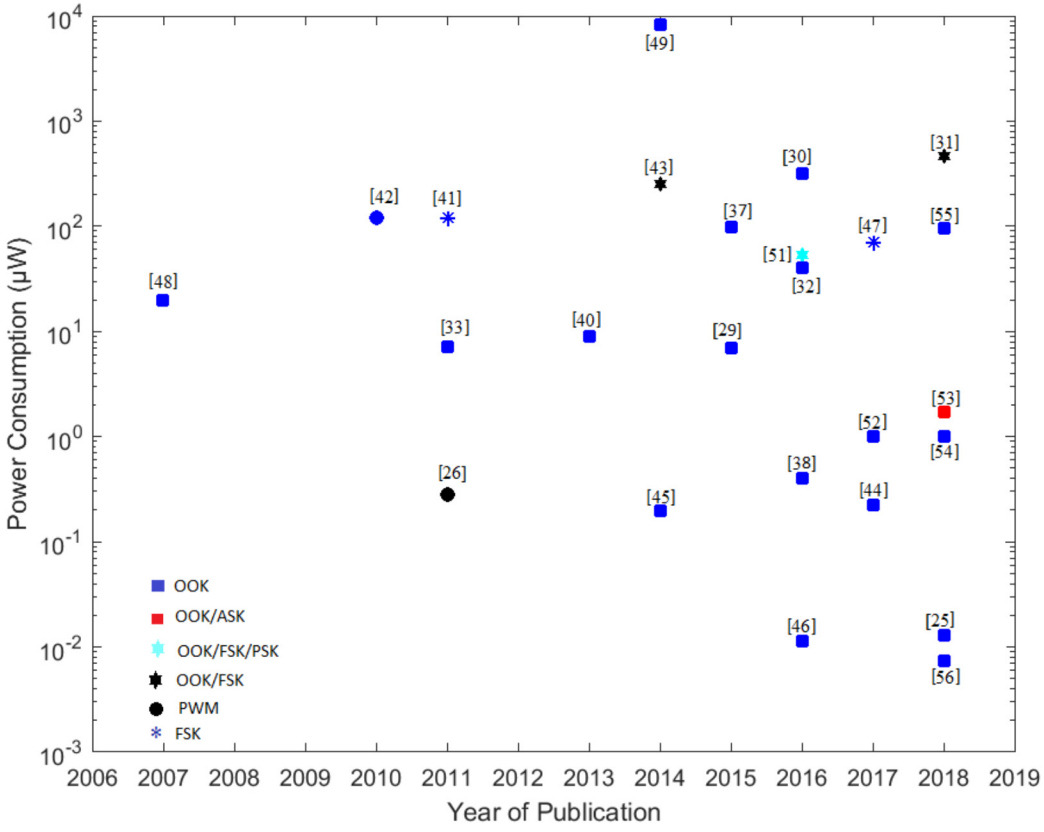

Figure 2.11: Power Consumption of state-of-the-art of WuRs

Table 2.1: Characteristics of available designed Wake-up Receivers

Ref.	Year	Frequency	Mod.	Pwr. supply	Sensitivity	Architec.	Techno.	Impl.
[44]	2007	915 MHz	OOK	20 μW	− 69 dBm	ED	Discrete	Prototype
[35]	2010	300 MHz	BPSK	120 μW	− 34 dBm	ILO	CMOS	Prototype
[19]	2011	433 MHz	PWM	278 nW	− 51 dBm	ED	CMOS	Prototype
[26]	2011	868 MHz	OOK	7.2 μW	− 60 dBm	–	CMOS	Prototype
[34]	2011	44.5 MHz	FSK	120 μW	− 90 dBm	ILO	CMOS	Prototype
[32]	2012	915 MHz	OOK	121 μW	− 83 dBm	ED	CMOS	Prototype
[33]	2013	60 GHz	OOK	9 μW	− 68 dBm	ED	CMOS	Prototype
[45]	2013	900 MHz	ASK	0	− 80 dBm	RFID tag	RFID	Prototype
[41]	2014	868 MHz	OOK	196 nW	− 55 dBm	ED	Discrete	Prototype
[36]	2014	902 − 928 MHz	OOK / FSK	250 μW	− 63 dBm	ILO	CMOS	Simulation
[28]	2014	868 MHz	OOK	0	− 33 dBm	ED	CMOS	Simulation
[46]	2014	2.4 GHz	OOK	8.25 mW	− 44 dBm	Sup.het.	Bi-CMOS	Prototype
[22]	2015	2.4 GHz	OOK	7 μW	− 80 dBm	Sup.het.	CMOS	Prototype
[20]	2015	915 MHz	OOK	0	− 43 dBm	ED	CMOS	Prototype
[21]	2015	2.4 GHz	OOK	0	− 19 dBm	ED	CMOS	Prototype
[30]	2015	2.4 GHz	OOK	99 μW	− 97 dBm	Het.	CMOS	Prototype
[47]	2015	900 MHz	–	0	− 86 dBm	RFID tag	RFID	Prototype
[48]	2016	433 MHz	OOK FSK PSK	54 μW	− 80 dBm − 78 dBm − 77 dBm	ILO	CMOS	Prototype
[23]	2016	900 MHz	OOK	320 μW	− 87 dBm	SRR	CMOS	Prototype
[25]	2016	28 MHz	OOK	40 μW	− 97 dBm	SRR	Discrete	Prototype
[31]	2016	868 MHz	OOK	400 nW	− 35 dBm	ED	Discrete	Prototype
[42]	2016	50 MHz	OOK	11.5 nW	− 60 dBm	ED	CMOS	Simulation
[40]	2017	550 MHz	OOK	222 nW	− 56.4 dBm	Sup.het	CMOS	Prototype
[43]	2017	868 MHz	FSK	70.2 nW	− 61 dBm	ED	Discrete	Prototype
[49]	2017	41 kHz	OOK	1 μW	–	SRR	CMOS	Prototype
[18]	2018	868 MHz	OOK	13 nW	− 54 dBm	ED	BCD	Prototype
[24]	2018	5.8 GHz	OOK/ FSK	470 μW	− 92.5 dBm	Sup.het.	CMOS	Prototype
[50]	2018	433 MHz	OOK/ ASK	1.7 μW	− 49.5 dBm	ED	Discrete	Prototype
[51]	2018	900 MHz	OOK	1 μW	− 58 dBm	ED	CMOS	Prototype
[52]	2018	2.4 GHz	OOK	95 μW	− 72 dBm	-	CMOS	Prototype
[53]	2018	433 MHz	OOK	7.4 nW	− 71 dBm	ED	CMOS	Prototype

ED = Envelope Detector; Impl = implementation; Techo = technology; Pwr = power; Mod = modulation

2.4.2 Sensitivity Vs Power Consumption

Sensitivity and power consumption are two key parameters of a WuRx. In classical receivers, the sensitivity is measured at bit error rate (BER) 10^{-3} that is the acceptable level of error for a good channel in communication system. BER is the number of error bits over an amount of transmitted bits, 10^{-3} BER means that over transmitted one thousand bits, we have one bit error; with this level of error rate, the probability of making an error in transmission is very low.

Since the Wake-Up Radio is not fundamental for data exchange, the only requirement is to get enough power level at the wake-up antenna to trigger the main radio.

There is always a trade-off between power consumption and sensitivity in the sense that high sensitivity requires high power consumption and subsequently, the two parameters are proportional. A design in [32] is a typical case to understand the link between the two parameters; we have for that circuit, a sensitivity of -56 dBm for power consumption of 63.5 μW while the increase in power to 121 μW provides the sensitivity of -83 dBm.

Figure 2.12 shows a graphical representation of state-of-art in Table 2.1 by considering their power consumption and sensitivity. As can be seen, no one Wake-up Radio out performs all the other in terms of power consumption and sensitivity. We can realize from the figure that, the majority of WuRs have their sensitivity lying between -70 dBm and -50 dBm, and their power consumption less than 100 μW. Some specific cases that drew our attention and we circle them in red. The references labelled (1) and (2) shown the very low power consumption in the circumstances 13 nW, 11.5 nW and 7.4 nW for the corresponding sensitivity of -54 dBm, -60 dBm

and -72 dBm respectively; which are very good performance on the Wake-Up Radio topic and can be exploited for the applications requiring very low power and high sensitivity. Circle (3) is for [24] and [34] with corresponding sensitivity of -92.5 dBm and -90 dBm respectively; these two cases correspond to high sensitivity WuRs with the power consumption relatively high, notably 470 μW and 120 μW. The cases of highest sensitivity are [25] and [30] with sensitivity of -97 dBm each; [25] operates with the carrier frequency of 28 MHz while [30] works in radiofrequency specifically 2.4 GHz; their power consumptions are 40 μW for [25] and 99 μW for [30].

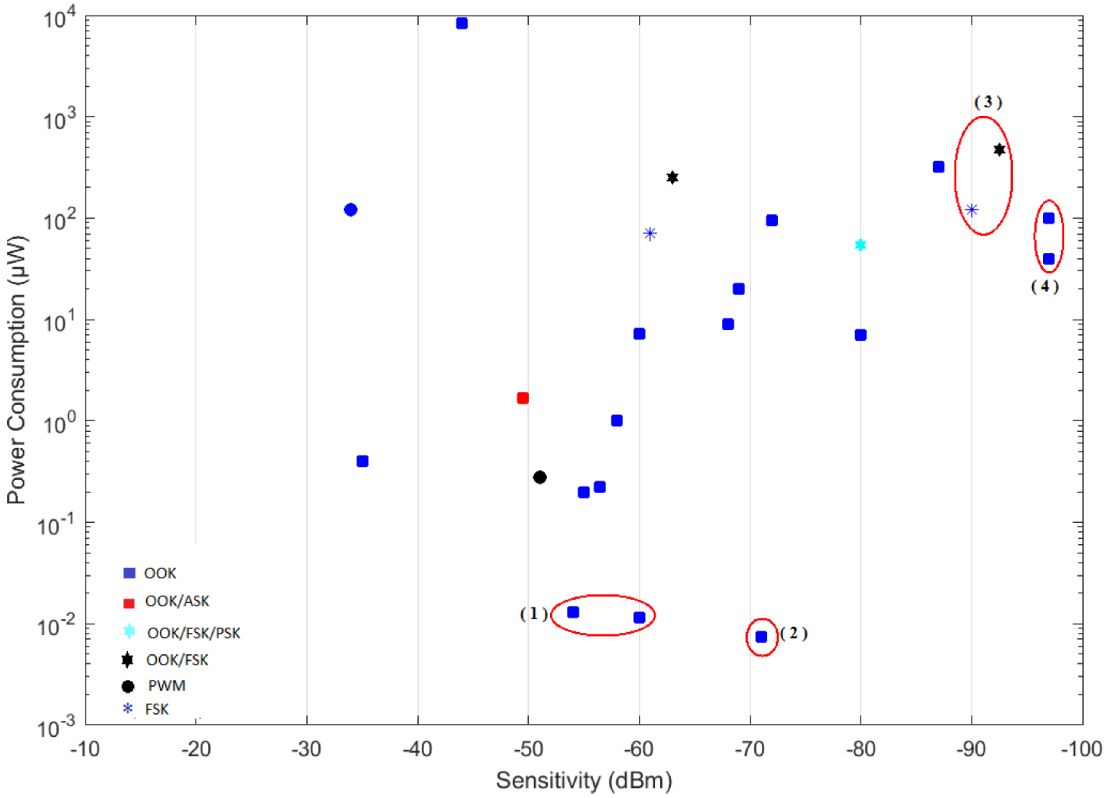

Figure 2.12: Power Consumption vs. Sensitivity

2.4.3 Power Consumption and Technology

In Figure 2.13, we represent the power consumption in function of sensitivity

Table 2.2: Technology of WuR and Power consumption

Power. Cons. \ Technology	BCD	CMOS	Bi-CMOS	Discrete	RFID
Power. ≤ 10 μW	[18]	[19], [20], [21], [22], [26], [28], [33], [40], [42], [51], [49]		[31], [41], [50]	[45], [47]
10 μW $<$ Power. ≤ 100 μW		[30], [48], [52]		[25], [43], [44]	
Power > 100 μW		[23], [24], [36], [34], [35]	[46]		

but taking into account the technologies. We realized that those parameters are not related even if it is admitted that CMOS integrated circuit is low power consumption technology with the counterpart of relatively high latency. Nevertheless, if we consider the data in Table 2.2, we can have the following discussions.

The single case working with BCD technology uses less than 10 μW; CMOS technology is the one that offers possibility to work with any range of power levels. The advantage of using CMOS integrated circuit comes from the fact that it generally has very low supply voltage and satisfies the condition of small size device that is very important in some cases (see section 2.2). The receiver in [46] which is implemented with Bi-CMOS technology works with 120 μW power. Discrete component technology implements low and medium power devices. Designs using RFID technology are very low-power since the tag are generally passive.

The choice of technology that will be used to implement a device can influence the selection of frequency and vice versa; for example, discrete components cannot be used to implement very high frequency circuits (above GHz), due to their radiation properties at high frequencies. The majority of WuRx are designed to work in ISM band either in Europe or in America and Japan; as mentioned elsewhere, Africa and specifically Cameroon follows Western European norms in telecommunications.

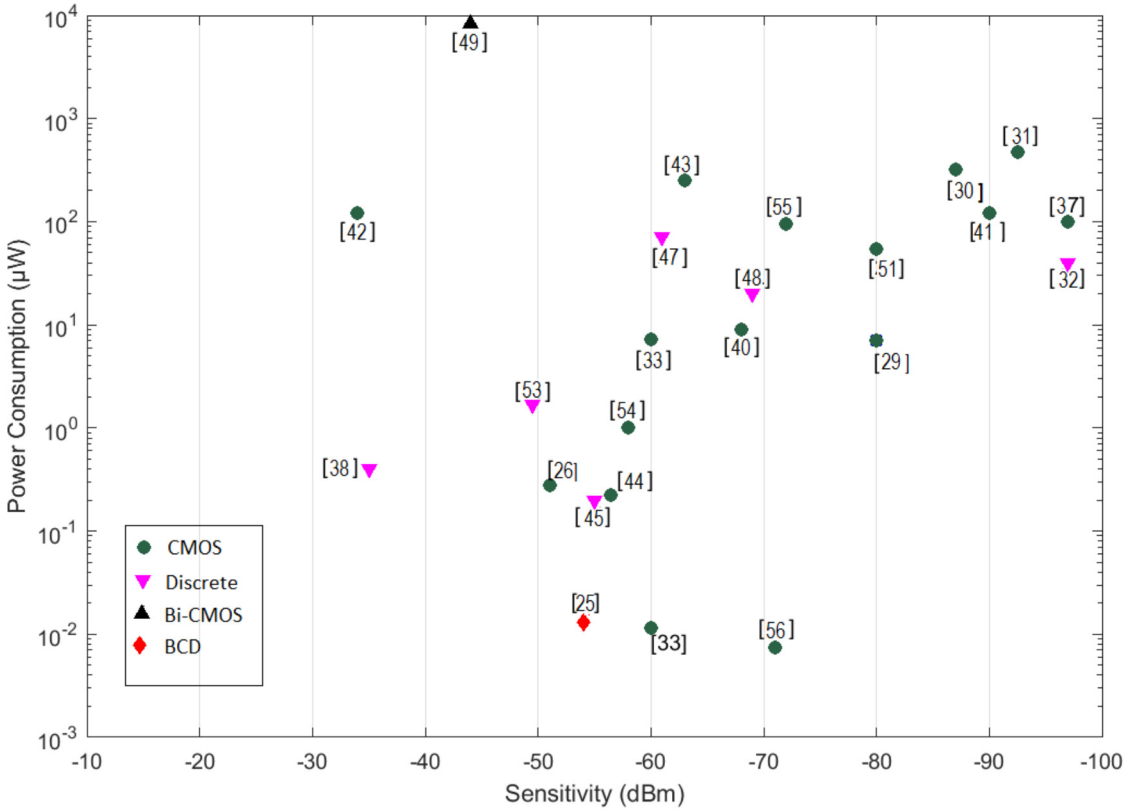

Figure 2.13: Power Consumption and Technology of WuR

In Table 2.3, we have different technologies with the frequency corresponding to each design. A double line divides the table into two-parts with the first one corresponding to sub GHz part and the second part in which there are devices operating above 1 GHz.

CMOS integrated circuit is used to implement WuR from ultra-low frequencies [34], [49] up to 60 GHz [33]. It is the only technology from the state-of-the-art that covers all range of frequency in the implementation of prototype. The single BCD implementation [18] that we have is working with 868 MHz ISM frequency. In [46] we find an implementation at 2.4 GHz, working in Bi-CMOS technology. All the implementation with discrete off-the-shelf components are working under 1 GHz; this is due to de dispersive nature of discrete components. If the frequency used in

Table 2.3: Technology of WuR and Frequencies

Frequency \ Technology	BCD	CMOS	Bi-CMOS	Discrete	RFID
41 kHz		[49]			
28 MHz				[25]	
44.5 MHz		[34]			
50 MHz		[42]			
300 MHz		[35]			
433 MHz		[19], [48],[53]		[50]	
550 MHz		[40]			
868 MHz	[18]	[26], [28]		[31], [43], [41]	
900 MHz		[20], [23], [36], [51]		[44]	[45], [47]
2.4 GHz		[21], [22], [30], [52]	[46]		
5.8 GHz		[24]			
60 GHz		[33]			

discrete component prototypes goes far beyond one gigahertz, the components will have a behavior different from the nominal one, thus causing operation failure by radiating and creating electromagnetic interference in the environment which leads to some power loss in the system.

It should be noted that the power consumption of system globally increases with the frequency, since the path loss increases with the frequency according to Friis formula. Moreover, the study presented in [54] shows that, for the same power consumption of 1.276 μW, a WuR design to work in dual frequency of 868 MHz and 2.45 GHz gives – 53 dBm and – 45 dBm sensitivity respectively, corresponding to a margin of 8 dB due to the circuit and systems behavior at different frequencies.

2.5 Applications of Wake-Up Radios

WuRs are used in very wide range of applications depending on their require-

ments, which are among others, the battery lifetime, wake-up range, wake-up latency, the size of devices and channel characteristics. Wake-Up Radios are devices generally designed for Wireless Sensor Networks (WSN), in order to activate main radio of nodes that will receive and transfer data before being switching off for next wake-up. The downside of WuR is that it adds the complexity to node because of additional secondary radio to be integrated; however, it is very helpful to reduce the overall energy consumption.

Many applications of WuRs are now registered in very large number of fields such as aeronautics, wireless body area network (WBAN), smart metering, industrial applications, smart city, wildlife monitoring, security and surveillance of systems, indoor localisation, asset tracking, smart grid and wearables. In this section, we are going to present some typically known cases of usage among the listed fields.

2.5.1 Wireless Body Area Network

WBAN communications are governed by IEEE 802.15.6 HBC PHY standard, which normalized the communication in the vicinity and into the human body, for medical and non-medical applications. IEEE 802.15.6 defines different layers which are Human Body Communications (HBC), Ultra-wideband (UWB) and Physical (PHY) layers as shown in Figure 2.14. [55]; Figure 2.15 presents different frequencies of that standard which are namely, for Medical Implant Communication Service (MICS), Wireless Medical Telemetry Services (WMTSs), Industrial Scientific and Medical (ISM) and Ultra-wideband (UWB) which can support high data rate applications.

WBAN is used to monitor body parameters like glucose level, heartbeat and

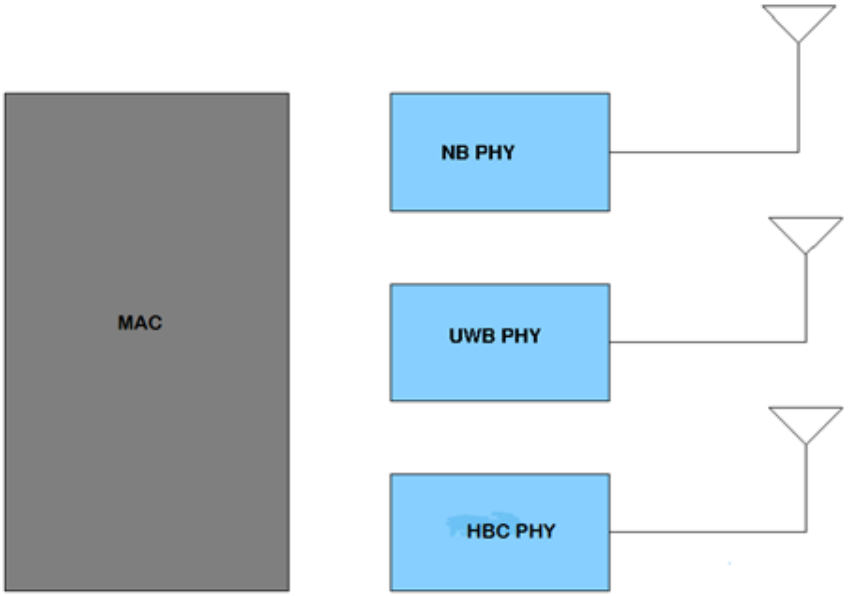

Figure 2.14: IEEE 802.15.6 MAC and PHY layers

body temperature, it requires around 20 to 50 sensor nodes. WuR in WBAN can be used as a trigger to activate high data rates node or as low power consumption, low data rate radio.

The WuR design in [25] is an example applicable for HBC, the use of 28 MHz frequency in that specific case causes the low free space loss (26 dB at 40 cm and 40 dB at 1 m). Since many applications in WBAN are in the vicinity of human body, the applicable WuR will require low sensitivity with the consequence of very low power consumption. It is reported in [56] that the receiver with a sensitivity of – 40 dBm is capable to receive the signal transmitted with 0 dBm power in WBAN.

According to the state-of-the-art, if we are to consider WuRs that can be matched with sensitivity requirement and power consumption below 10 μW, as recommended in [13], if additionally, we consider size constraint, we will be able to say that WuRs in [18, 19, 20, 21, 22, 26, 33, 40, 42, 51, 49] match with WBAN applications.

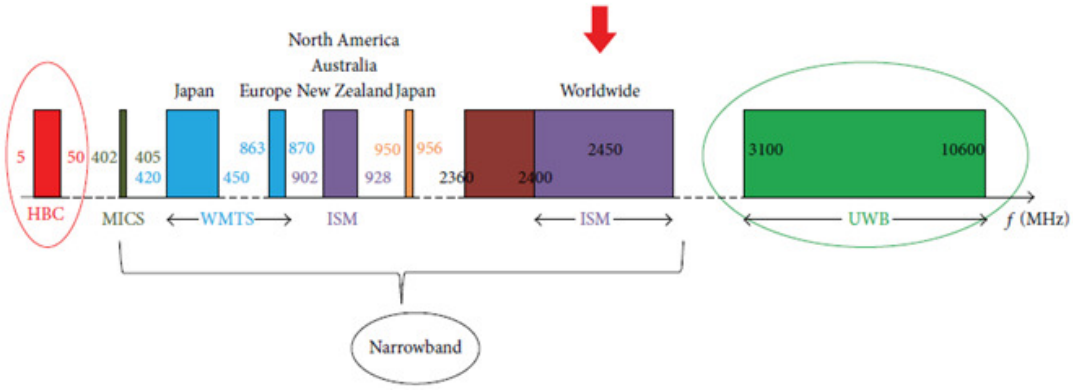

Figure 2.15: Frequency bands in IEEE 802.15.6 standard [55]

2.5.2 Smart metering

Smart metering offers the possibility to read a measurement from distance on home meter that can be gas, water or electricity meter. In Cameroon, for example, a technician is on the field every month to read water and electricity meter, it happens that sometimes there is no access to the meter since people are not always in their house. Smart metering allows reading meter without necessity to access meter; the typical distance is 15 meters. The used WuR on the smart meter will reduce the power consumption of transmitter that sends the value appearing on meter.

The pathloss for smart metering was measured at 15 meters to be 100 dB, the similar value was obtained for multiple floor scenario at distance 10 meters as indicated in [16]. The standard IEEE 802.15.4g that govern globally Smart Utility Network (SUN) in which smart metering belong specifically, restricts the maximum power radiated at 25 dBm in European band 868 MHz, therefore, this application will require very high sensitivity to compensate cover need due to high demand of path loss. In this context the minimum required sensitivity is – 75 dBm. An out of band WuR is designed and implemented in [57], working at 868 MHz frequency, with current consumption of 2.8 μA. By using a CR2032 coin cell with 230 mAh as

supply, the estimated lifetime of the battery was found to be 7 years.

From the state-of-the-art, the solutions proposed in [25] and [48] that are all with power consumption less than 55 μW and sensitivity better than – 75 dBm, matched with the smart metering application.

2.5.3 Wildlife monitoring

The global vision of IoT has permit to derive other aspects of specified applications which is wildlife monitoring, such as Internet-of-Birds. In [58], an example of wildlife monitoring is presented using four larger flamingos (Phoenicopterus roseus), which are tracked with attached devices. In the corresponding study, the system deployed for monitoring should follow some size and weight constraints. For the specific case of birds, the device should be a maximum of 5 % the total weight of bird, and the shape should be optimized to reduce impact on its movement. For that bird species weighing between 0.6 – 1 kg, a device of about 31 g was designed, working under 500 mAh and 3.7 V lithium polymer battery. The energy efficiency of the system was measured and yielding a performance of 540 days by considering no battery self-discharge, or 397 days with consideration of 2 % battery self-discharge. This specific application on birds can be extended to other wildlife monitoring; WildScope [59] project used the same process to attach sensor nodes on deers and foxes for the tracking purpose and study of their behaviour and interactions.

The used of WuR for wildlife monitoring aims to make use of energy efficiency in order to enhance the battery lifetime of device and avoid capturing the animal for battery exchange. By following the reference study in [27] that specifies the range for wildlife monitoring above 30 meters and low consumption requirement,

the WuRs that matched with the corresponding applications from state-of-the-art are [22], [25], [48] and [44].

2.5.4 Security and surveillance

The security of people and facilities often relies on surveillance systems generally use camera for recording and sending data. The used of smart system based on WuR embedded on wireless sensor node, minimize the energy depletion in such a system. The typical case in [60] presents the used of pyroelectric infrared (PIR) sensors, to detect human motion and send the WuS to activate camera. If there is no event in the coverage area, camera nodes will be in sleep mode. The PIRs are deployed in dense area with overlapping in coverage so that, there is redundancy in case of breakdown of node camera. That study shows for some cases, the used of duty-cycling MAC takes advantage in terms of power consumption on WuR without addressing, but could not out perform addressing based WuR.

Depending on the coverage area involved in the security and surveillance application, the same WuRs performance working for wildlife monitoring matched with this application, but they should also include addressing capability like in [61]. This application can also be extended to smart cities application using Wake-up Radio receivers for energy breakdown in smart systems.

2.5.5 Indoor localisation and asset tracking

Indoor localization is the process of locating a person or an object in an indoor environment. This technique is generally used in commercial businesses or shopping malls. It is special since the GPS signal cannot be received. Sometime this

application must rely on wireless sensor nodes. An application example is found in [62], implementing a sub 10 μW WuR for asset tracking, operating at 434 MHz and battery intended to last for years (20 years in some cases). From the state-of-the-art, all the WuRs with power consumption lower than 10 μW matched with this application.

2.5.6 Wearables

Wearable devices such as smart bracelet, smart clothes, and equipment for fitness and health tracking are also subject of battery lifetime challenge. The WuR mechanism was proposed in the case study [31] for wearables to optimize the energy depletion of battery. In that particular case, the performance obtained for Wake-Up Radio consuming only 400 nW power with – 35 dBm sensitivity is satisfactory for such an application.

2.5.7 Other possible applications of Wake-Up Radio

The challenge of reducing power consumption in many applications is still pending. The WuR solution will be a great opportunity to reduce the power consumption for those applications. In aeronautic for example, the used of thousands Wireless Sensor Nodes [16], [63] will benefit from the power efficiency due to WuR attached to each node; the currently known system in used in aeronautic, work with ultra-low-power receiver, but there is still to implement wake-up systems.

They are many applications in which the WuR device will decrease drastically their energy consumption such as smart grid, smart lighting, automation of application, etc. We cannot surely give an exhaustive list of applications that may require

WuR, but its use will in every case increase potentially the lifetime of systems.

In order to make it possible, there is still a great deal of work on standardization of the WuRx. This work, which is still in its very early stages, particularly with the 802.11ba standard as presented in the work presented in [64], still has to overcome certain limits. In that standard, the target power consumption is 1 mW with a complex access and identification method that will necessarily require the use of a microcontroller. This order of power consumption remains high compared to WuRx that do not require a microcontroller.

2.6 Conclusion

This chapter is dedicated to the state-of-the-art of WuRs, we presented an overview on requirements and characteristics of wake-up devices, we then made their classifications based on different parameters like their energy supply source, architectures, implementation technologies and identification methods. In the rest of this chapter, we analyse different parameters, then we present non-exhaustive state of the art of the applications that can be implemented with WuR.

We can immediately say from state-of-the-art that many applications are still working under duty cycle strategy for power efficiency, instead of WuR which offers the advantages of low latency and avoidance of useless overhearing of channel. Furthermore, some scarce cases of WuR utilisation implemented are still prototypes and are still to become commercial device available on the market. For this reason, the most implemented prototype was for experimental purposes. The future scope of research on Wake-Up Radio receivers should focus on boarding those systems on wireless sensor nodes that are widely used in a very large scope of applications.

Chapter 3

Contribution to the improvement of quasi-passive Wake-Up Radio

3.1 Introduction

One of the challenges of this thesis is to improve the WuRx system. In the previous chapter, important parameters of Wake-Up Radio are defined, and among others we have the sensitivity on which we will focus in this chapter. The sensitivity is the lowest signal level which may be received properly by the radio receiver.

For the purpose of increasing sensitivity, the hierarchical method which consists in dividing the system into functional blocks in order to better define the possibilities of improvement have been chosen. Analysis has shown that the detector block defines the sensitivity of the proposed WuRx, and its improvement will surely impact the global sensitivity. The approach here is to analyze the behavior of the detector in order to find out margins of improvement.

The work done so far on the detector's design was essentially based on the

use of HSMS diode family and lumped elements L matching circuits, what limits them to operate on a narrow frequency band. The choice of a RF diode here will be determined by methodological analysis of large range of RF components. The solution proposed in this chapter is to use a wideband, high efficiency rectifier in order to increase the communication range of such quasi-passive WuRx compared to the initial architecture [65]. Theoretically, the use of matching network with three degrees of freedom (in Pi or in T), allows obtaining a wider bandwidth.

The rest of this chapter is organized as follows: section 3.2 describes the concerned quasi-passive wake-up radio identified the means of a frequency imprint. Section 3.3 discusses the sensitivity of the overall system, based on the improvement of the detection circuit, the performance improvement is demonstrated by the means of circuit-system co-simulations performed by using Keysight's ADS Software. The conclusion is given in section 3.4.

3.2 Quasi-passive wake-up radio

As stated earlier, the Wake-Up radio is a very low power secondary radio that is attached to the main radio receiver. The principal radio is powered off when there is no information to be transferred, and enables only if the wake-up signal announces the availability of data to be sent. The main objective of WuRx is the mitigation of power consumption of radio frontend during the listening mode.

The peculiarities of the studied of quasi-passive WuRx are on the one hand, its ability to associate the wake-up radio function to its addressing capability, and on the other hand the use of a multicarrier OFDM signal as WuS which is independent of any baseband processing. It was firstly developed in CITI Laboratory as

presented in [65] to tackle principally the idle power consumption issues in Wireless Sensor networks (WSNs), that find their applications in: environmental monitoring [66], [67], home appliances automation and monitoring [68], [69], industrial process monitoring and actuation [70], security and surveillance [71], agriculture [72], health care [73], etc. But with today rapid development of Internet of Things, such a WuRx can be embedded in any connectable object for the energy consumption reduction. In this section a general description of quasi-passive WuRx is given with simulation results.

3.2.1 Description

The majority of WuRx as we have shown in previous chapter, does not have addressing capability. Figure 3.1 shows the possible usage of this specific WuRx. If at a given time, the transmitter which is represented here as the gateway, wants to collect any information from the node numbered j (j is an integer number chosen between 1 and N) , it sends the WuS corresponding with the jth identification number. All nodes will receive the WuS signal, but only the node with the corresponding ID should wake-up by switching on its frontend for the beginning of data exchanges. At the end of communication, the node goes back off and waits for the next matching wake-up signal. During the idle time of node, only WuRx is on.

The block diagram of quasi-passive WuRx is presented in Figure 3.2. The received wake-up signal from the antenna is divided into two equal parts by means of a passive power divider. The two parts are then filtered by the direct and complementary bank of filters. The filter bank on the direct path has the same exact frequency shape as the identifier, then its path will allows signal ID to pass. The

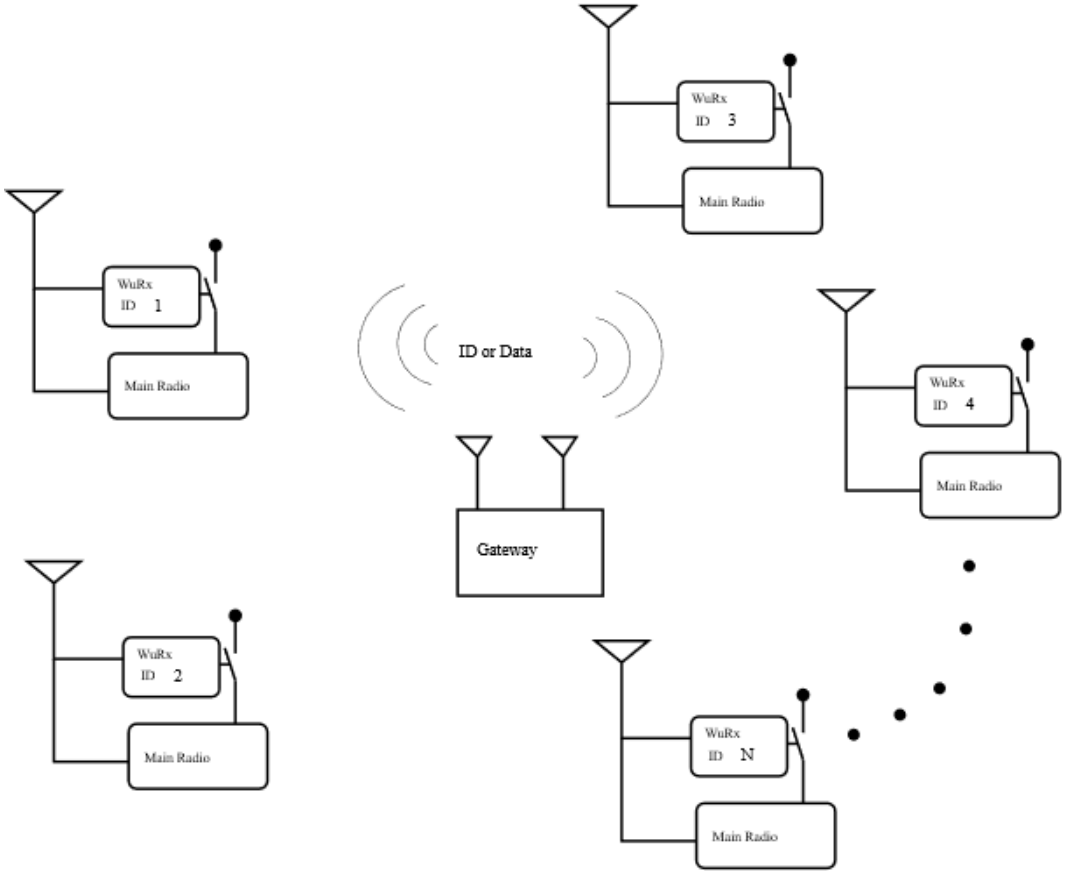

Figure 3.1: ID based wake-up mechanism

filter bank on the complementary path, a complementary shape (a pass-band filter on the complementary path where there is a stop band filter on the direct path and vice versa). Obviously, after filtering, the power level of the signal at the output of the direct path is higher than the power level of the signal at the output of the complementary path when the identifier is received. At the output of each bank of filters, there is an envelope detector that will transform the RF signals (V_{RF1} and V_{RF2}) into a proportional DC voltage (V_{DC1} and V_{DC2}). The subtractor which is conceived base on active circuitry, and also plays the role of a voltage amplifier, collects at its input the voltages from the detectors. The subtractor's output voltage is compared to a threshold voltage by using a Schmitt trigger. The reference level $V_{threshold}$ is tuned in such a way that, if the identifier is received, the voltage V_{sub}

at the output of the subtractor becomes superior to $V_{threshold}$ and V_{COM} drives the main receiver's power supply to ON.

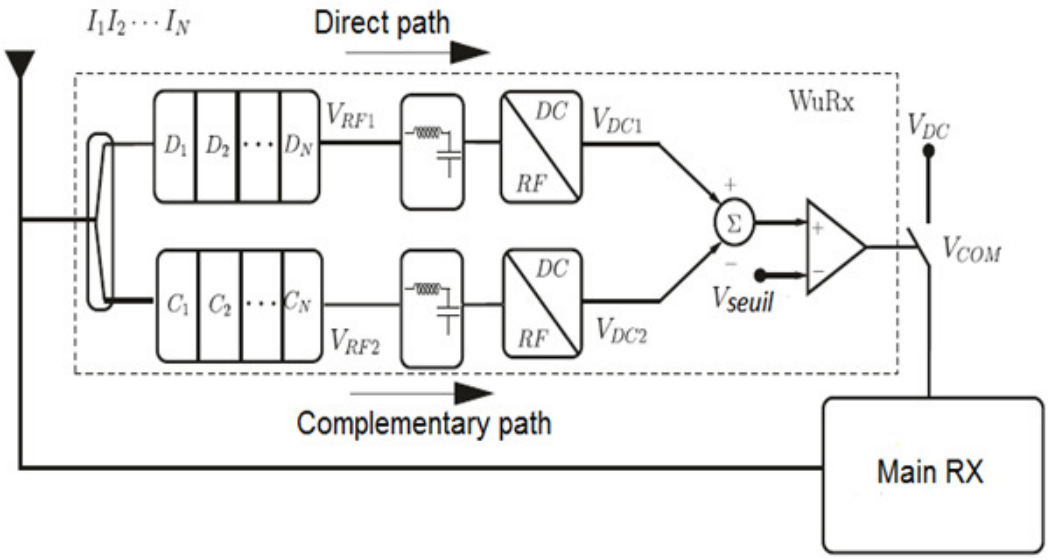

Figure 3.2: Block diagram of CITILab WuRx [65]

The identifier to address this wake-up receiver is formed based on an OFDM signal. The total number of subcarriers in the OFDM signal is divided into N groups. The pattern of the sub-bands of direct path filter bank is the same as that of the identifier signal. If a given sub-band of a direct filter is associated to a logical "1" and is a pass-band, its complementary sub-band will be associated to logical "0" and will be a stop-band.

The bank of filters on the direct and complementary path is represented in Figure 3.3. They are 0 dB filters each with bandwidth of $\frac{BW}{N}$, with BW the total bandwidth of the OFDM signal and N the number of sub-bands; the output rejection is considered as – 50 dB. The central frequency of i$^{\text{th}}$ filter is given by the following equation:

$$f_i = f_0 + (\frac{(2i-1)-N}{2N})BW, \tag{3.1}$$

with i=(1,2,...,N), and f_0 the central frequency (2.45 GHz) of the channel.

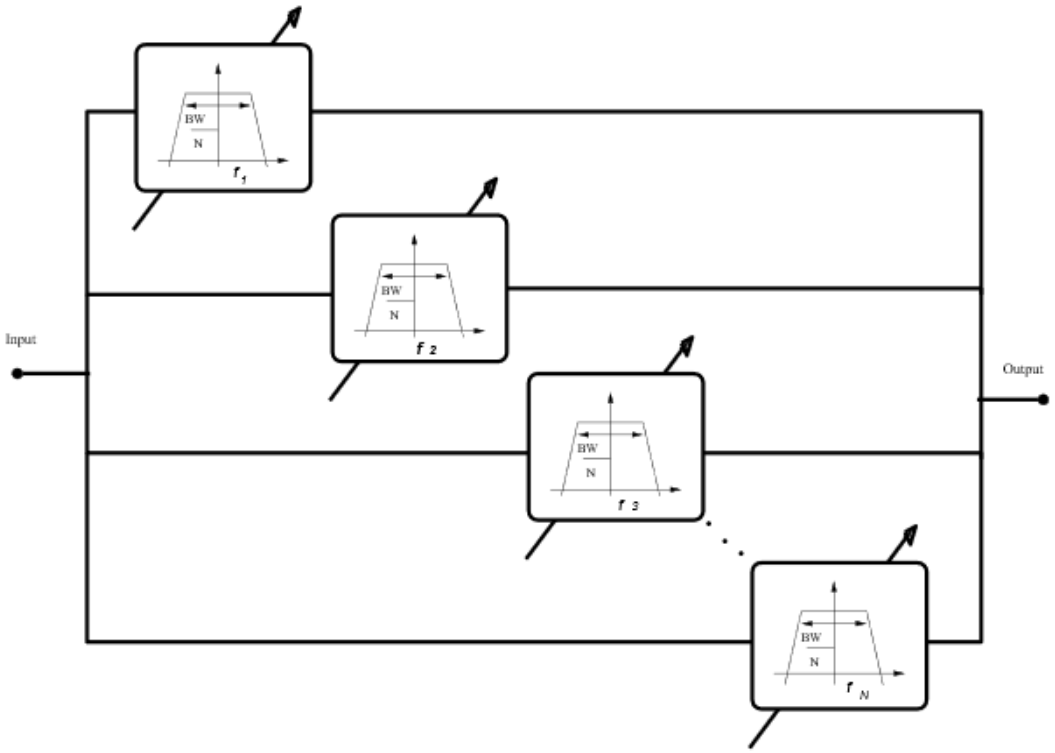

Figure 3.3: Block diagram of bank of filters

The direct path filter (D_K) , the complementary path (C_K) and the identifier (I_K) are modeled as followed :

$$\begin{cases} I_K \in (I_N ... I_k ... I_1); \text{ with } I_k \in (0,1); \forall k \in (1 \cdots N) \\ D_K \in (D_N ... D_k ... D_1); \text{ with } D_k \in (0,1); \forall k \in (1 \cdots N) \\ C_K \in (C_N ... C_k ... C_1); \text{ with } C_k \in (0,1); \forall k \in (1 \cdots N) \end{cases} \tag{3.2}$$

The number N is chosen by respecting technological constraints, notably taking into account the feasibility of filters' quality factors. It is important to mention that, not all the $2^N - 2$ combinations can be used as identifiers (here the first identifier in the range is represented by $000\ldots0$ and the last by $111\ldots1$ are not taken into account). To avoid a false wake-up and decrease energy consumption of the overall system, three conditions must be fulfilled when choosing the identifiers.

Firstly, an identifier should provide an energy level on the direct path higher than the one provided at the complementary path. The second condition is that the eventual surrounding signals (such as WiFi signals that have the same band as the identifier) should not be able to provide enough energy to activate the WuRx. The last condition is that only the assigned identifier is able to activate the WuRx. The conditions are summarized in the following three equations:

$$\begin{cases} \sum_{L=1}^{N} D_{K,L} \cdot I_{K,L} - \sum_{L=1}^{N} C_{K,L} \cdot I_{K,L} > 0 \\ \sum_{L=1}^{N} D_{K,L} \cdot \Pi - \sum_{L=1}^{N} C_{K,L} \cdot \Pi \leq 0 \\ \sum_{L=1}^{N} D_{K,L} \cdot I_{T,L} - \sum_{L=1}^{N} C_{K,L} \cdot I_{T,L} \leq 0 \ , \forall T \in (1 \cdots 2^N - 2) \end{cases} \tag{3.3}$$

Where Π is an OFDM signal with the same bandwidth as the one of the identifier. If we are in case where N = 4, Π will be 1111.

In Figure 3.4, we have an example of signal identifier for the case of filters with fourth sub-bands. If random data is sent on a subgroup of sub-carriers, the power level on the sub-band is greater with respect to the noise level which corresponds to a logical “1”. When no data is sent, on a subgroup of sub-carrier, the power level is near the noise floor and this codes a logical “0”. Since the total bandwidth is 20 MHz, each sub-band occupies a space of 5 MHz.

Considering the condition of equations (3.3) that helps to avoid a false wake-up. It comes that, out of $2^N - 2 = 14$ (with $N = 4$) possible identifiers, only six of them are fulfilling all the requirements of a robust receiver not liable to false wake-up. Those identifiers are presented in Table 3.1.

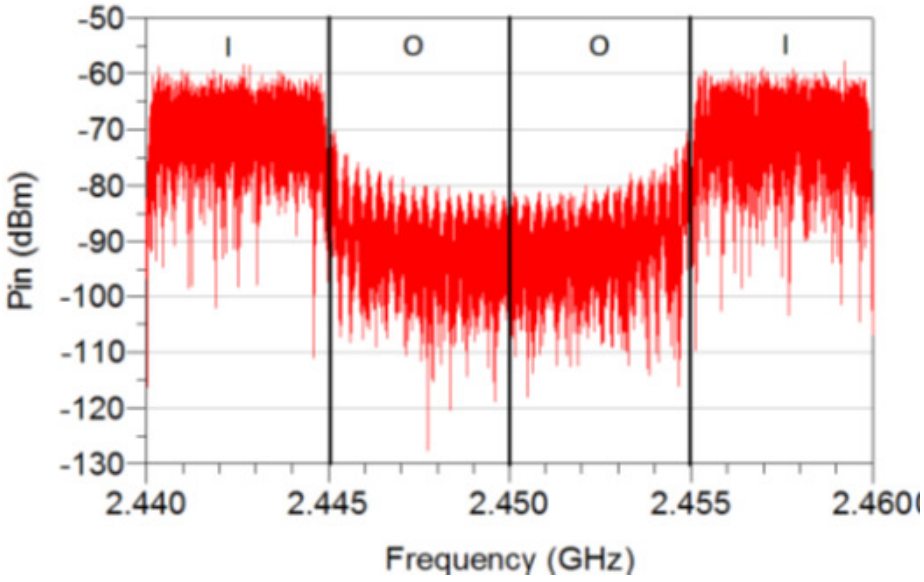

Figure 3.4: An Example of identifier (1001)

Table 3.1: Identifier, direct path and complementary path filter

Identifier	Direct path	Complementary path
0011	0011	1100
0101	0101	1010
0110	0110	1001
1001	1001	0110
1010	1010	0101
1100	1100	0011

3.2.2 Simulation

Figure 3.5 represents a global architecture of the quasi-passive Wake-Up Radio as it is figured in the simulator. Keysight's Advanced Design System (ADS) software is used to perform all the simulations in this section.

The identifiers are created by modifying the base-band part of an 802.11 g emitter, and emitting the resulting signal around a carrier frequency of 2.45 GHz and bandwidth of 20 MHz. The total 64 sub-carriers are used, corresponding to spacing

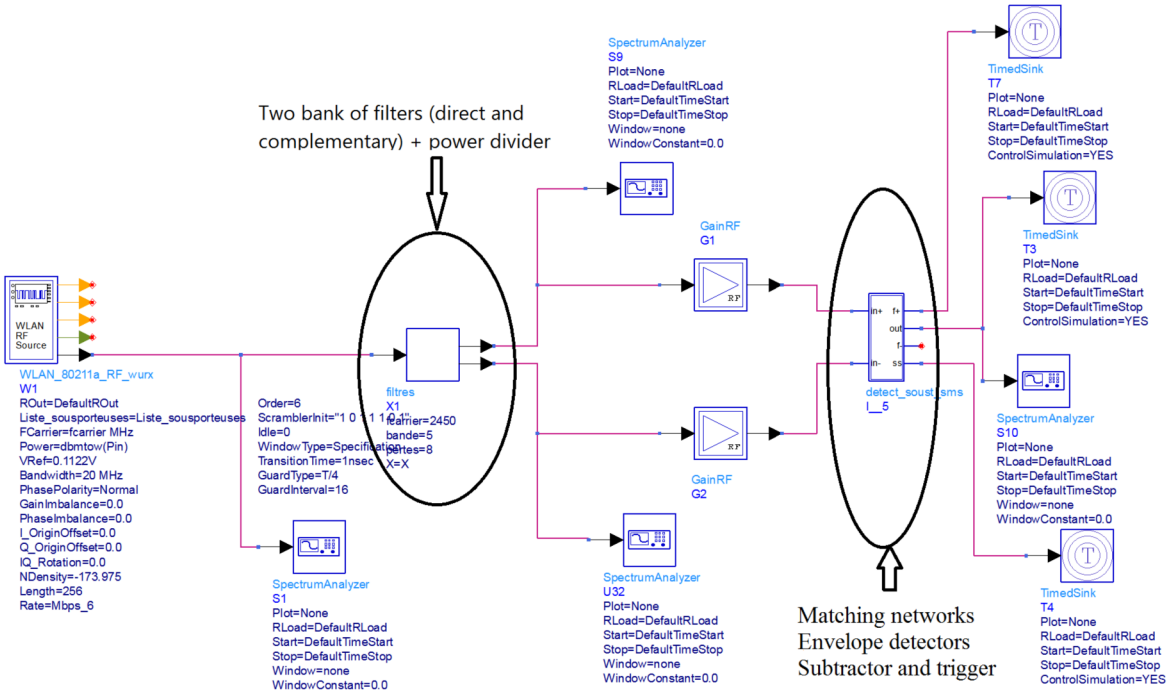

Figure 3.5: Global simulation of the quasi passive WuRx

of 312.5 kHz. The emitted signal is also known as Wi-Fi signal, that uses OFDM modulation.

To deliver the maximum power from the filters to the envelope detectors, an impedance matching network must be calculated. In Figure 3.6, the matching network and detector are characterized at central frequency of 2.45 GHz, yielding the responsivity and reflection coefficient in Figure 3.7 (a) and (b), for power sweeping range of – 50 dBm to – 10 dBm.

In Figure 3.8, the part circled in global simulation as “matching network, detector, subtractor and trigger” is represented. The impedance matching circuits have been designed to provide the best matching at low power levels at the 2.45 GHz working frequency. It can be observed that the one detector is for the direct path and the other for complementary path. The detector behaviour for this simulation

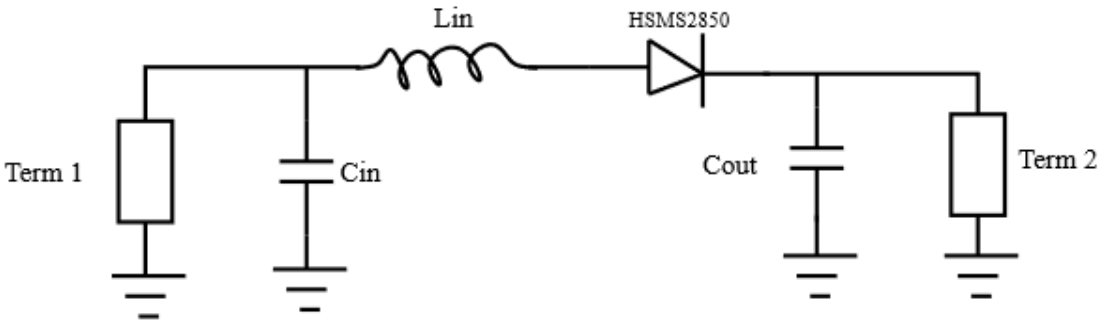

Figure 3.6: Impedance matching network and detector

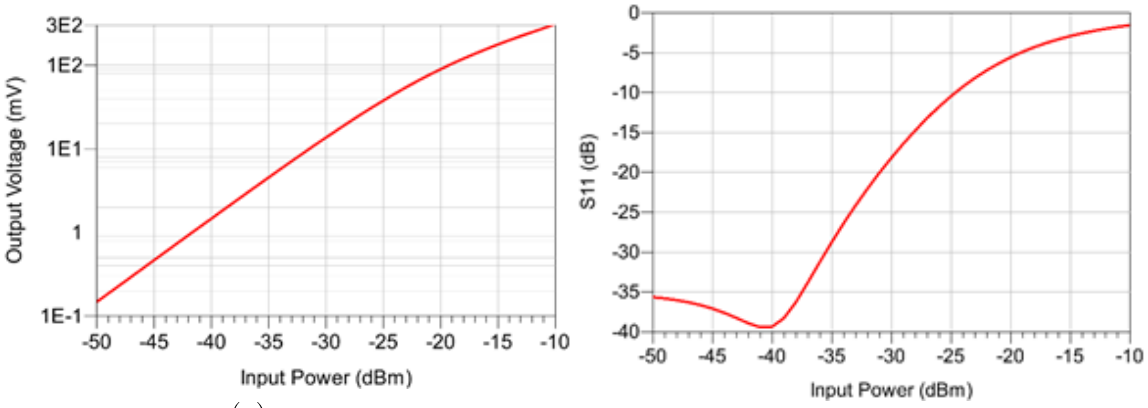

(a) (b)

Figure 3.7: (a) responsivity and (b) reflection coefficient of detector

is as depicted in Figure 3.7. When the simulation is carried out with all parts, the output of detectors on direct and complementary path for correct identifier and input power of – 25 dBm is showed in Figure 3.9. When the identifier is sent during 500 μs, the voltage output of direct path is always above the voltage of the complementary path. The direct path voltage is applied to the positive input of subtractor while the complementary path is applied to the negative input of subtractor. The difference of two voltages is amplified by the gain given by the following equation (3.7).

The amplified output of the subtractor is displayed in Figure 3.10. It represents

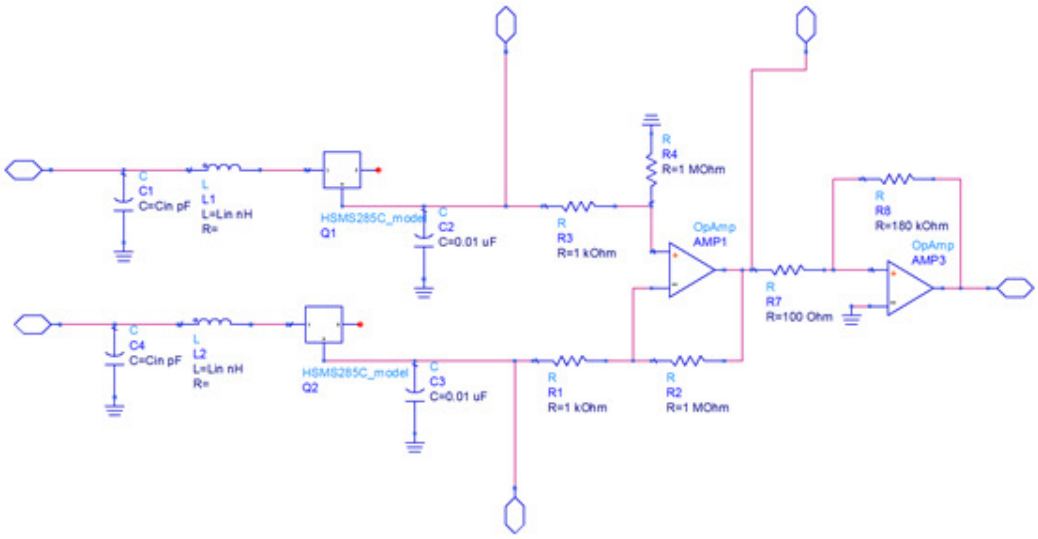

Figure 3.8: The matching network, detectors, subtractor and trigger

the mathematical value of equation (3.4), given by:

$$Vsub = \sum_{L=1}^{N} D_{K,L}.I_{K,L} - \sum_{L=1}^{N} C_{K,L}.I_{K,L} \tag{3.4}$$

Av is the voltage amplification of the difference between the direct path and complementary path obtained by the computation of subtractor done in the following equations:

$$V_{+} = \frac{V_{DC1}/R_3}{\frac{1}{R_3} + \frac{1}{R_4}} = \frac{R_4 V_{DC1}}{R_3 + R_4} \tag{3.5}$$

and

$$V_{-} = \frac{\frac{V_{Sub}}{R_2} + \frac{V_{DC2}}{R_1}}{\frac{1}{R_1} + \frac{1}{R_2}} \tag{3.6}$$

If at this stage we consider $R1 = R3$ and $R2 = R4$, then if we equate the two equations, we obtain:

$$V_{Sub} = \frac{R_2 V_{DC1}}{R_1} - \frac{R_2 V_{DC2}}{R_1} = A_V(V_{DC1} - V_{DC2}) \tag{3.7}$$

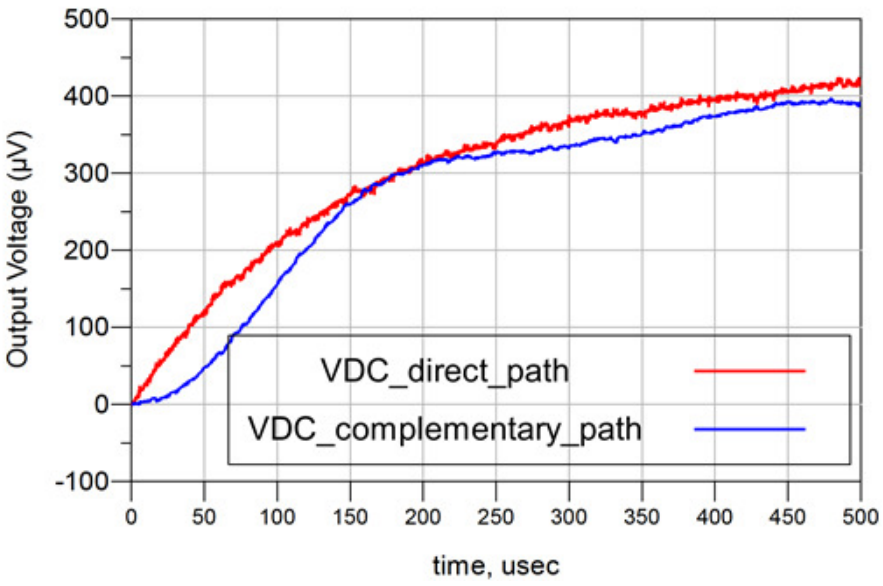

Figure 3.9: The envelope detectors output

with $A_V = \frac{R_2}{R_1}$

If the amplified difference $A_V(V_{DC1} - V_{DC2}) < V_{ref}$, the main radio will remain off; and when it becomes greater than the reference meaning $A_V(V_{DC1} - V_{DC2}) > V_{ref}$, the Schmidt trigger switches on the main radio and communication start. At this stage, the output of the trigger is given in Figure 3.10, while the evolution of subtractor's output as function of input power is given by Figure 3.11.

In the case of the circuits we are considering here, the sensitivity of the receiver is defined by that of the rectifier circuit (envelope detector) and it is highly desirable to increase this sensitivity.

3.3 High-efficiency rectifier for sensitivity improvement

The sensitivity or the capability of receiving low power signal in most receivers and in particular the wake-up receiver types, in the absence of a low noise amplifier,

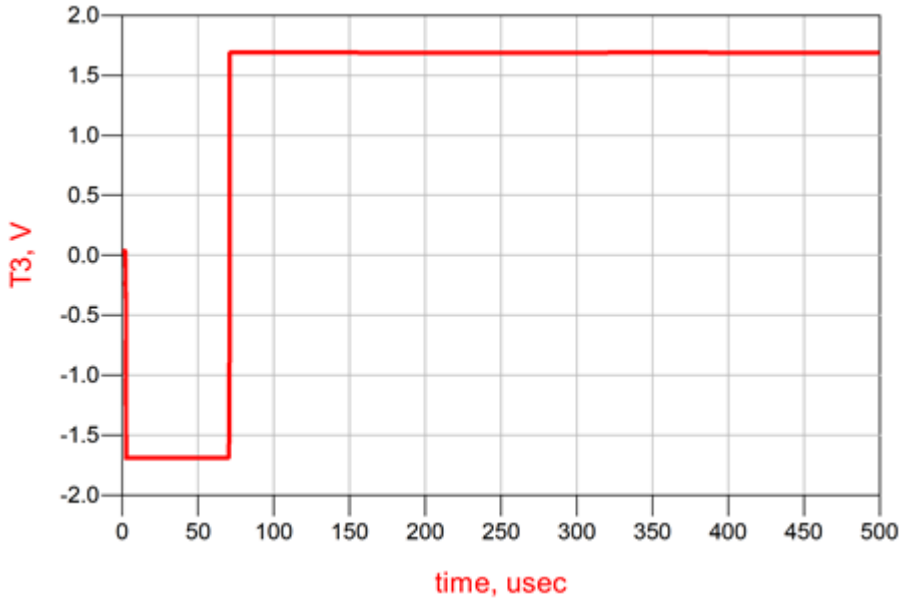

Figure 3.10: The output signal of Schmidt Trigger when $A_V(V_{DC1}$ - V_{DC2})>V_{ref}

depends on the sensitivity of the detection diodes when its used diodes. To choose these diodes, one must make a study on the sensitivities of the diodes, but also on their conversion efficiency for input signal having low power levels. In this section, we present the technique used to improve the range of WuRx, which consists on the one hand in the choice of the diodes and on the other hand the choice of the impedance matching design method.

The work done so far on the rectifier's design was essentially based on the use of L matching circuits, which limits them to operate on a narrow frequency band. The solution proposed in this section is to use a wideband, high efficiency rectifier in order to increase the communication range of such quasi-passive WuRx compared to the initial architecture [65]. Theoretically, the use of matching network with three degrees of freedom (in Pi or in T), allows obtaining a wider bandwidth. Moreover, the butterfly stub in microstrip technology allows obtaining a robust rectifier, having low variation of the electrical characteristics (central frequency and bandwidth) with

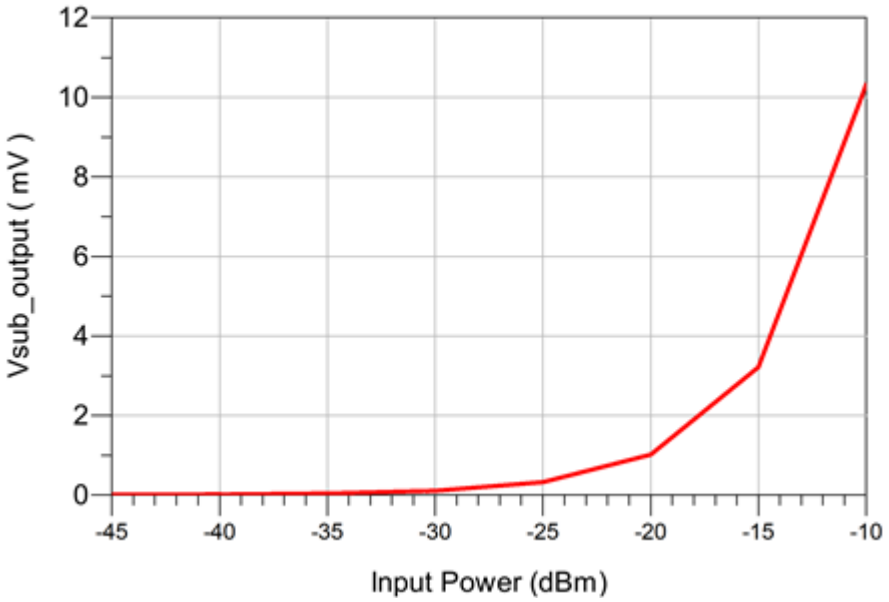

Figure 3.11: The variation of subtractor output voltage

respect to the technology dispersion.

3.3.1 HSMS 2850 vs SMS7630

Sensitivity is one of the most important parameters that characterize receivers. It depends in almost all receivers' cases, either on a low noise amplifier (LNA) placed at the input of the receiver, or on the detection diodes. In the cases using LNA, very low power RF signals above the noise floor with acceptable signal-to-noise-ratio is received and amplified. The detection diodes have capability to sense very weak power RF signals and output a power that can be processed by the receiver.

The WuRx considered here works with detection diodes system, and was originally build to operate with HSMS 2850 Schottky diode. The later component was originally used to build the quasi-passive Wake-up Radio, because of its availability off-the-shelf, but also because it presents an advantage in terms of responsivity [73] on the similar components operating in RF on low power ranges.

The choice of the diode is guided mainly by the consideration of two characteristic parameters, that are the sensitivity and the conversion efficiency. The spindiode presented in [74], of which we have retrieved the characteristics (Figure 3.12) in order to evaluate performance in WuRx, is a very highly sensitive diode but with drawback of having very low power conversion efficiency of less than 1% [75] in the range of low power input.

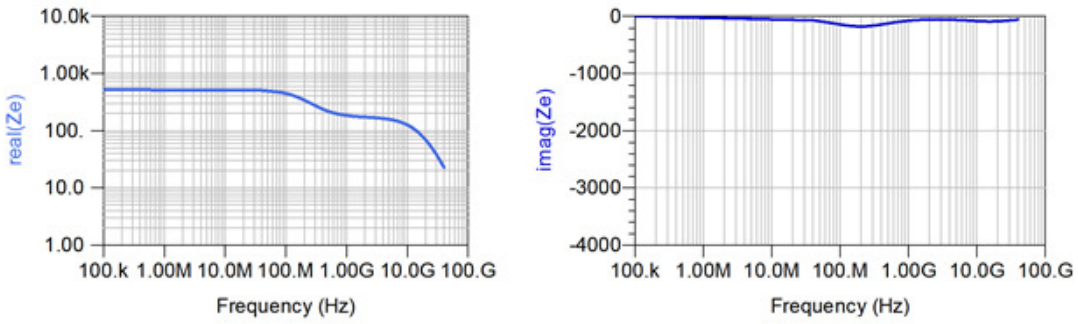

Figure 3.12: Impedance simulation (Real part and Imaginary part) of spindiode [74]

Besides a study in [73] that proved HSMS2850 to be better than HSMS2820. Here the challenge is to find a diode of better sensitivity than the later ones. Some characterization work was done on those components to provide the results presented in figures below.

Figure 3.13 shows the conversion efficiency as a function of the input RF signal strength for the HSMS2850 and SMS7630 diodes in a configuration which is matched in impedance at - 25 dB. For the input RF power ranging from - 50 dBm to - 10 dBm, we obtain an increasing conversion efficiency from 0% to a slightly less than 30% and from 0% to a slightly less than 60% respectively for HSMS2850 diodes and SMS7630.

Figure 3.14 shows the value of the output voltage as a function of the RF input power. For RF input power ranging from - 50 dBm to - 10 dBm, the DC output

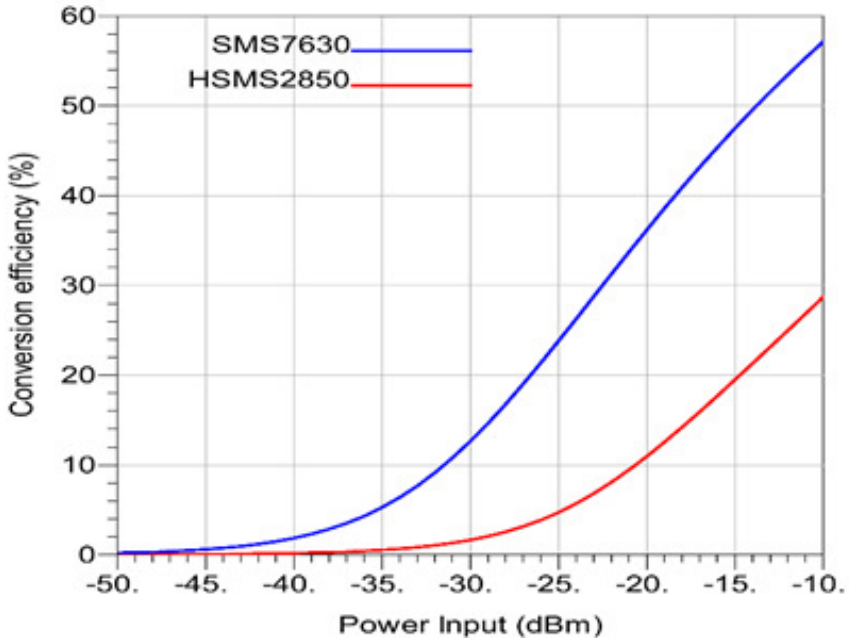

Figure 3.13: Comparison of conversion efficiency of HSMS2850 diode and SMS7630, for input RF power varying from - 50 dBm to -10 dBm

voltages vary from 0 to 300 mV and from 200 μV to 400 mV for the HSMS2850 and SMS7630 diodes respectively. From the point of view of very low RF power rectifying, this difference is significant and cannot be neglected under any circumstances.

In both cases, it may be observed the advantage of the SMS7630 diode on the HSMS2850 diode which is the one which was originally used in the quasi-passive WuRx. From this simulation results, it may be observed that the use of the Skyworks Schottky SMS7630 diode will produce better results and undoubtedly improved the overall sensitivity of the system.

Following what we have demonstrated the advantage of the SMS diode over the HSMS diode, it is now important to determine for which values of the load resistor the conversion is optimal. To do this, we have first, by using only the SMS7630 diode, varied the load resistance by measuring the efficiency for a fixed power of -30 dBm (1μW) as shown in Figure 3.15. Then we varied the RF input powers of the

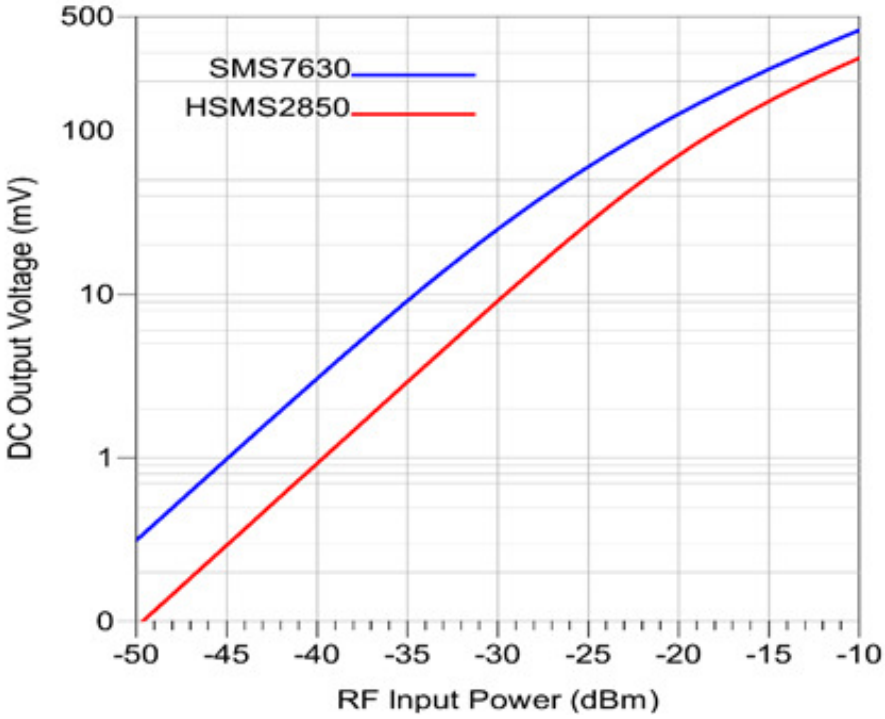

Figure 3.14: DC output voltage of SMS7630 and HSMS2850 according to input RF power.

rectifier circuit for two resistance values notably 1 KΩ and 5 KΩ while measuring the output voltages as shown in Figure 3.16. Indeed, as can be seen from Figure 3.15, the conversion efficiency of the SMS7630 based rectifiers at – 30 dBm input power is maximum for a 5 KΩ resistor. Moreover, one can remark that for various load resistance values, the rectifier based on the SMS7630 diode has better conversion efficiency compared to the rectifier based on HSMS2850, initially presented in [65]. Indeed, this conversion efficiency is 12.7 % at maximum compared to 2 % of the rectifier based on the HSMS2850. In Figure 3.16, we can see that, for two resistance values, 5 KΩ and 1 KΩ, using the SMS7630 diode, the variation of the output voltage is more important at the optimal load resistance compared to 1 KΩ. We have respectively the variations 200 μV at 400 mV and 0 μV at 200 mV.

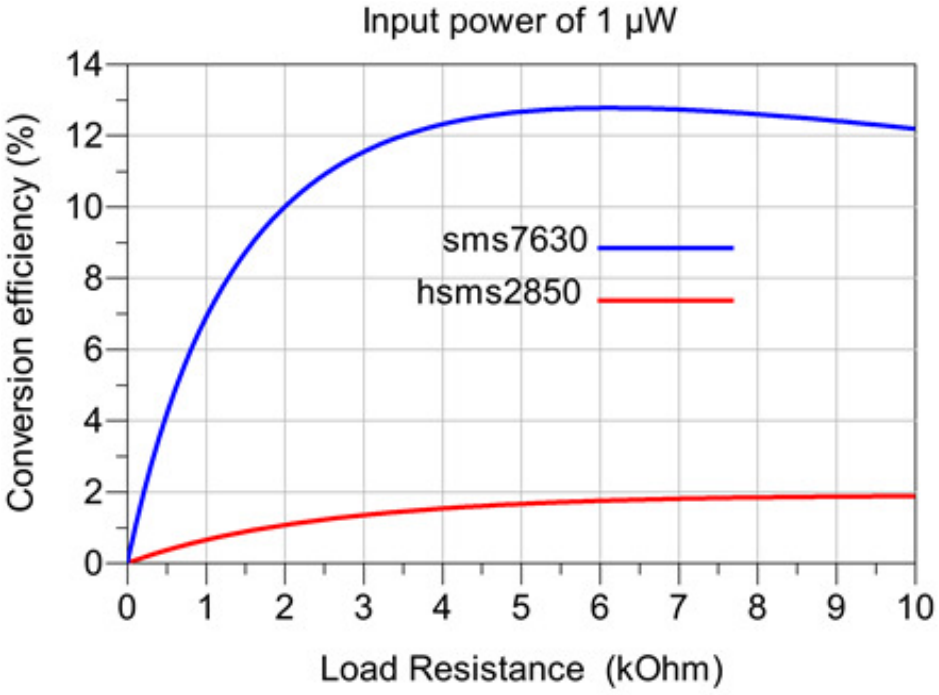

Figure 3.15: Conversion efficiency of SMS7630 and HSMS2850 when input power is 0 dBm, with varying load from 1 Ohm to 10 KΩ

3.3.2 Sensitivity Improvement

Sensitivity being defined as the smallest power value that a receiver can detect, and give an interpretation or make the difference with a noise, its improvement for a specific system requires a careful choice of components as well as a perfect adaptation of the different stages. An impedance matching network is used for optimum power transfer from one stage of a circuit to another. By definition, it is a device that will perform an impedance transformation between two RF blocks, in order to optimize the energy transfer. The common and efficient way to achieve this function is by combining passive elements, such as inductors, capacitors and transmission lines. Depending on the way these elements are layouted, a specific impedance transformation can be achieved. The choice of the most appropriate matching network

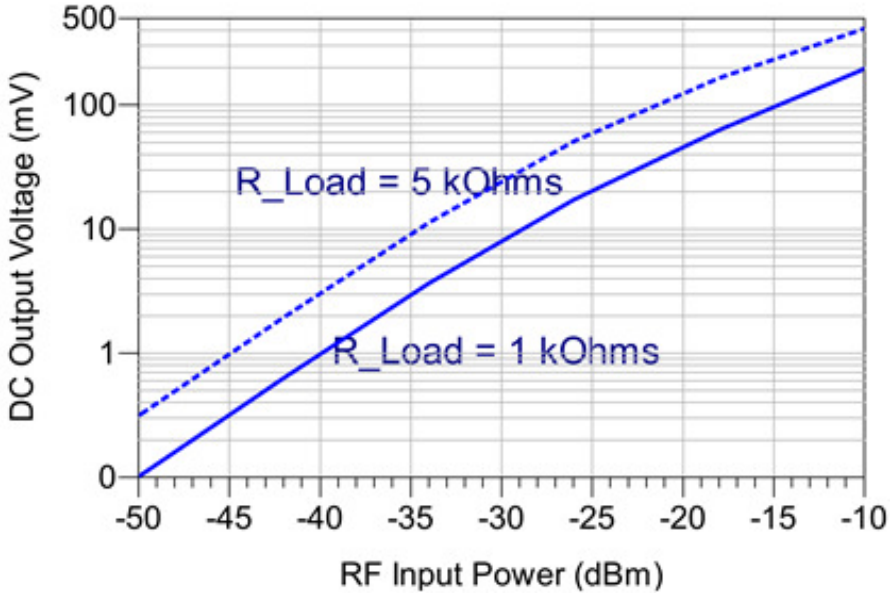

Figure 3.16: DC output voltages as function of RF input powers for load resistances 1 k Ohm and 5 k Ohm, using only SMS7630 diode

topology depends crucially on its application, the existing technology and several criteria, such as quality factor, insertion loss and space requirements. Impedance matching topologies are presented in [76], and further special arrangements are shown in Figure 3.17. Thus, we have the L topology as used in the initial circuit and presented in Figure 3.6, 2L, PI and T.

The study we did in subsection 3.3.1 allowed us to replace the HSMS2850 diode structure with an SMS7630 diode structure. While taking into consideration the bandwidth required so that the identifier signal would not be attenuated in the band, the targeted matching bandwidth is 20 MHz, corresponding to the bandwidth of the wake-up signal presented in Figure 3.4. Given the need for a wide adaptation band, we have used the Π topology, which we discuss in more details in the next chapter. As it can be seen in Figure 3.18, the rectifier is well matched from 2435 MHz to 2465 MHz, on required bandwidth (20 MHz around 2.45 GHz). Furthermore, one

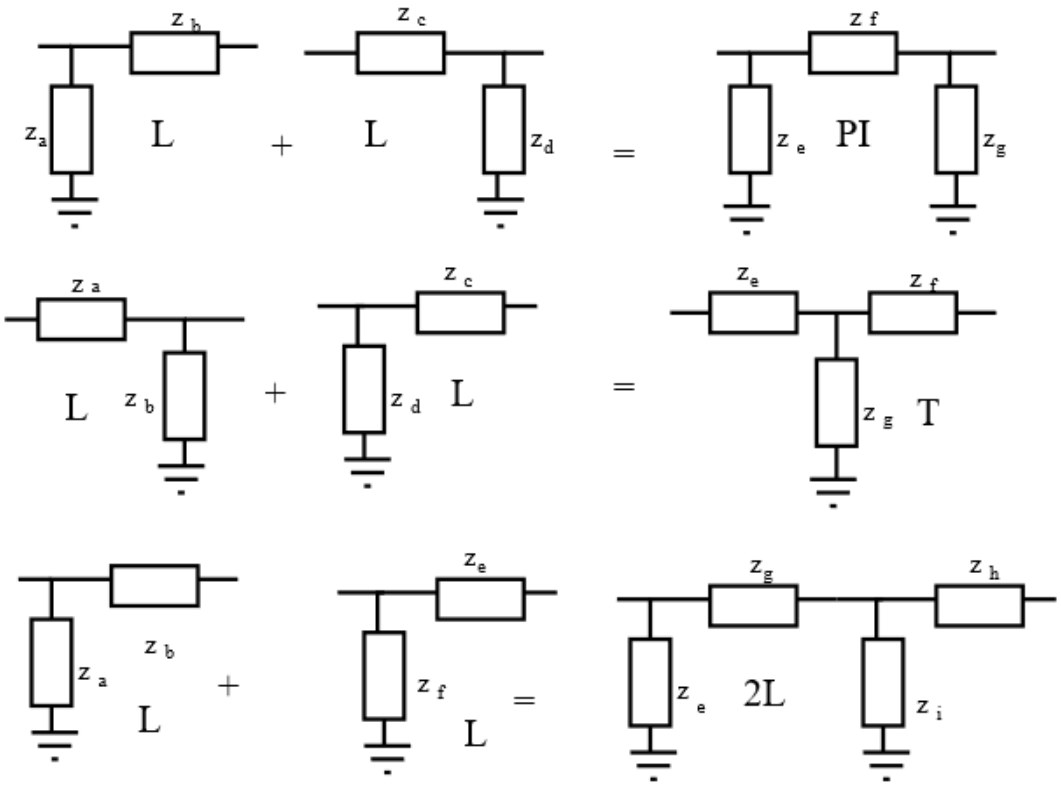

Figure 3.17: Matching Network topologies, L, T, Pi and 2L. In these topologies, Zn (with n $\in a, b, c, d, e, f, g, h, i$) represents reactive elements

can remark that the in-band ripple of the reflection coefficient is higher in the case of the SMS7630 based rectifier. However, this ripple (which create 4 dB variation between S11 min and S11 max) does not affect the wake-up radio's sensitivity.

Using the six viable identifiers in Table 3.1, we repeated under ADS the simulations of the original system, as well as the new system, which uses a new impedance matching network that covers the necessary bandwidth (20 MHz) at central frequency of 2.45 GHz, as well as the more sensitive SMS7630 diode. We obtained a gain around 5 dB for each of the identifiers as shown in Figures 3.19, 3.20, 3.21, 3.22, 3.23, 3.24. These gains for each of the identifiers induce an increase in the range, i.e. the distance between the transmitter sending a wake-up signal and the WuRx receiver. The transmitter power used for the experimental validation [77]

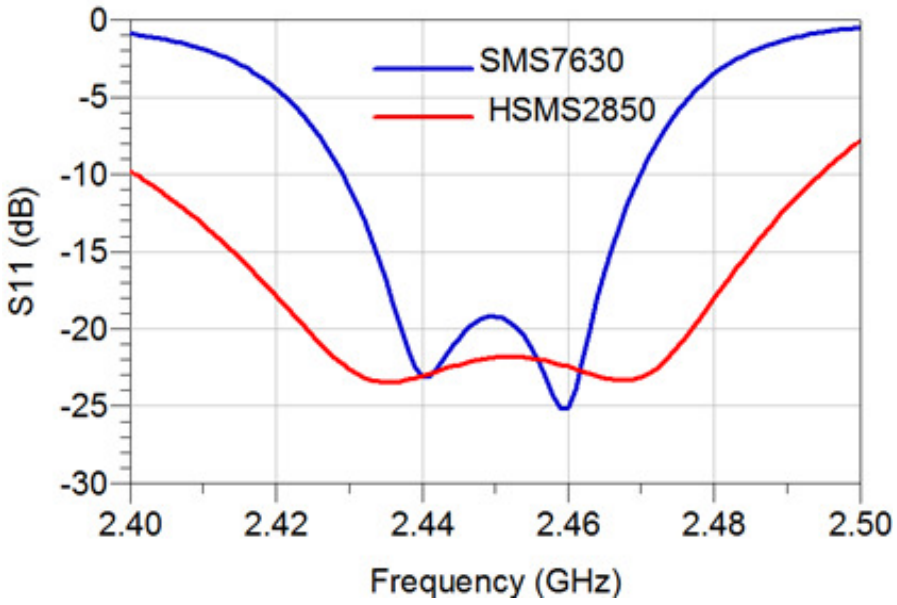

Figure 3.18: Reflection coefficient S11(dB) at the rectifier's input for HSMS2850 and SMS7630

was 20 dBm, for an initial sensitivity of -45 dBm. These two parameters enable to determine the distance between the transmitter and the receiver if a free space propagation scenario is taken into account, considering the carrier center frequency of 2.45 Ghz. The following equations are then used. These two parameters enable to determine the distance between the transmitter and the receiver in free space propagation, considering the carrier center frequency of 2.45 GHz. The following equations are then used:

$$S_R = P_E - \alpha \tag{3.8}$$

where S_R is the sensitivity of receiver

P_E : The power of the emitted signal

α: The attenuation due to propagation in free space.

$$\alpha = 20\log_{10}(4\pi df/c) = 20\log_{10}(4\pi f/c) + 20\log_{10}(d) \tag{3.9}$$

Since the carrier frequency is $f = 2.45$ GHz, $c = 3{\times}10^8$ m/s, and d the distance between emitter and receiver. We can express the attenuation as in equation (3.10).

$$\alpha = 20\log_{10}(4\pi \times 2.45{\times}10^9/3{\times}10^8) + 20\log_{10}(d) = 40.225 + 20\log_{10}(d) \quad (3.10)$$

By subtituting equation (3.10) in equation (3.8) and replacing the power of emitter by its value, we get :

$$S_R = 20dBm - 40.225dB - 20\log_{10}(d) = -20.225dBm - 20\log_{10}(d) \quad (3.11)$$

Considering the sensitivity value of - 45 dBm, we determine from equation (3.11) the distance 17.328 meters, which is the original distance [65]. If we now consider the gain obtained for each of the viable identifiers, equation (3.8) arises in a new term which is as follows:

$$S_R = P_E - \alpha + G_r \quad (3.12)$$

G_r corresponds to the gain obtained for each of the identifiers and it is summarized in Table 3.2, as well as the distance margins obtained, using equations (3.8) - (3.12) for the calculations.

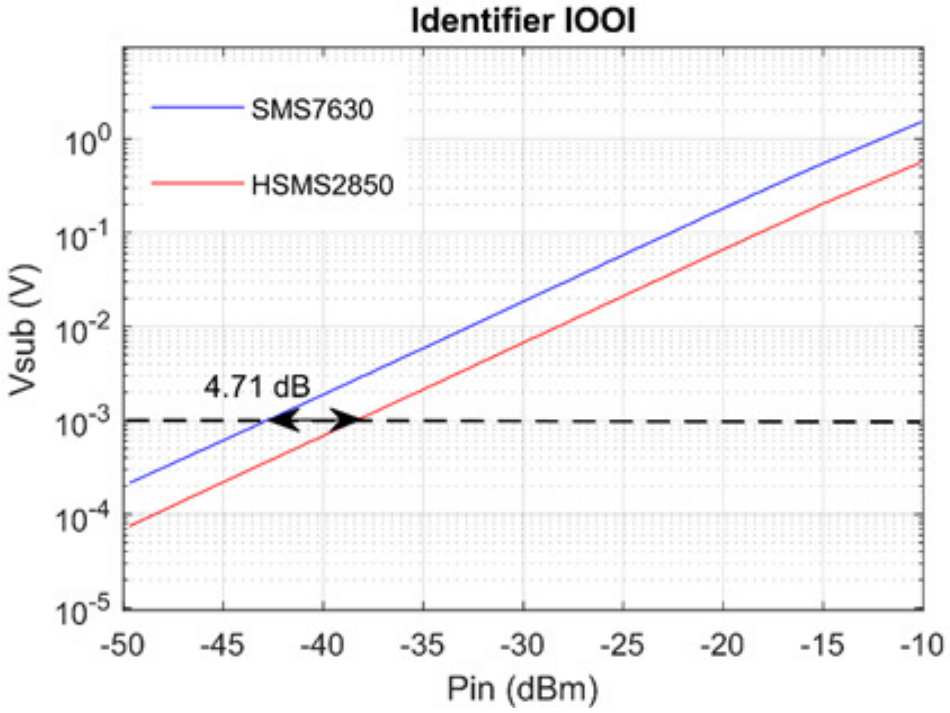

Figure 3.19: Variation of the original output voltage and the new output voltage of substractor for identifier 1001

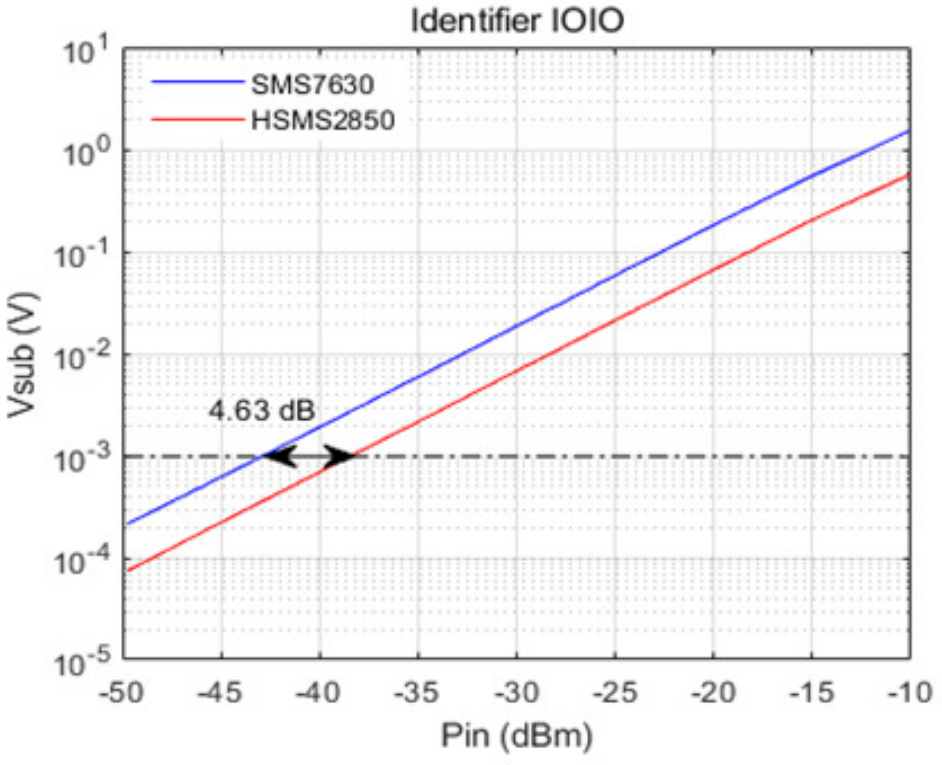

Figure 3.20: Variation of the original output voltage and the new output voltage of substractor for identifier 1010

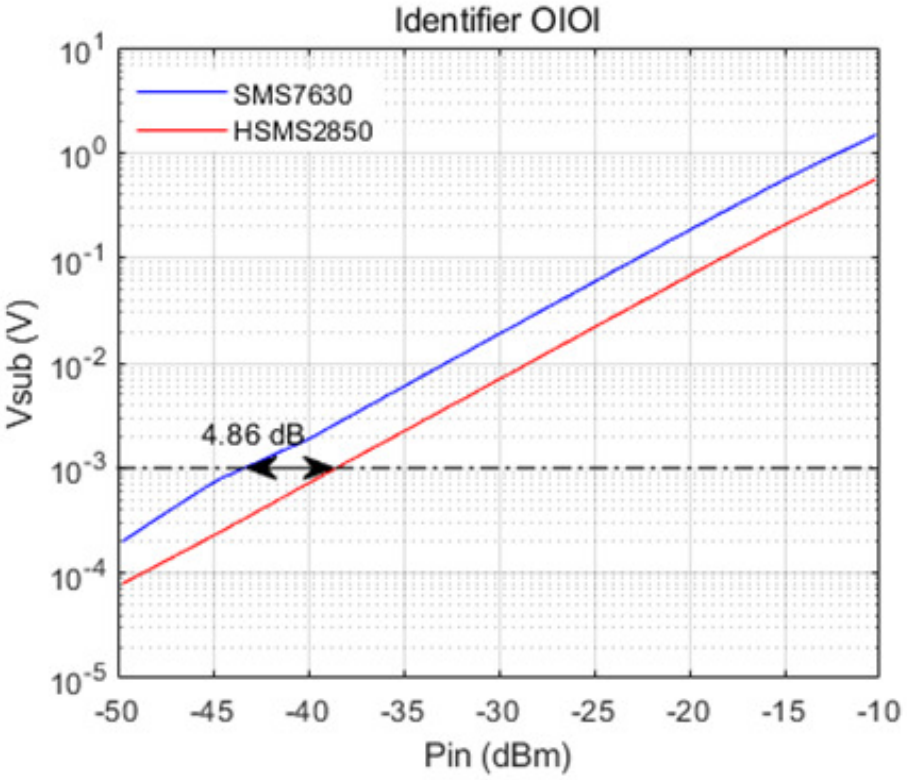

Figure 3.21: Variation of the original output voltage and the new output voltage of substractor for identifier 0101

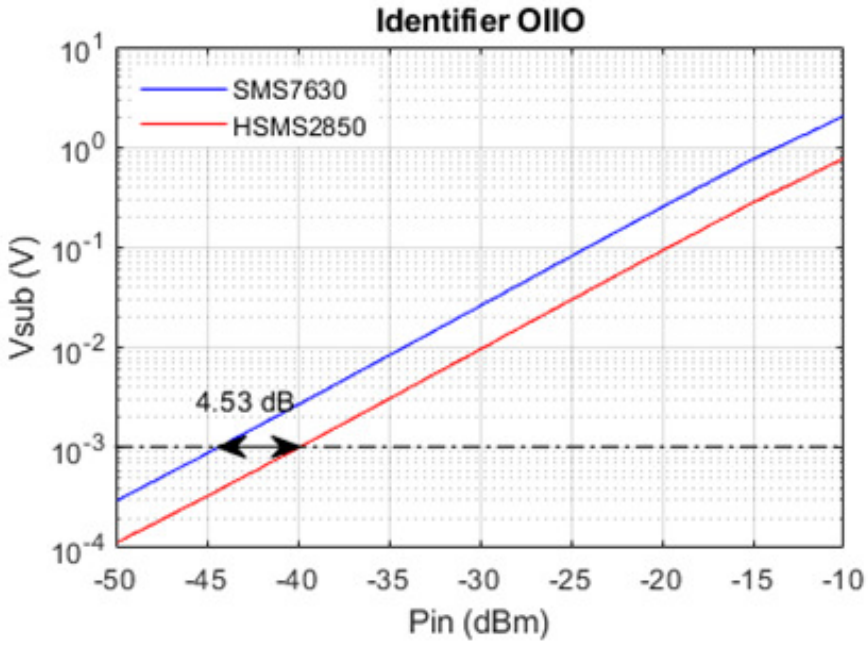

Figure 3.22: Variation of the original output voltage and the new output voltage of substractor for identifier 0110

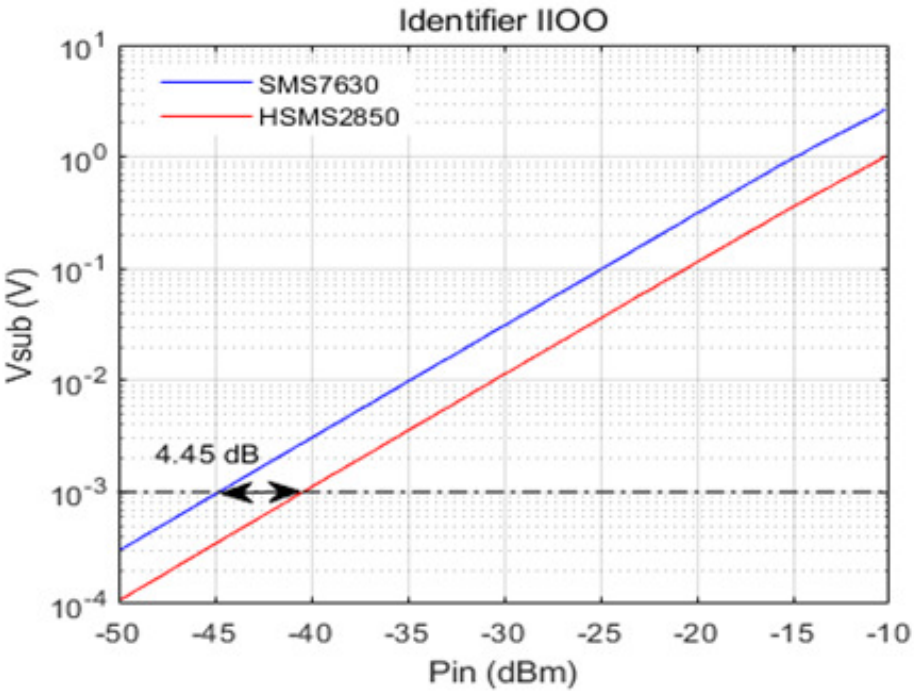

Figure 3.23: Variation of the original output voltage and the new output voltage of substractor for identifier 1100

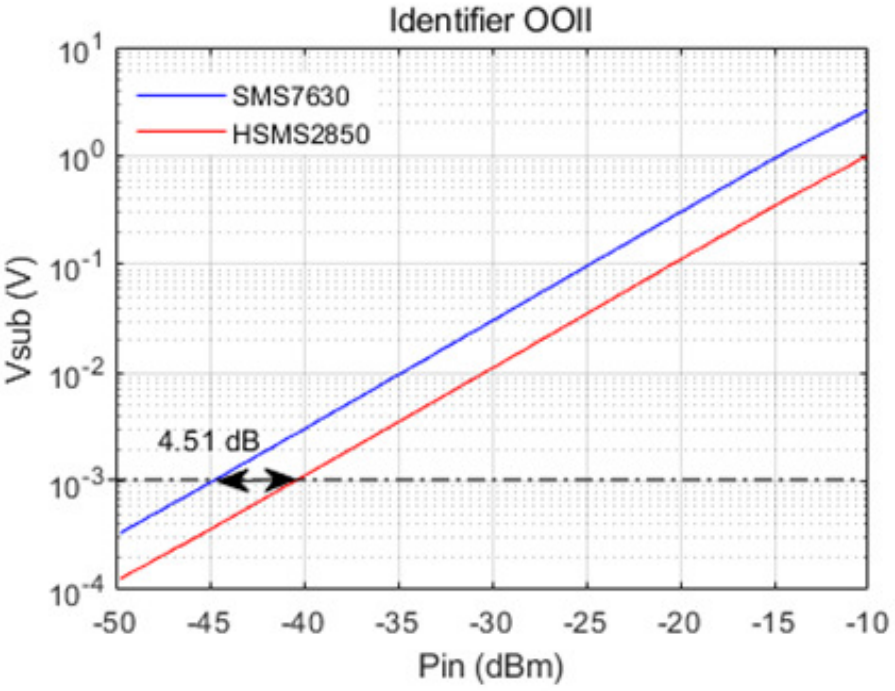

Figure 3.24: Variation of the original output voltage and the new output voltage of substractor for identifier 0011

Table 3.2: Sensitivity and communication range increase for the six viable identifiers

Identifier	Gain (G_r) [dB]	Total distance [m]	Increase in distance [m]
1001	4.71	29.802	12.47
1010	4.63	29.529	12.20
0110	4.53	29.191	11.86
0101	4.86	30.321	12.99
1100	4.45	28.923	11.59
0011	4.51	29.123	11.79

3.4 Conclusion

This chapter allowed us to present the quasi-passive WuRx as originally conceived. It is a peculiar energy saving system, which aims at an integration with wireless sensor networks as well as with the Internet of Things more widely. For most of the components in this circuit, RF identification is used instead of the microcontroller-based identification found in the literature.

Moreover, this chapter, we applied a rigorous simulation technique that allowed us to select from among the low-power RF diodes the one that offered an advantage in terms of conversion efficiency but also the determination of the optimal load. We also used a Pi impedance matching network that enables to cover a large bandwidth by minimizing power loss over this band. We have thus achieved a wideband high-efficiency rectifier to improve the communication range of a quasi-passive wake-up radio receiver. Enhancements to the rectifier have resulted in a gain of approximately 5 dB for each of the viable identifiers, which corresponds to an improvement in communication range of an average of 12 meters.

Despite the architecture that allows identification in RF (and not with a microcontroller), there are still passive circuits that must be supplied. These circuits consume little energy and it is possible, under certain conditions, to power them from the energy harvested through the ambient electromagnetic field. Thus, we will have a WuRx autonomous from the supply source of the communicating device that contains it.

Chapter 4

Design of energy harvesting circuit for autonomous wake-up radio

4.1 Introduction

The radio interface of a connected device is the part that consumes a lot of energy, even in the absence of information to be transmitted (standby mode). This causes a great waste of energy especially when there is no data exchange. It then becomes necessary to improve the efficiency of these interfaces or to find ways to put the radio front-end into a standby mode.

Ideally, the standby mode should be zero energy consumption, more precisely, exempted from the main energy source of the connected device. Since the WuRx is a very low-power consumption device, the solution of power supplying it from an energy harvesting circuit is feasible; the harvested energy in this case should be equal or greater than the required energy by WuRx for its supply. Depending on the application, several sources of energy may be considered in order to be harvested

Table 4.1: Summary of London's underground RF energy harvesting measurement campaign [pinuela13]

Bands	Frequencies (MHz)	Average power density	Maximum power S_{BA} (nW/cm^2)
DTV	470 − 610	0.89	460
GSM900 (MTx*)	880 − 915	0.45	39
GSM900 (BTx**)	925 − 960	36	1.93
GSM1800 (MTx)	1710 − 1785	0.5	20
GSM1800 (BTx)	1805 − 1880	84	6.39
3G (MTx)	1920 − 1980	0.46	66
3G (BTx)	2110 − 2170	12	240
WiFi	2400 − 2500	0.18	6

* BTX = base station transceiver; ** MTX = mobile transceiver

such as piezoelectric energy [78], wind [79], hydroelectric [80] and solar energy [81]. Moreover, from our perspective, the RF energy harvesting [82, 83] draws a particular attention.

There are several sources of ambient RF energy that may be harvested [83], namely Digital Television Broadcasting (DTV), cellular networks, or wireless local area networks (WLAN) access points. Depending on whether one is in a rural, urban or semi-urban environment, one of the sources can be dominant over the others [83]. Similarly, proximity or distance from transmitters will make a significant difference on the availability of energy of the considered source.

In Cameroon, as in other developing countries, the increasing number of mobile phone users over the last two decades has made possible the installa-

tion of a very large number of base stations, transmitting signals power on 850/900/1800/2100/2600 MHz frequencies. The power potential on some of these frequencies measured elsewhere is available in Table 4.1. This cause the omnipresence of ambient RF energy to be harvested in those frequencies.

In [84], energy harvester circuit has been designed, operating at 900 MHz. Because of the input power of 0 dBm, 450 μW power was recovered with the conversion efficiency of 45%. On another note, the experiment in [85] proves the RF efficient energy harvesting from a DTV-UHF tower situated at 4.1 km away, with the reported harvested power of 60 µW. The Effective Radiated Power (ERP) is of 960 kW, the tower operates at frequencies 674 to 680 MHz. The receiver is equipped with a 5 dBi gain antenna. The harvested power is sufficient to supply continuously a commercial thermometer/hygrometer. Another implementation [86] of DTV EH from a tower situated at 6.6 km results in the harvesting of an average 20 μW power. These examples can be extended to GSM 1800 MHz and even 3G mobile networks by considering that, the installation of the base station for mobile communication follows the same rule as for GSM network, thus leading to similar considerations.

Moreover, WLAN has become an omnipresent network in almost all working environments, thus giving the possibility to harvest RF energy. Authors in [87] shows that it is possible to harvest energy from Wi-Fi sources operating at 2.4 / 5 GHz to supply a large number of devices like low-power cameras, temperature sensors, etc. A most demonstrative implementation [88], has proved the highest conversion efficiency of 33.7 % when placed at 40 cm distance from the source, yielding to power of 76.3 μW at the output. In Table 4.2, we have gathered the operating frequency bands of RF signal sources.

Table 4.2: Some RF sources signal and frequency bands

Frequency band	Frequency range (MHz)
VHF	30 − 300
FM	87.5 − 108
UHF	300 − 3000
TV	470 − 862
GSM800	UL 824.2 − 848.8 DL 869.2 − 893.8
GSM900	UL 890 − 915 DL 935 − 960
GSM1800	UL 1710 − 1785 DL 1805 − 1880
UMTS	UL 1920 − 1980 DL 2110 − 2170
LTE	UL 791 − 821, 880 − 915, 1710 − 1785, 1920 − 1980, 2500 − 2570 DL 832 − 862, 925 − 960, 1805 − 1880, 2110 − 2170, 2620 − 2690
WiFi	2400 − 2483, 5150 − 5875
ISM	433, 915, 2450, 5800

Despite its low conversion efficiency, compared to other sources of energy (whether solar or wind which availability can be conditioned by other parameters like weather); RF energy is permanently available. It is in fact the most suitable source of energy for the applications that requires continuously supply. **The aim of this work is to couple two techniques that are Wake-up Radio (WuRx) and EH in order to optimize the energy consumption of the connected devices**. More precisely, the approach proposed here is to power supply the wake up radio by the energy collected from RF energy harvesting. For this reason, the

object to be supply has a standby mode that is independent from its main energy source. This is particularly efficient for low power devices and applications.

In some other scenarios, especially those in which the connected device is far away from the energy source, the energy collected by the harvesting circuit is not sufficient. In these particular cases, wireless power transfer solutions may be employed [89].

On the one hand, we are assisting to a decrease in terms of energy consumption of the WuRx and on the other hand to an increase in the energy harvesting circuits' efficiency. It becomes obvious that the combination of the two approaches may bring a zero-energy consumption standby mode. This work aims to use RF energy harvesting for the supply of WuRx. The coupling of Wake-up Radio and Energy Harvesting will help to make "deploy and forget" device as far as energy supply is concerned. Indeed, the energy consumption of the battery of the device will be only in the active state. Its implementation will be of great importance for Wireless Sensor Networks (WSN) and Internet of Things.

The rest of this chapter is organized as follows: Section 4.2 briefly describes the quasi-passive WuRx to be power supplied by an energy harvesting circuit. Section 4.3 presents the general considerations of the energy harvester circuits. The proposed circuit with performance improvement is presented in section 4.4. The circuit-system simulation results together with the obtained results after implementation are presented in section 4.5. Section 4.6 gives the conclusion and draws the perspectives of this work.

4.2 Quasi-passive wake-up radio power supplied by Energy Harvesting circuit

The Quasi-passive Wake-Up Radio to be power supplied is an ID-based WuRx that uses wideband multicarrier signals as the identifiers. Its architecture described in [65] includes, on one hand, the passive part made up of power divider, envelope detectors together with their impedance matching circuits and two banks of filters of which, one for the direct path and the other for the complementary path. On the other hand, the active part is composed of a voltage subtractor and a Schmidt trigger. Therefore, the energy that should be harvested will be used for the supply of the active components. An experimental validation of this WuRx was presented in [77]; the only components that require to be power supplied are the subtractor and the Schmidt trigger. Due to their low-power demands, the off-the-shelf components ISL28194 and TLV3691 were chosen to implement the wake-up radio's active part. Their respective consumption is given to be 1.65 μW and 375 nW, thus, the instantaneous consumption is 2.025 μW. Figure 4.1 is our proposition for autonomous WuRx.

4.3 Energy Harvesters: An overview and investigation

In RF energy harvesting, Schottky diodes are used rather than any other type of diodes. They have a considerable advantage over PN junction diodes in terms of switching speed. If the semiconductor is of the N-type, the dominant charges

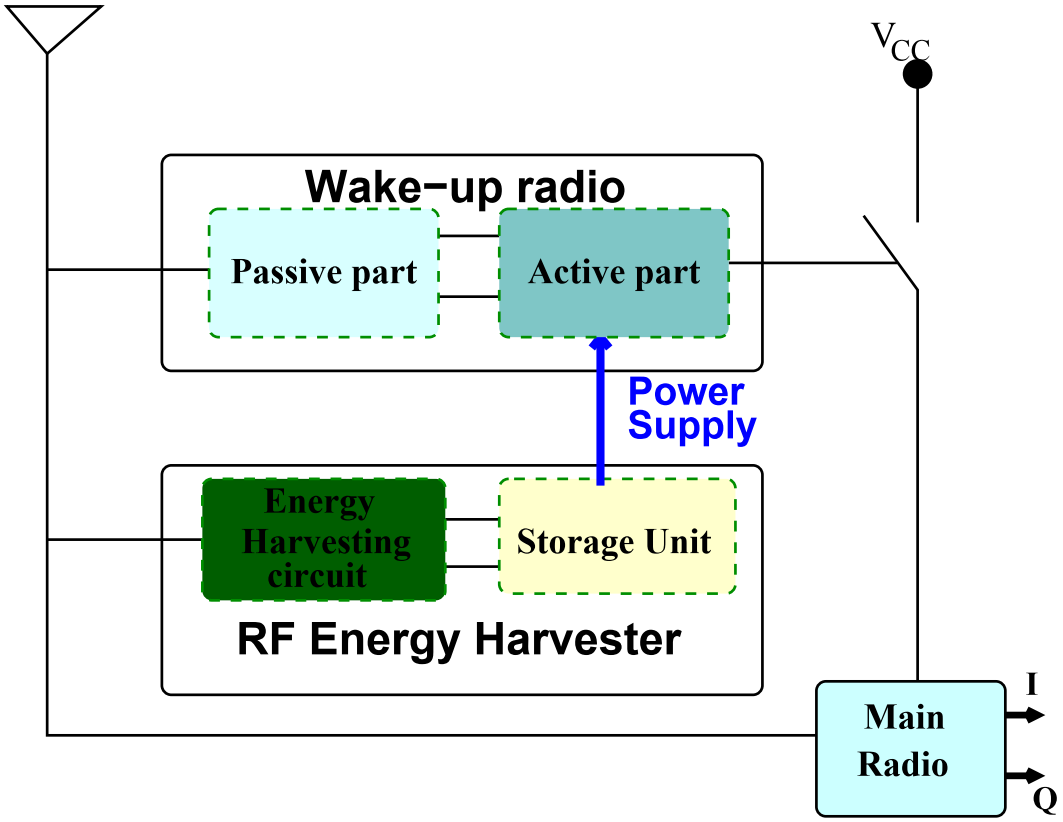

Figure 4.1: The proposed autonomous wake up radio. The active part of the wake up radio is power supplied by an RF energy harvesting circuit. The wake-up radio drives the power supply of the main radio

(electrons) are rapidly injected into the conduction band of the metal contact and become free electrons. There is no slow recombination process of the n- and p+ charge carriers, as in the case of PN diodes, which results in a reduced switching time. This time is essentially dependent on the junction capacitance. It is of the order of a few hundred picoseconds for small signal diodes [74], compared to a few hundred nanoseconds for PN diodes. This makes Schottky diodes ubiquitous in RF detectors as well as in mixers, where they can operate at frequencies up to several tenths of GHz.

At the same time, Schottky diodes have very low series resistance compared to that of the PN ones, offering the advantage of lower threshold voltages than their PN counterparts. These features are advantages in power rectification applications because the losses in the diodes will be reduced.

The diode threshold voltage plays an important role in RF-DC conversion efficiency because the amplitude of the incident signal is often lower than the diode threshold voltage. High operating frequencies require fast rectification devices. The characteristics of the Schottky diodes are the ones recommended for use in RF-DC rectification circuits.

4.3.1 State of the art of the RF harvesting circuit

In this subsection, some of the most recent and important related works will be presented on the subject with their characteristics; we must not lose sight of the fact that the ultimate aim of these circuits is to harvest radio energy for a contribution to the energy consumption of various systems. To the best of our knowledge, the harvesting of radio energy as it stands today really began in 2005 with the work

presented in [90]. In this pioneering work, a series of 4 passive antennas made of transmission lines (Engraved on the FR4 PCB) interlaced in a square spiral was used. Each of the antenna was matched in impedance with a rectifier using a dual-diode bridge HSMS2820. The interlacing of antennas in that work aimed at collecting the maximum of energy on a physical surface different from the effective surface of an antenna at the considered frequency (915 MHz). The result obtained was a power of 80 milliwatts harvested at a distance from 20 cm from a 5 W emission.

The most commonly used radio frequency energy harvesting circuits are essentially the one listed in Table 4.3. These are the series, shunt, voltage doubler, Dickson, Greinacher and Cockcroft-Walton topologies. These different topologies are employed in the design of rectifiers that operate in several frequency bands as can be seen in Table 4.3. These topologies that are represented in the following section and will be used later as case studies for the demonstration. The Cockcroft-Walton topology is not used in the next steps and will not be depicted since it is a multiple diode version of the voltage doubler topology. It is clear that most of the works presented here are recent and use almost the same diodes as those we have chosen for our study.

4.3.2 Parameters of RF/DC converter

a. Overview of small-signal diode parameters

The block diagram of a common RF energy harvester is presented in Figure 4.2. It is made up of an antenna, an input HF filter which is used for impedance matching between the antenna and the rectifier, the rectifier's diode plus parallel capacitor, the storage unit to store the harvested energy and load to be supplied. Depending

Table 4.3: Characteristics of some recent energy harvesting circuits

Reference	Year	Frequency (GHz)	Max. eff. [%] / Inp. Pwr.[dBm]	Topology	Diode	Subtrate	Load (kOhm)
[91]	2020	2.2	50% / 0 dBm	Series	SMS7621	RO5880	0.2
[92]	2020	0.9 / 1.8 / 2.45	52%, 50%, 46.5% / 0 dBm	Series	HSMS2852	FR4	3.8
[93]	2020	2.4	69.3% / 5.5 dBm	Voltage doubler	SMS7630	RO4003C	2
[94]	2020	2.4 / 5.2	63.38%, 65.4% / 13 dBm	Series	HSMS2860	FR4	0.15
[95]	2020	5.8	81% / 15 dBm	Shunt	HSMS286F	RO4350B	0.45
[96]	2019	5.8	66% / 20 dBm	Shunt	HSMS2860	F4B	0.12
[97]	2019	1.4	74.8% / 10 dBm	Voltage doubler	SMS7630	FR4	1
[98]	2019	2.4 / 5.8	63%, 54.8% / 12.3 dBm	Series	HSMS2860	FR4	0.6
[99]	2019	0.9 / 1.8	57.5%, 52.6% / − 5 dBm	Series	HSMS2850	RO5880	7
[100]	2019	0.920	24% / − 4 dBm	Dickson	SMS7630	FR4	0.050
[101]	2018	2.45	17% / 0 dBm	Greinacher	HSMS2862	Textile	10
[102]	2018	1.1 − 1.35	63% / 10 dBm	Voltage doubler	SMS7630	FR4	2
[103]	2018	2.45	68% / 5 dBm	Cockcroft-Walton	HSMS2850	FR4	5
[104]	2018	2.5	69 % / 3.5 dBm	Voltage doubler	HSMS2850	RO3003	1
[105]	2018	2.45	27 % / 10 dBm	Shunt	HSMS2850	RO350B	0.68
[106]	2018	0.9 / 1.8	20.2%, 22.59% / − 11.8 dBm	Greinacher	—	CMOS	70
[107]	2017	0.93	12.6 % / − 15.4 dBm	Dickson	—	CMOS	0.50
[108]	2017	2.45 / 5.8	57.1 %, 39.2% / − 0 dBm	Voltage doubler	SMS7630	RO5880	5
[109]	2017	2.45	57 % / 0 dBm	Shunt	SMS7630	RO3203	2.47
[110]	2017	2.45	37 % / 0 dBm	Voltage doubler	SMS7630	FR4	2.4

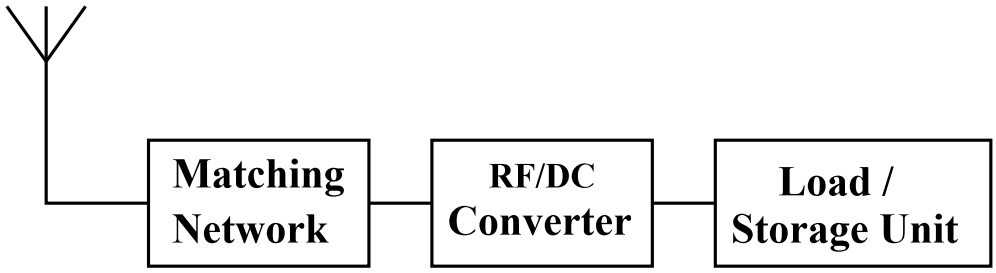

Figure 4.2: Block diagram of an RF energy harvester

on the application, the storage unit may be a battery or a super-capacitor.

In general, the energy harvester has the role of transforming the power contained in electromagnetic waves available at its input, into a DC voltage susceptible to energize the load (the WuRx's active part in our case). It is mainly characterized by its conversion efficiency η given by the following expression:

$$\eta[\%] = \frac{P_{DC}}{P_{RF}} \cdot 100 \tag{4.1}$$

where P_{DC} is the DC power at the output of the storage unit and P_{RF} is the instantaneous power at the input of the matching circuit.

In RF energy harvesting, Schottky diodes are used rather than any other types of diode. The small-signal model is presented in Figure 4.3 and the electrical parameters of some common Schottky diodes are listed in Table 4.4.

Table 4.4: Parameters of some commonly used Schottky diodes

Diodes	HSMS2820	HSMS2850	HSMS2860	SMS7630
R_S (Ω)	6	25	6	20
C_{j0} (pF)	0.7	0.18	0.18	0.14
V_j (V)	0.65	0.35	0.65	0.34

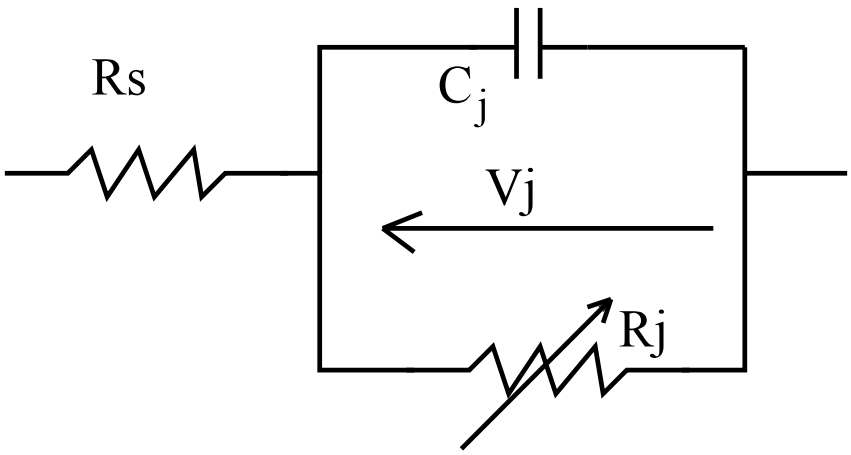

Figure 4.3: Small signal model of Schottky diode

In the equivalent model depicted in Figure 4.3, R_S represents the series resistance, C_j and R_j are respectively the junction capacitance and the junction resistance. The junction capacitance C_j is given by:

$$C_j = C_{j0}\sqrt{\frac{V_j}{(V_j + V_{DC})}} \tag{4.2}$$

where C_{j0} is zero bias diode's junction capacitance, V_{DC} is the output voltage across the load resistance and V_j is the voltage across the semi-conductor metal junction.

The junction resistance R_j is variable and depends on the externally applied bias current I_b, on the saturation current I_s, on the ideality factor n, and on temperature T. It is expressed as:

$$R_j = \frac{8.33 \times 10^5 \cdot n \cdot T}{Ib + Is} \tag{4.3}$$

These parameters are impacting the rectifier's overall efficiency. More globally, the overall efficiency depends on the amount of RF power at the diode level and the amount of power delivered to the load (4.1).

b. The efficiency of circuit

As explained in [74], the global efficiency of the circuit takes into account the matching efficiency η_M, the conversion efficiency η_{RF-DC} and transfer efficiency from the diode's output to the load $\eta_{DC-Load}$. It can be express as:

$$\eta = \eta_M \cdot \eta_{RF-DC} \cdot \eta_{DC-Load} \tag{4.4}$$

The matching efficiency η_M depends on the reflection coefficient (4.5). Minimizing this reflection coefficient, especially at low power levels, leads to an increase in matching efficiency.

$$\Gamma_0 = \frac{Z_D - Z_S}{Z_D + Z_S} \tag{4.5}$$

here Z_S is the source internal impedance. In our case, it corresponds to the rectifier's antenna impedance. Z_D is the RF/DC's impedance at the considered frequency. Depending on the internal parameters of diodes presented in Figure 4.3, we can give the following expression [105]:

$$|\Gamma_0|^2 = \frac{\left[R_j + (R_S - 50)\left(R_j^2 C_j^2 \omega^2 + 1\right)\right]^2 + R_j^4 C_j^2 \omega^2}{\left[R_j + (R_S + 50)\left(R_j^2 C_j^2 \omega^2 + 1\right)\right]^2 + R_j^4 C_j^2 \omega^2} \tag{4.6}$$

Some practical considerations are done to simplify the previous equation. Since the frequency is high (2.4 GHz in this case), here we consider $\omega = 2\pi f = \infty$. This lead to the approximation of reflection coefficient to:

$$|\Gamma_0| = \frac{R_j + (R_S - 50)}{R_j + (R_S + 50)} \tag{4.7}$$

Having the reflection coefficient defined in equation (4.7), the matching efficiency

will be given by:

$$\eta_M = \left(1 - |\Gamma_0|^2\right) \tag{4.8}$$

As shown in [111] that the RF/DC's conversion efficiency η_{RF-DC} is defined by :

$$\eta_{RF-DC} = \frac{1}{1 + A + B + C} \tag{4.9}$$

$$\begin{cases} A = \dfrac{R_L}{\pi R_S}\left(1 + \dfrac{V_j}{V_{DC}}\right)^2 \left[\theta\left(1 + \dfrac{1}{2\cos^2(\theta)}\right) - 1.5\tan\theta\right] \\ \\ B = \dfrac{R_S R_L C_j^2 \omega^2}{2\pi}\left(1 + \dfrac{V_j}{V_{DC}}\right)\left(\dfrac{\pi - \theta}{\cos^2\theta} + \tan\theta\right) \\ \\ C = \dfrac{R_L}{\pi R_S}\left(1 + \dfrac{V_j}{V_{DC}}\right)\left(\dfrac{V_j}{V_{DC}}\right)(\tan\theta - \theta) \end{cases} \tag{4.10}$$

where θ is a dynamic variable which depends on the input RF power, also called forward bias turn-on angle. The resistance R_L models the rectifier's load. It corresponds to the input impedance of the storage unit. The DC power transfer to storage unit efficiency, from rectifier circuit $\eta_{DC-Load}$ is expressed as :

$$\eta_{DC-Load} = \frac{1}{1 + \frac{R_T}{R_{Load}}} \tag{4.11}$$

Where R_T is the Thevenin equivalent resistance seen by the load.

The rectifier's antenna surface plays an important role in the amount of power collected by the energy harvester. Indeed, one simple model is to consider the free space transmission. In this case, the RF power received by the antenna may be expressed by:

$$P_{RF} = \frac{P_t G_t A_{eff}}{4\pi r^2} \tag{4.12}$$

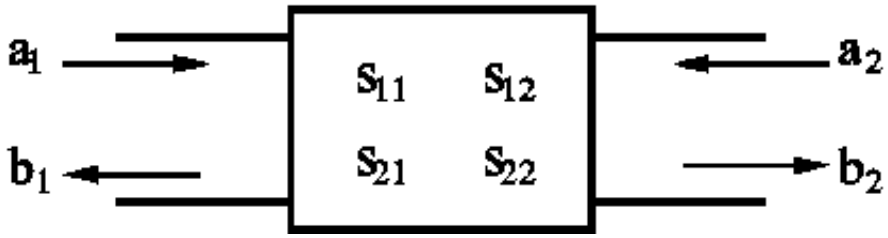

Figure 4.4: Diagram of a two port network

Where: P_{RF}: RF power level at the antenna's input

P_t: power radiated by the transmitter

G_t: gain of transmitting antenna

A_{eff}: antenna's effective aperture

r: distance between the transmitting and the receiving antennas

The effective area of the antenna can be computed if the typical case [89] of 4 dBi gain and a frequency of 2.45 GHz are considered:

$$A_{eff} = \frac{G\lambda^2}{4\pi} \tag{4.13}$$

Where λ: is the wavelength (m), G is the linear gain of the antenna.

c. S-Parameters

Most of the microwave circuits deal with power quantities rather than current and voltage quantities; the reasons are that circuits in high frequencies is generally based on power transfer from one stage to the next one, and the current and voltage measurement are proving very difficult in RF whereas that of power is easier [112]. Consequently, microwave theory models devices, circuits and systems through parameters that can be obtained through quantities of power.

In the case of linear circuit elements or elements that are non-linear but operate

with small signals in such a way that they can be considered linear, a system or network can be characterized only through parameters measured at the input and output ports of the system, without having to bother about the exact content of the system. Once these parameters have been determined, it is possible to predict the exact behaviour of this system at any external stimulation, once more, without having to know its structure.

S-parameter simulation is a small-signal simulation most often used to characterize passive RF components or to determine the small signal characteristics of a device in precise polarization or temperature conditions. The non-linear components are therefore linearized around of the operating point. The resulting linear circuit is analyzed as a multi-port network. Each port is sequentially stimulated by small signals and the response is measured and transformed into S-parameters. Figure 4.4 shows the representation of different power waves getting in or coming out from a quadripole, with:

a_1 : power wave entering Port 1;

b_1 : power wave leaving Port 1;

a_2 : power wave entering Port 2;

b_2 : power wave out of Port 2.

The S parameter element's for such a system are related to power wave as:

$$b_1 = a_1 S_{11} + a_2 S_{12} \tag{4.14}$$

$$b_2 = a_1 S_{21} + a_2 S_{22} \tag{4.15}$$

In these relationships, the S_{ij} terms represent :

S_{11} : reflection coefficient of Port 1;

S_{22} : reflection coefficient of Port 2;

S_{21} : transmission coefficient from 1 to 2;

S_{12} : transmission coefficient from 2 to 1.

The S parameters are defined with respect to a characteristic impedance which is usually 50Ω. They are given by:

$$S_{11} = \frac{b_1}{a_1}|_{a_2=0} \tag{4.16}$$

$$S_{12} = \frac{b_1}{a_2}|_{a_1=0} \tag{4.17}$$

$$S_{21} = \frac{b_2}{a_1}|_{a_2=0} \tag{4.18}$$

$$S_{22} = \frac{b_2}{a_2}|_{a_1=0} \tag{4.19}$$

When $a_2 = 0$, the quadripole is said to be matched at the output; if $a_1 = 0$, then the quadripole is matched at the input. Each of the S-parameters are computing while the quadripole is matched either at the input or at the output.

4.3.3 RF energy harvesting circuit topologies

Radio frequency energy harvesting circuits are usually designed around four functional blocks. The antenna, which represents the source to be placed at the input of the circuit, the impedance matching network that allows the source to transmit the maximum power to the next block, the rectifier block which is the rectification block in the strict sense, and then the load. The rectifier includes a capacitor and is followed by the last block which is the load for which the DC power

from the rectifier is intended.

Figure 4.4 presents the various topologies of circuits used for radio frequency energy harvesting.

4.3.4 Survey of energy harvesting topologies and data analysis

This survey is conducted by simulation where a feasible impedance matching of $S_{11} = -25dB$ at an input power of - 30 dBm was chosen as shown in Figure 4.5. For all the five structures submitted to study, the matching network is just after the source for both families of HSMS and SMS diodes. The choice of the HSMS 2850 diode is guided by a study carried out in [73], which shows that it offers an advantage over many other RF diodes and is commonly used for RF applications. The SMS 7630 diode is chosen because it is almost ubiquitous in rectifiers, as shown in the study we present in the Table 4.3. Furthermore, in [113], it was shown that for the specific case of the rectifier using the diode in series, the SMS 7630 diode was better than the HSMS 2850 diode. For these reasons, three diodes that are HSMS2850, HSMS2860 and SMS7630 will be used for the survey study.

In Figure 4.5 simulation results of the conversion efficiency of the five topologies mentioned above are presented. In order to achieve this, each topology was constructed using the three most commonly used diode types mentioned above.

As can be seen, this study was carried out on the power band from – 30 dBm to 30 dBm, corresponding to the power range from 1 microwatt to 1 Watt. This power band is the same one in which can be found the radiated energy in the case of wireless power transfer, and the ambient RF Energy. The result obtained on each graph was

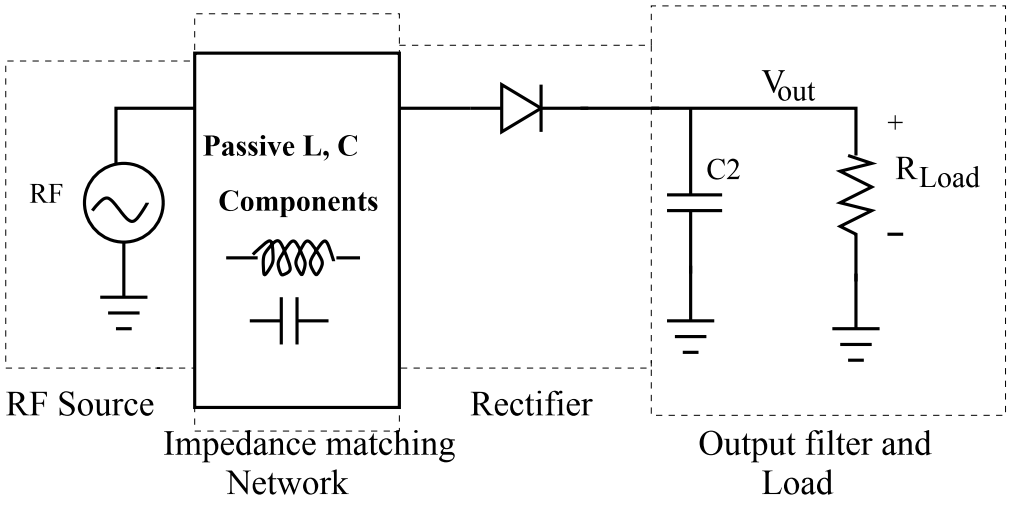

(a) Series topology

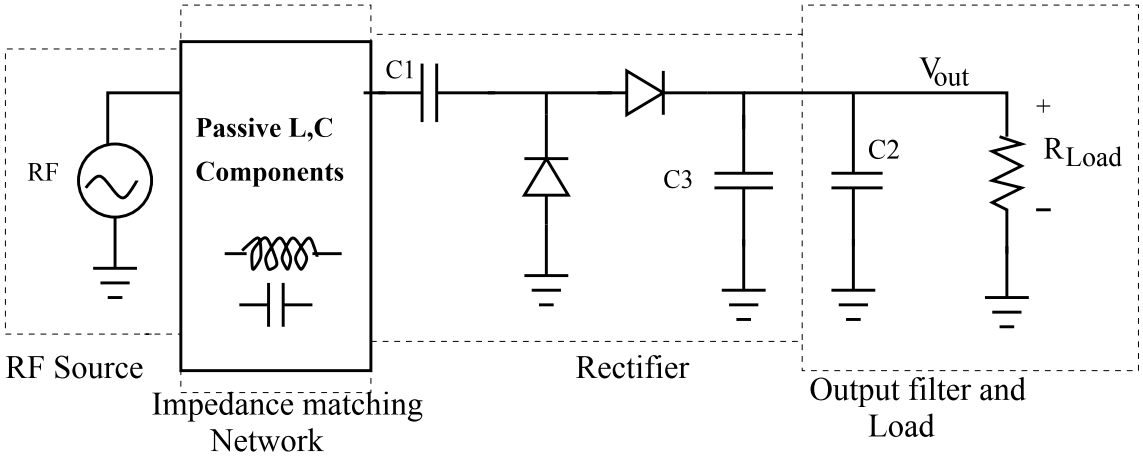

(b) Voltage doubler topology

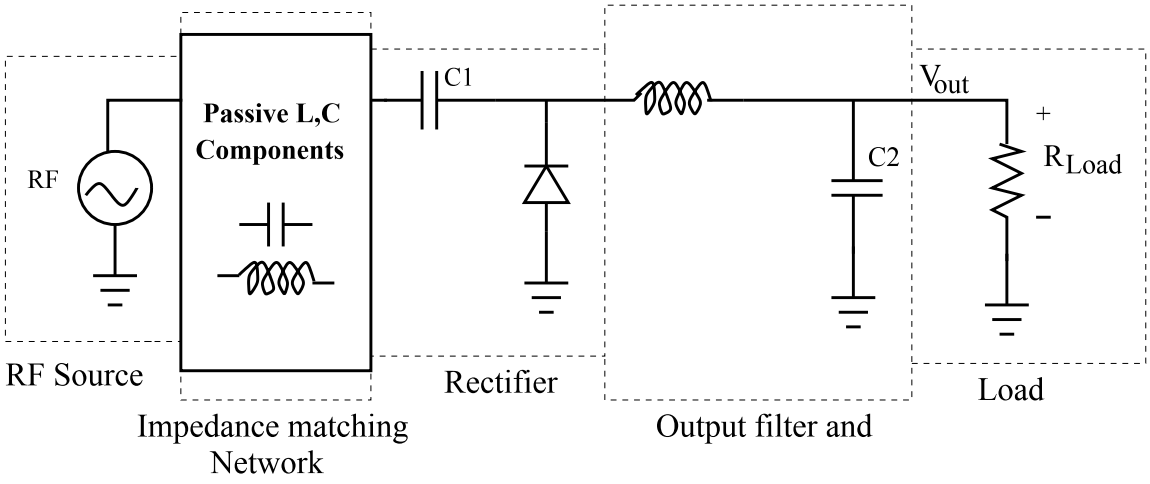

(c) Shunt topology

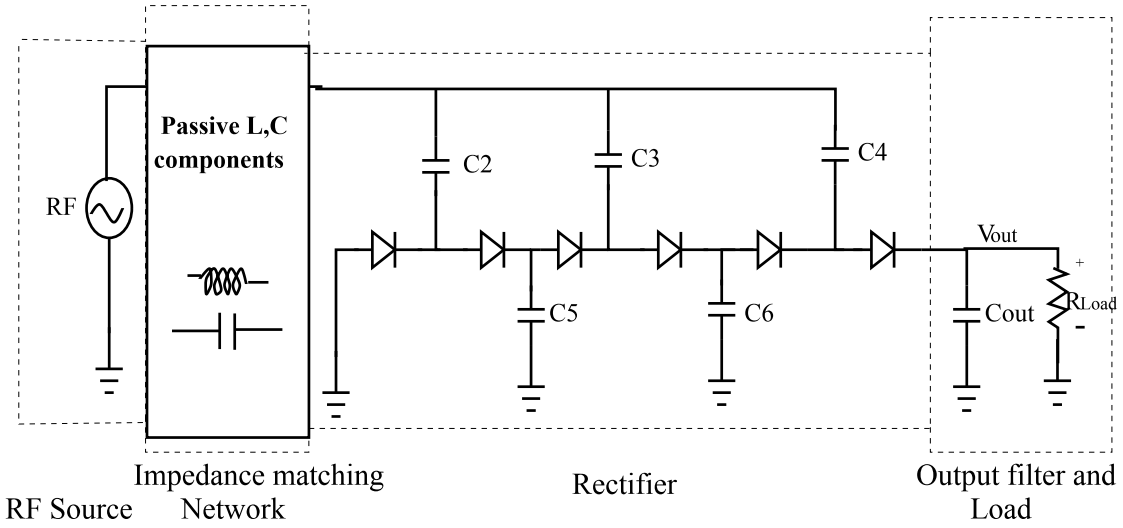

(d) Dickson topology

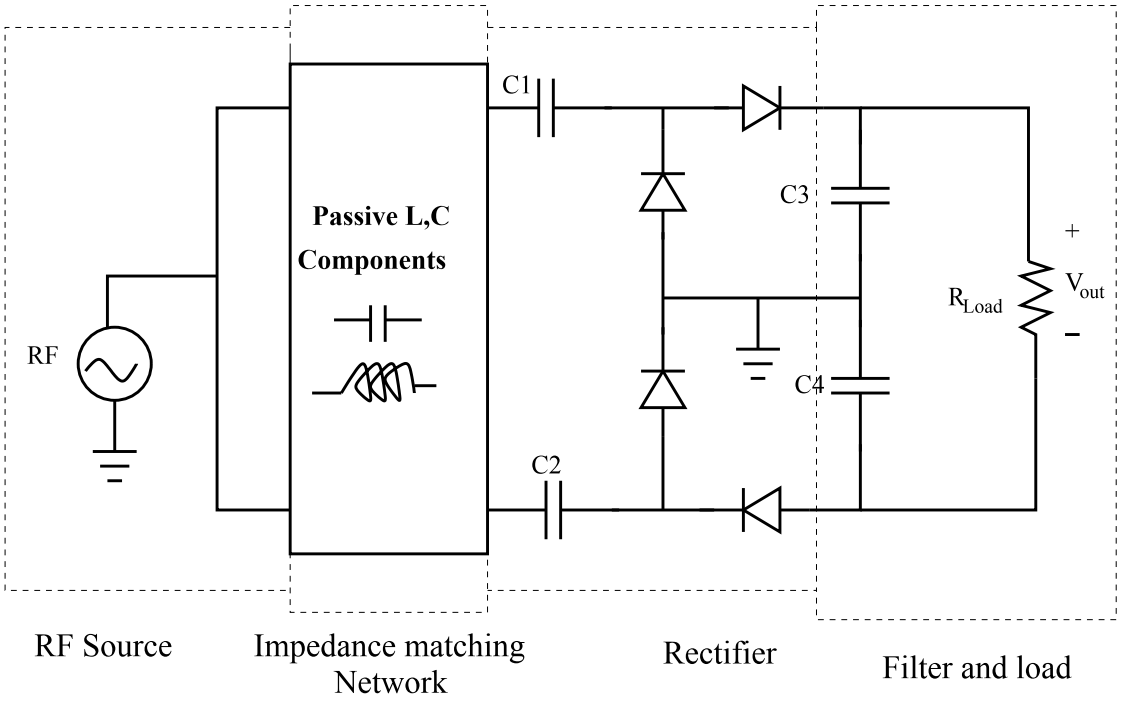

(e) Greinacher topology

Figure 4.4: Topologies of circuits used for radio frequency energy harvesting

done by optimizing the load resistance (Figure 4.5) using the "Optimization tool" of the Keysight's ADS software. In the above cases, the working frequency is 2.45 GHz and all the results are summarized in Table 4.5. In the same table, a summary

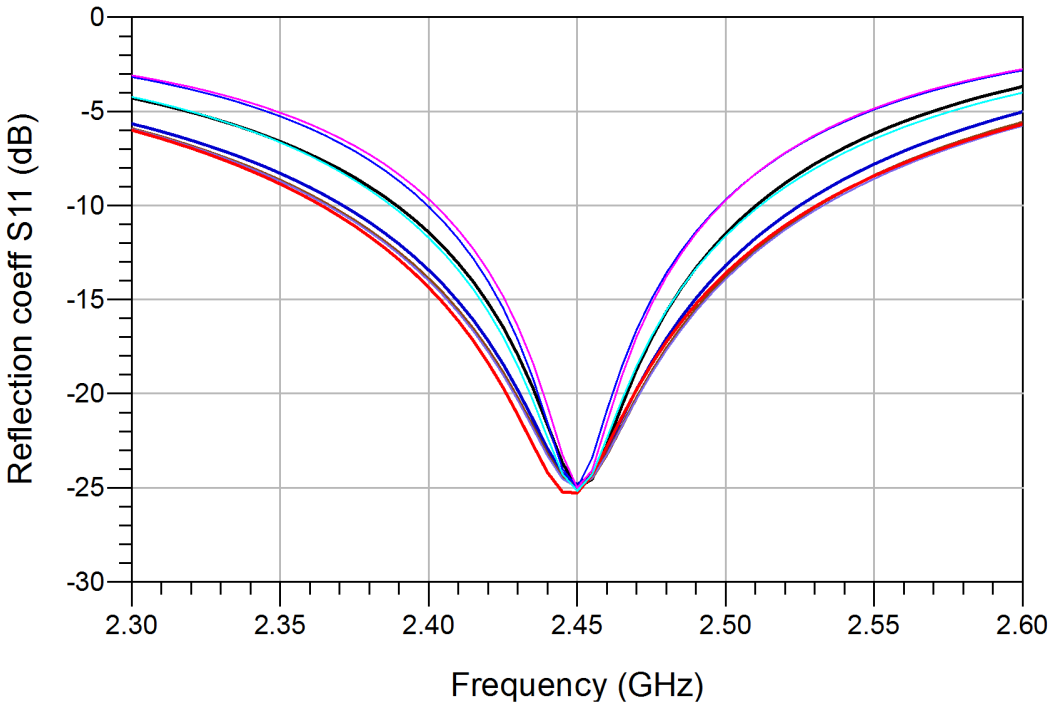

Figure 4.5: Reflection coefficient of all the rectifier topologies in simulation at frequency 2.45 GHz with input power - 30 dBm

of the simulation results of the different topologies with the optimized load values for each case is also presented. By varying the input power from – 30 dBm to 30 dBm, we determine the power of maximum efficiency.

A simple analysis shows that Dickson diode structure HSMS2860 which has an efficiency of 85.71 % at 25 dBm input power is the best structure for RF energy harvesting. If, on the contrary, we are in an environment where the power that arrives at the antenna is very low, around - 4 dBm, then the SMS7630 diode series topology, which reaches its maximum efficiency at 66.66 %, is the best. At this power (– 4 dBm), the Dickson topology has an efficiency of only 34 %.

As shown in this same Table 4.5, there is a wide range of loads to be placed at the output of the rectifier circuit to achieve maximum efficiency. These loads are varying depending on the topology and the diode used, from a few tens of ohms to

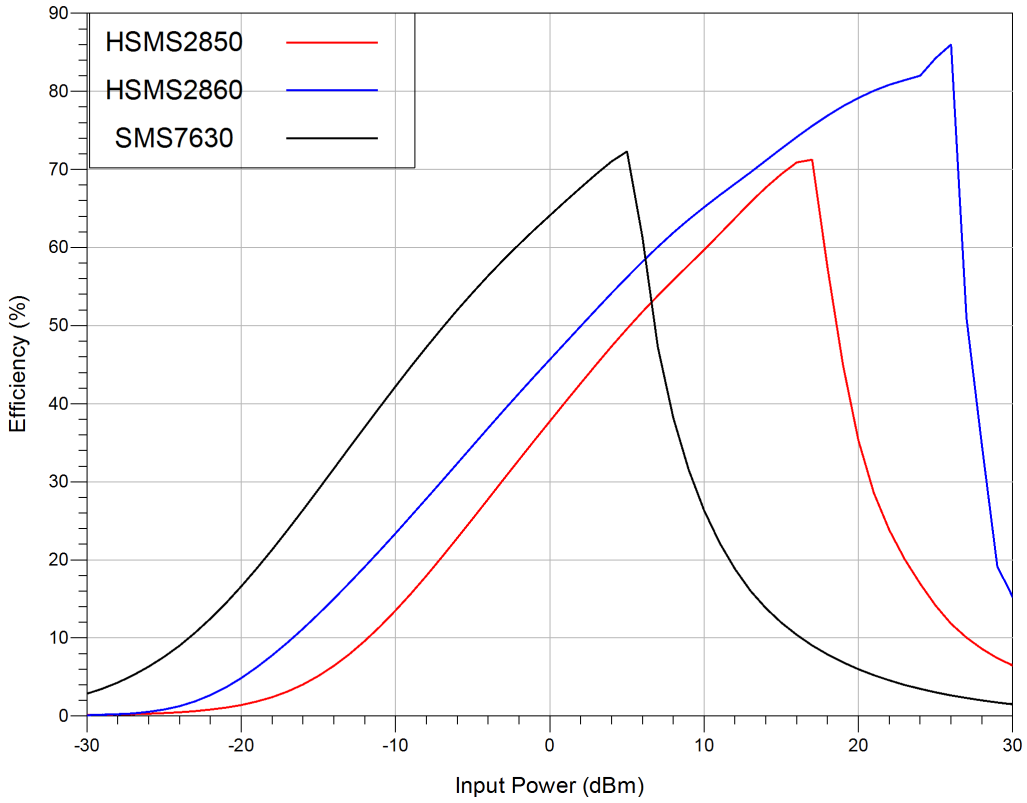

(a) Dickson topology

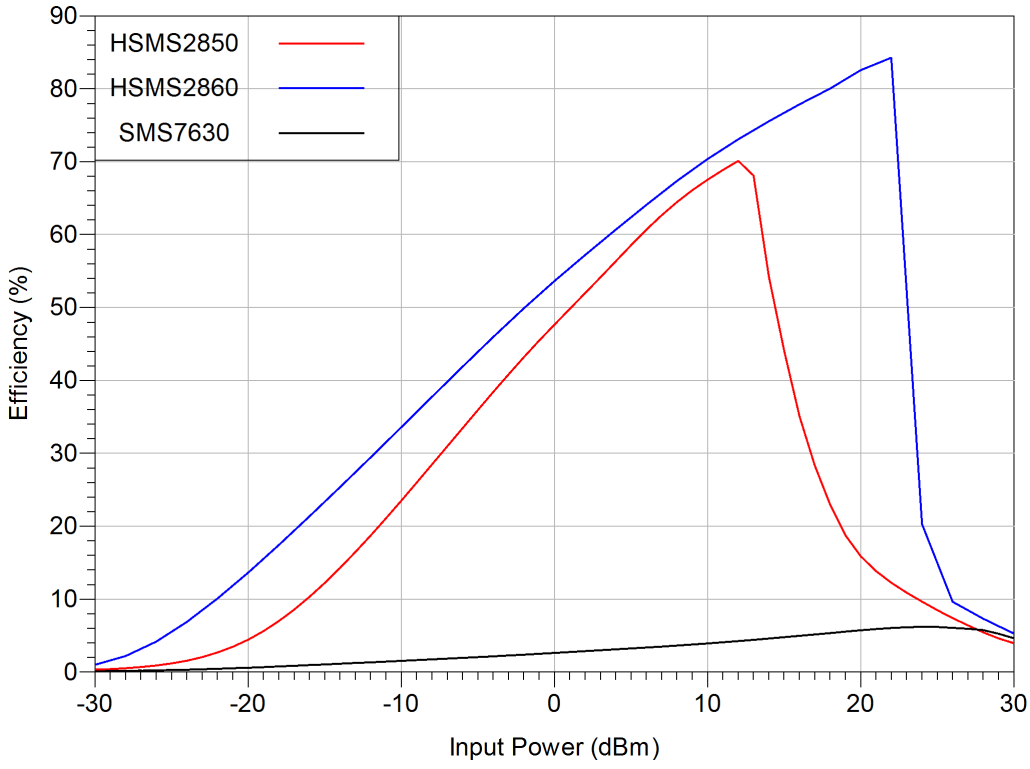

(b) Greinacher topology

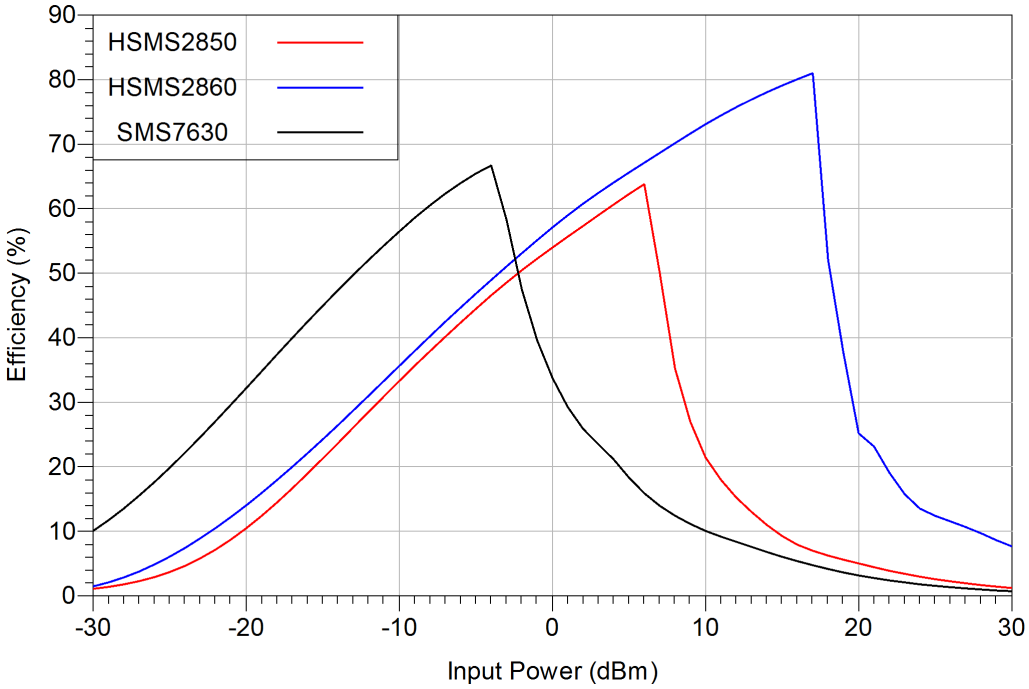

(c) Series topology

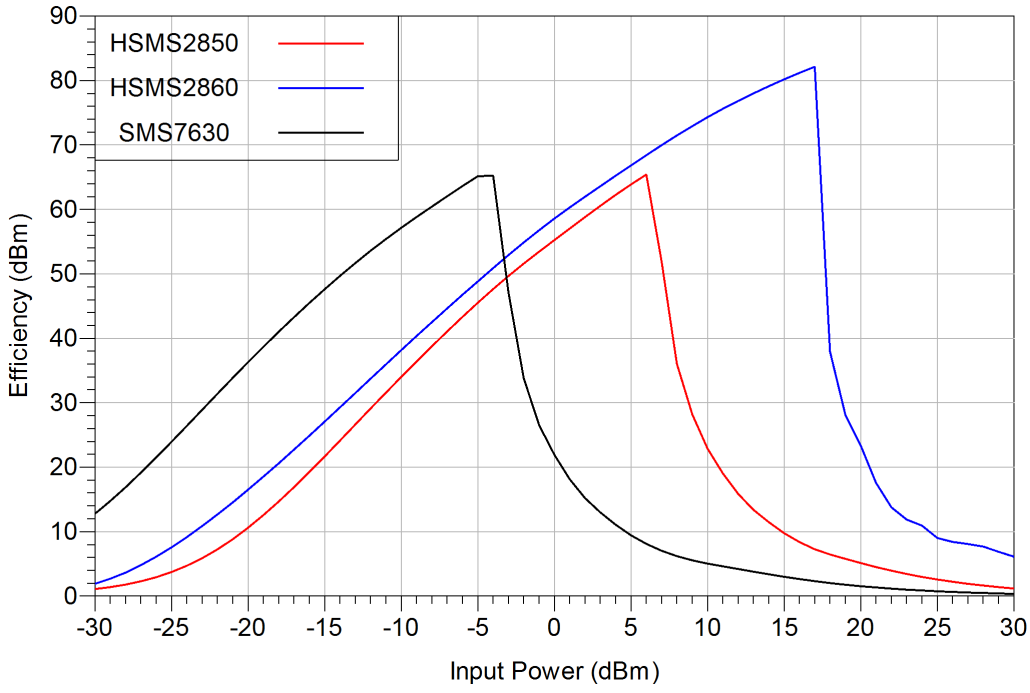

(d) Shunt topology

a few tens of kilo ohms.

It should be noted that during the simulation, whatever the value of the load

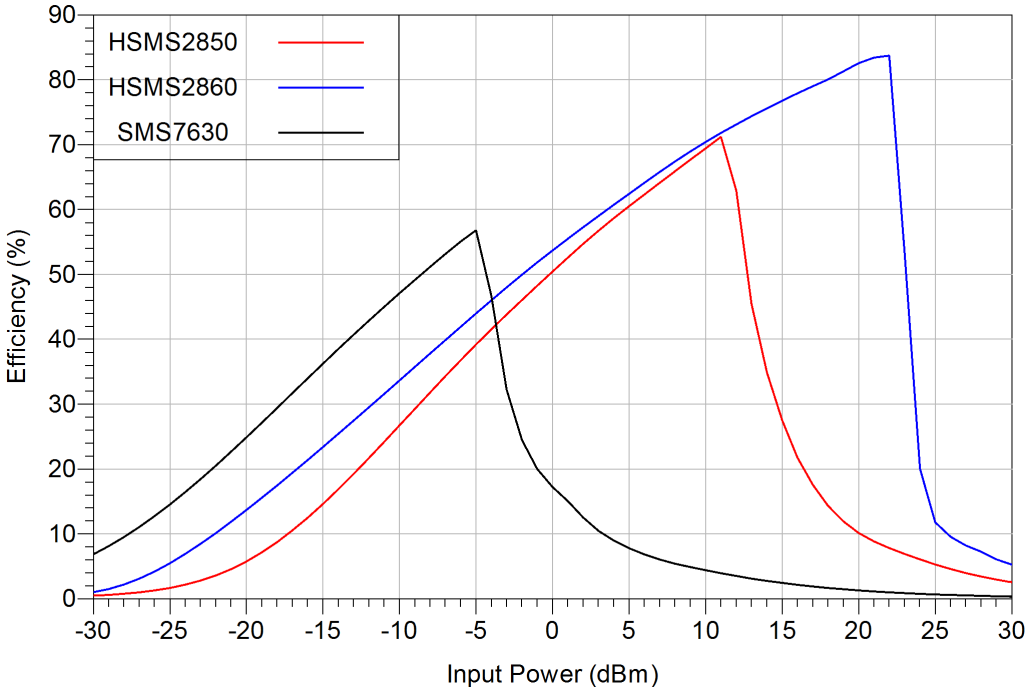

(e) Voltage doubler topology

Figure 4.5: Rectification efficiency simulation survey of different topologies (Dickson, Greinacher, Series, Shunt and voltage doubler) using diodes HSMS2850, HSMS2860 and SMS7630. Here the simulations are done at frequency 2.45 GHz; for each topology, the color code are red for HSMS2850, blue for HSMS2860 and black for SMS7630

resistance, it does not have a significant influence the reflection coefficient (S11) that is used for impedance matching. This is due to the fact that S11 is and RF parameter and the load is in the DC part. However, this value of the load resistance has a great influence on the efficiency of the system. Therefore, to determine the optimum load, it must be varied by measuring the efficiency of the system.

From the discussion above, it can be deduced that the choice of topology and diode of the energy harvesting circuit to achieve maximum efficiency must depend on the input power available to be captured. If, for example, 0 dBm of power is to be harvested in the 2.45 GHz band, it can be seen from graphical analysis that we have an efficiency of 60 % for the shunt topology with HSMS2860 diode and

HSMS2850 diode series topology. For the same power, the Dickson topology with the SMS7630 diode has an efficiency of 63 %. These last three circuits are therefore the ones to be considered since they have the highest efficiencies at 0 dBm input power.

With this obtained result, it can be said that the choice of diode for an energy harvesting circuit depends on the power source available and the related topology to be considered. This means that one diode is only better than the other if a specific situation is considered.

4.3.5 Energy harvesting topologies and frequency impact investigation

To evaluate the influence of frequency on the radio frequency energy harvesting circuits, the five previous topologies have been taken again and matched in impedance at 5.7 GHz frequency, with a realizable reflection coefficient S_{11} of – 25 dB, as in the previous cases. The reflection coefficient plots can be seen in Figure 4.6 where graphs represent the impedance matching for all the five topologies with the three most commonly used diode types highlighted. In this Figure 4.6 there are 15 plots, some of which overlap with the others and make them invisible.

This frequency is chosen for the same reason as 2.45 GHz, that is Wireless Local Area Network (WLAN) frequency band most often used for Wi-Fi and likely to have radio frequency energy.

In the following, we present in Figure 4.6, the curves corresponding to the simulation of the above studied topologies at the 5.7 GHz frequency band. In Figure 4.6, as in the case of Figure 4.5, there are 15 graphs, which represent the five topologies,

Table 4.5: Simulation of efficiency at frequency 2.45 GHz

Topology	Diode Type	Max Eff.(%)	Pwr of max. Eff.(dBm)	Pwr of 10% Eff.(dBm)	Load Res.(kΩ)
Dickson	HSMS2850	71.13	17	– 12	7
	HSMS2860	85.71	25	– 17	30
	SMS7630	71.56	5	– 23	20
Grein-acher	HSMS2850	70.1	12	– 16	2
	HSMS2860	84.2	16	– 22	15
	SMS7630	6.15	23	—	0.1
Series	HSMS2850	63.97	7	– 20	2
	HSMS2860	81.03	16	– 22	3
	SMS7630	66.66	– 4	– 30	2
Shunt	HSMS2850	65.36	6	– 20	2
	HSMS2860	82.09	16	– 23	4
	SMS7630	65.46	– 5	– 31	5
Voltage doubler	HSMS2850	71.20	11	– 17	3.3
	HSMS2860	84.58	20	– 22	15
	SMS7630	56.78	– 5	– 28	5

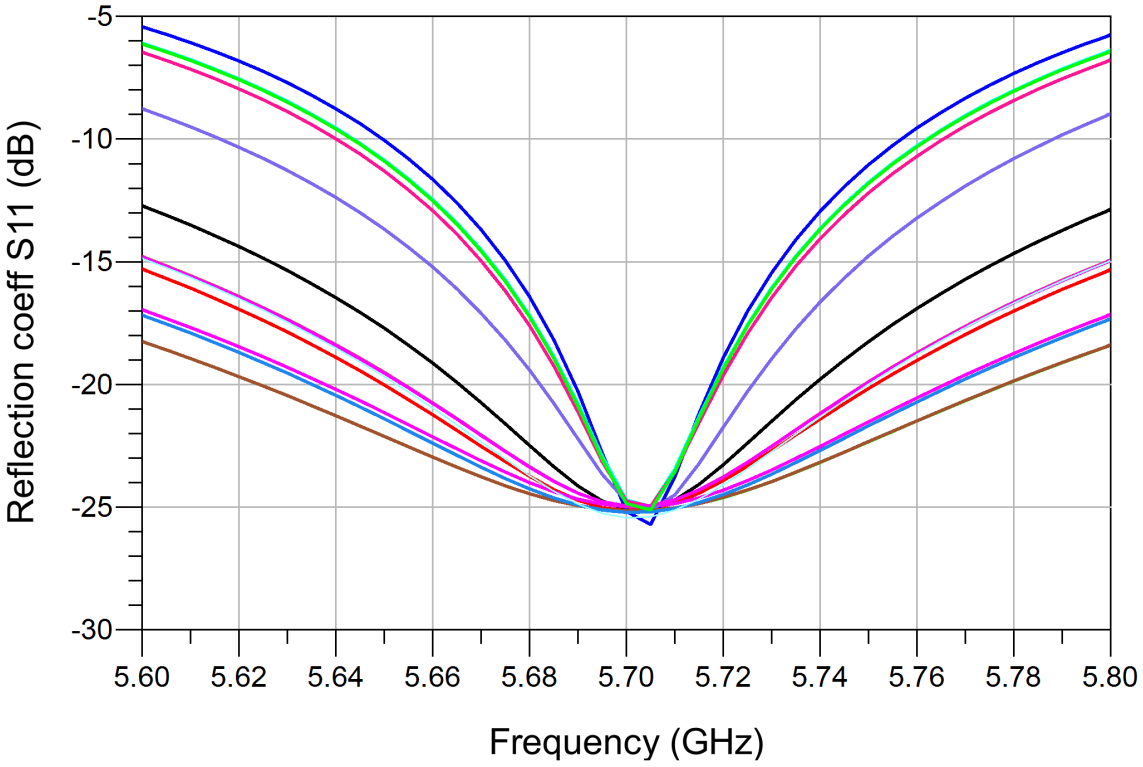

Figure 4.6: Reflection coefficient of all the rectifier topologies in simulation at frequency 5.7 GHz with input power - 30 dBm

each of which uses the 3 identified diodes.

The results shown in Figure 4.6 are summarized in Table 4.6. From these results, in addition to the general observations already made in the case of 2.45 GHz frequency, it can be said that whatever the topology and diode used for RF energy harvesting, better results are obtained at 2.45 GHz band than at 5.7 GHz band. It is important to mention that the considered diodes are working on the frequency bands considered and above. This leads to the conclusion that the higher the frequency, the lower the energy harvested with these known circuits. This overall drop in conversion efficiency is not subject to a general rule of proportionality; for example, the conversion efficiency of the voltage doubler topology with the HSMS2860 diode drops from 84.58 % to 72.88 %, which is a relative loss of 11.7 % when moving from 2.45 GHz to 5.7 GHz bands, whereas this relative loss is 35.61 % for the Dickson

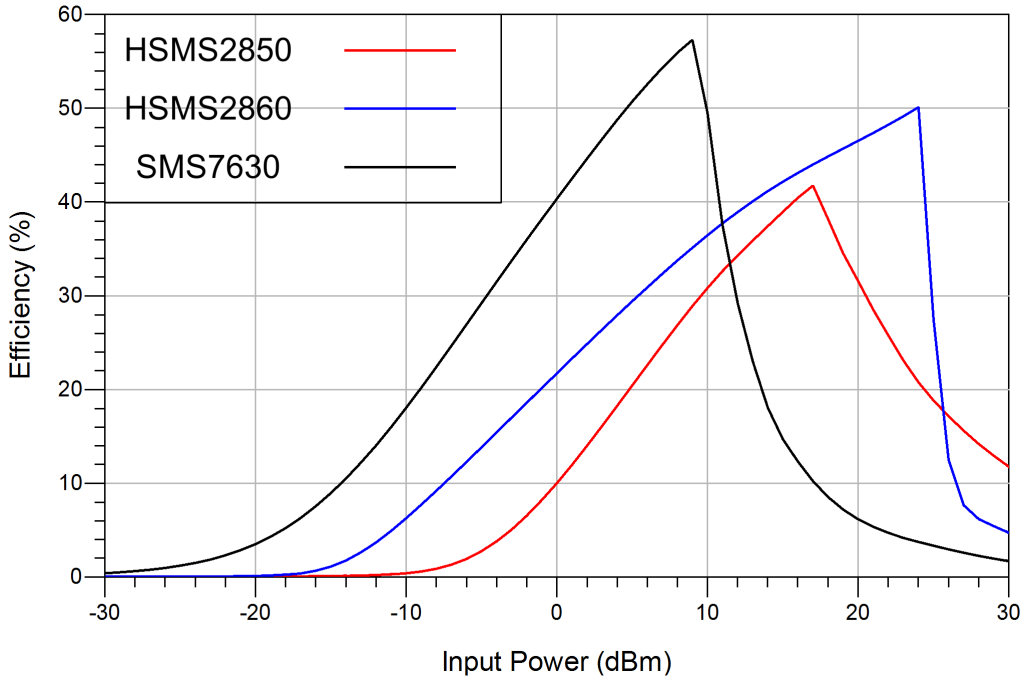

(a) Dickson topology

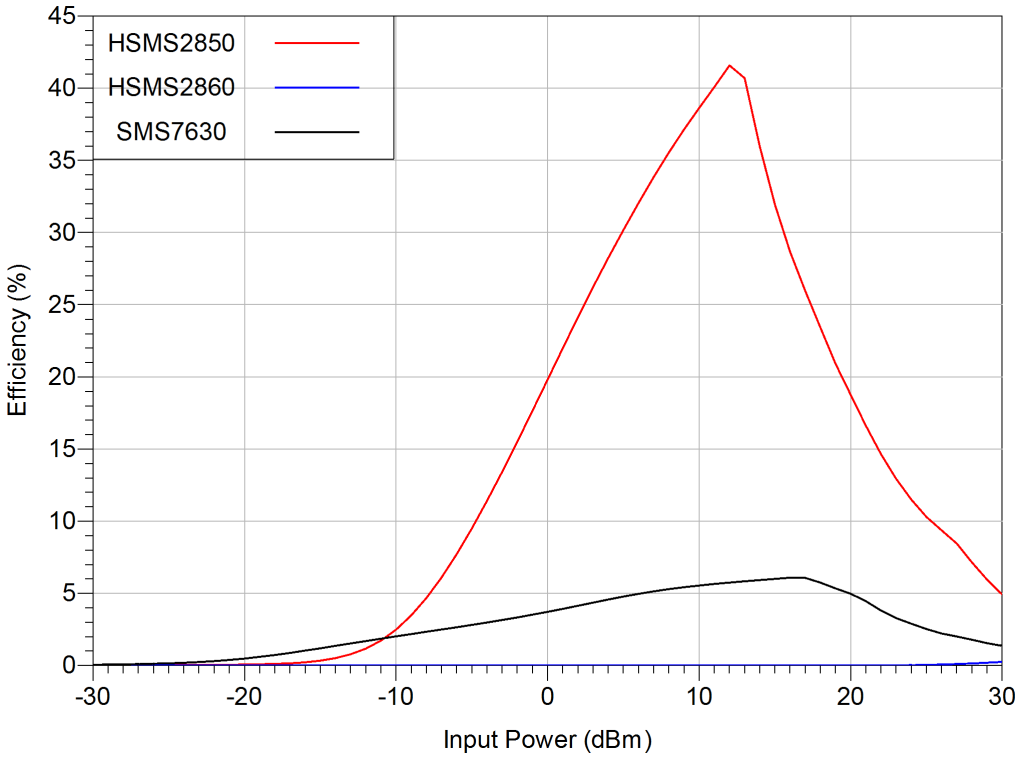

(b) Greinacher topology

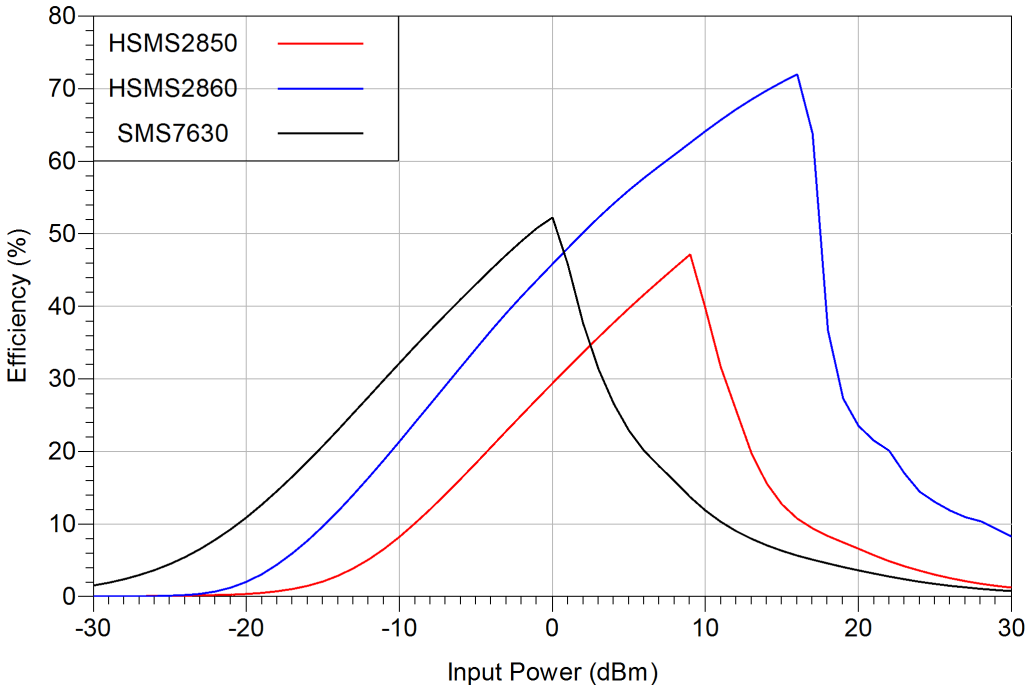

(c) Series topology

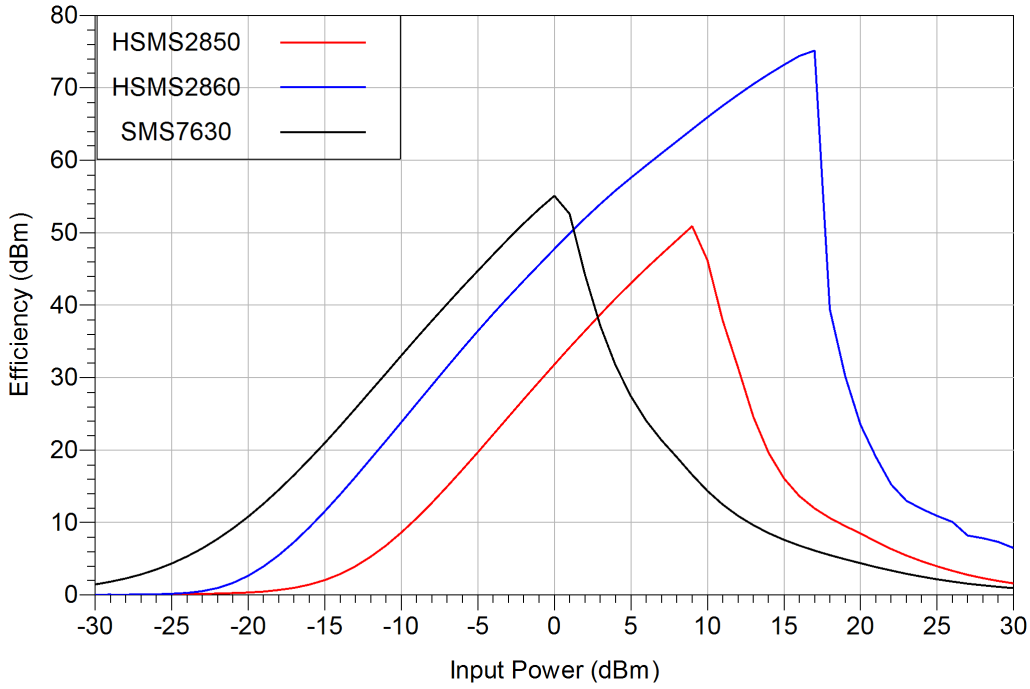

(d) Shunt topology

topology with the HSMS2860 diode in both bands.

Furthermore, it is observed that the input power at which the maximum conver-

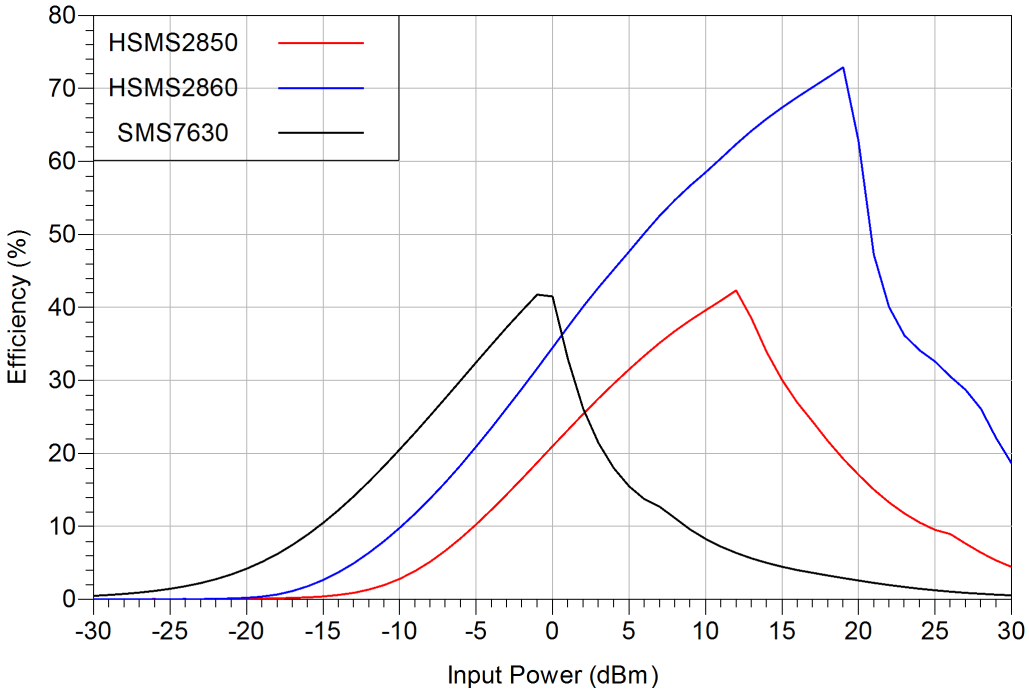

(e) Voltage doubler topology

Figure 4.6: Rectification efficiency simulation survey of different topologies (Dickson, Greinacher, Series, Shunt and voltage doubler) using diodes HSMS2850, HSMS2860 and SMS7630. Here the simulations are performed at 5.7 GHz; for each topology, the color code are red for HSMS2850, blue for HSMS2860 and black for SMS7630

sion efficiency is achieved can change in some cases from one frequency band to the other.

4.4 Tools for circuit analysis and design

4.4.1 Simulation tools

The choice of working environment was conditioned not only by the RF frequencies range around which our circuits operate, but also by its availability and the flexibility it offers in terms of simulation tools. For these reasons, we chose ADS (Advanced Design System) working environment from Keysight Technologies, which

Table 4.6: Simulation of efficiency at 5.7 GHz

Topology	Diode Type	Max Eff.(%)	Pwr of max. Eff.(dBm)	Pwr of 10% Eff.(dBm)	Load Res.(kΩ)
Dickson	HSMS2850	41.73	17	0	1.5
	HSMS2860	50.10	24	– 7	30
	SMS7630	57.28	9	– 14	10
Grein-acher	HSMS2850	41.58	12	– 5	0.5
	HSMS2860	0.25	30	—	0.5
	SMS7630	6.08	16	—	0.3
Series	HSMS2850	47.16	9	– 9	0.7
	HSMS2860	71.98	16	– 15	1
	SMS7630	52.23	0	– 21	0.9
Shunt	HSMS2850	50.88	9	– 9	0.6
	HSMS2860	75.12	17	– 16	1.5
	SMS7630	55.07	0	– 21	0.8
Voltage doubler	HSMS2850	42.30	12	– 5	0.6
	HSMS2860	72.88	19	– 10	1
	SMS7630	41.73	– 1	– 15	1

was available at the CITI laboratory, but which also provides a large number of tools dedicated to the design of RF circuits. ADS provides a library with a large variety of components (active and passive); on the one hand it enables to perform time analyses (transient), and frequency analyses (S Parameters, Harmonic Balance, Large Signal S Parameter) with optimization possibilities, and on the other hand it offers

the possibilities to simulate electromagnetic (momentum) and SPICE (Simulation Program with Integrated Circuit Emphasis) circuits.

a. Time domain (transient) simulation

Simulation is of paramount importance in that it allows to verify the circuit theory before any implementation. This verification in the time domain is done either at the macro or behavioural level, taking into account the whole circuit, or at the components level.

The behavioural model analyses the mathematical relationship that describes the circuit. The construction of behavioural blocks is easily achievable, and their simulations are hundreds or thousands of times faster compared to macro level simulations. The macro model analyses the blocks of each circuit using equivalent models. This model can involve both real and ideal components.

Component-level simulation is the simulation of all the interconnected elements of the circuit as represented in circuit theory. This level of simulation provides the highest accuracy, although it generally requires more simulation time than other types of simulation [114].

Figure 4.7 is a representation of the iterative algorithm for the operation of the SPICE time domain simulation program.

A transient simulation like SPICE operates exclusively in the time domain. The dependence of currents and voltages is summarized here in a set of integro-differential equations of the circuit under analysis, which are then solved by the simulator. This results in a time non-linear analysis. The transient analysis is performed fully in the time domain and consequently cannot take into account the frequency-dependent behaviour of distributed elements such as microstrip elements, S-parameter ele-

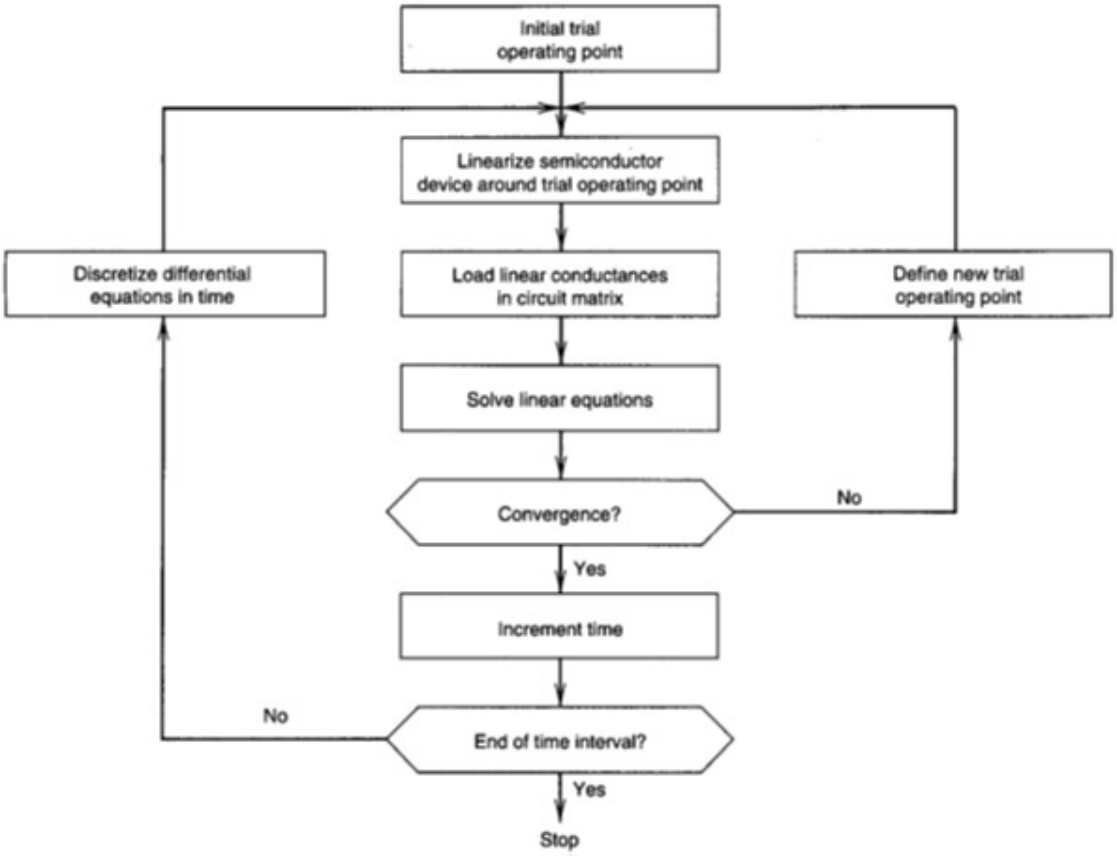

Figure 4.7: SPICE solution algorithm
[114]

ments, etc. Accordingly, in a transient analysis, these elements must be expressed in simplified, frequency-independent models such as lumped equivalent components, constant loss and dispersion-free transmission lines, short circuits, open circuits, etc.

For this time domain simulation case, the frequency behaviour of distributed elements such as microstrip elements, S-parameter elements, cannot be taken into consideration. Such assumptions and simplifications are generally quite acceptable for low frequencies [103].

b. S-Parameters simulation

S-Parameters simulation allows the linearization of the components of a linear or non-linear circuit at high frequencies around an operating point characterized by its optimal frequency. The circuit thus characterized, its behaviour can be predicted for any known input signal. These parameters do not take into account the content of the network, and are as easy to measure and use in RF, as any other parameters. They are conceptually simple, analytically convenient, and capable of providing a great insight into a measurement or design problem [115].

c. Harmonic Balance simulation

Harmonic Balance (HB) simulation is a non-linear circuit analysis that proceeds simultaneously in the time and frequency domain. This simulation method was first discussed in 1937, but the modern version applicable to simulators appeared in 1976 [116].

This basic choice as a method of circuit analysis consists in decomposing circuits into linear and nonlinear subsystems, having the same number of ports. This decomposition reduces the number of variables to be optimized.

Linear sub-entities are analysed in the frequency domain by conventional multi-port techniques, while non-linear sub-entities are analysed in the time domain by appropriate equations.

The conversion from the time domain to the frequency domain is done by the Fast Fourier Transform (FFT). The technique used is particularly suitable, and calls for the mathematical formalization of the problem, as a non-linear algebraic system is in the form $E(X) = 0$. This formulation is based on the Kirchhoff Current Law which sum all the currents to each node at zero. E is a vector of the HB error to be evaluated numerically, and X is a set of harmonic state variables. The strategy for solving this equation is chosen from a wide range of algorithms. Newton's strategy, which is iterative, has overall very good performance in the resolution of the equation, but may still fail to converge if the chosen starting point is not close enough to the solution, specifically in the case of highly non-linear systems. There is very low probability to obtain the result on the first iteration.

A trade-off is found between Newton's iterative algorithm and other methods in order to improve convergence when needed [117]. An algorithm based on the update of the Hessian formula is first used for the simulation, then the Newton's iterative algorithm is used to improve the result. Harmonic Balance simulation is a digital solution technique for analogue circuits that operate in steady-state, quasi-periodic and periodic regimes.

The simulation process is summarized in the block diagram in Figure 4.8. This type of analysis is convenient for the study of circuits such as amplifiers, mixers, oscillators, multipliers that operate in wide signal mode.

HB analysis has advantages over time simulation, especially in the case of high-

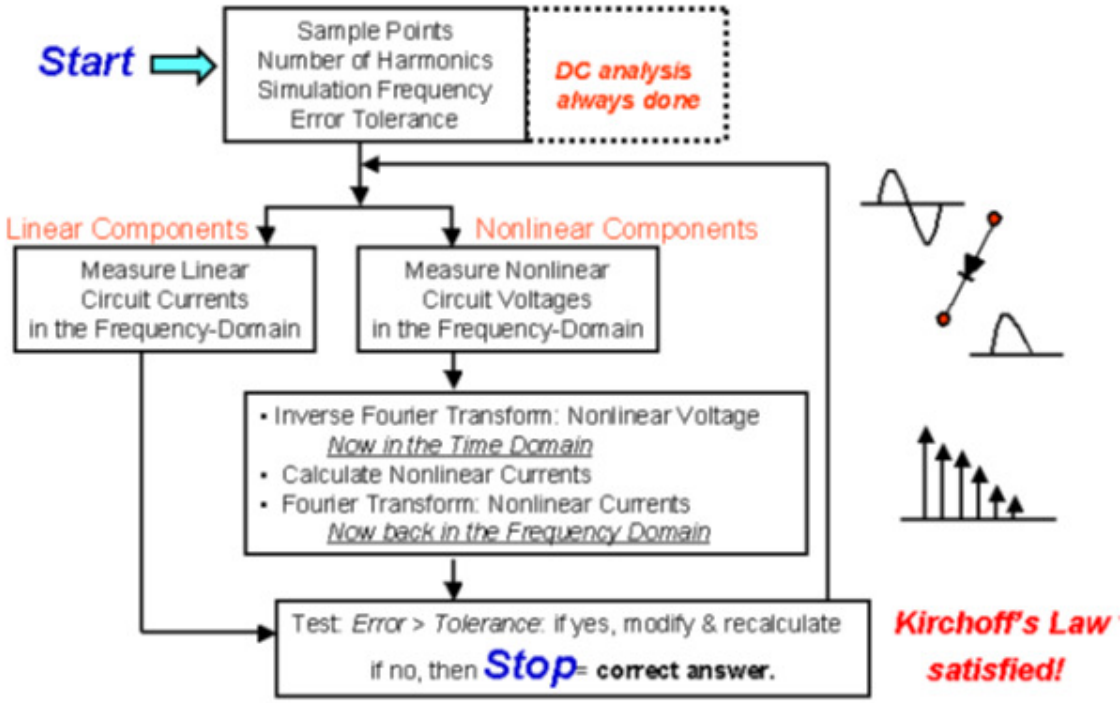

Figure 4.8: Overview of Harmonic Balance simulation [118]

frequency circuits [118]:

- The steady-state behaviour of a system is generally the one of interest to circuit's designers. The time constants to reach this steady state are often logged with respect to the operating frequency of the circuit, what would result in considerable simulation time. HB simulation provides the steady state directly.

- HB simulation is faster in solving typical high-frequency problems than time algorithms. The harmonics generated in a non-linear circuit are often of a much higher order than the fundamental. This would make time simulations much slower because the simulation step depends on the smallest period.

- The high-frequency behaviour of many linear models is better represented in the frequency domain. Their use in the time domain would lead to problems

of accuracy, causality or stability.

d. Large Signal S-Parameters (LSSP) simulation

Compared to S-Parameter simulations which are based on the linearized small-signal circuit, LSSP simulation are based on the simulation of a full large signal non-linear circuit with harmonic balance method. The solution of harmonic balance simulation involves nonlinear effects such as compression since it is a large signal simulation technique. The large-signal S-parameters can therefore vary along with the power levels. Like the S-parameters being small signals, the large-signal S-parameters are defined as the ratio between reflected and incident waves:

$$S_{ij} = \frac{B_i}{A_j} \tag{4.20}$$

We defined the incident and the reflected waves as:

$$A_j = \frac{V_j + Z_{0j} I_j}{2\sqrt{R_{0j}}} \ , \ B_i = \frac{V_i - Z_{0i}^{*} I_i}{2\sqrt{R_{0i}}} \tag{4.21}$$

where:

V_i , V_j are Fourrier coefficients of the voltages at ports i and j at the fundamental frequency

I_i, I_j are Fourier coefficients of the currents at ports i and j at the fundamental frequency

Z_{0i} , Z_{0j} characteristic impedances at ports i and j

R_{0i} , R_{0j} real parts of Z_{0i} and Z_{0j} [119].

The determination of the "large signal" S-parameters of a two-port system is

carried out as described below:

- Port 2 is loaded with an impedance equal to its complex conjugate impedance.
- A signal of power P_1 set by the user is applied to port 1 through a source having an impedance equal to the complex conjugate impedance of this port.
- Using a Harmonic Balance simulation, the currents and voltages at ports 1 and 2 are calculated.

These information are used to compute the parameters S_{11} and S_{21}.

- Port 1 is loaded with an impedance equal to its complex conjugate impedance.
- A signal of power $P_2 = |S_{21}|^2 P_1$ is applied to port 2 through a source having an impedance is equal to the complex conjugate impedance of this port.
- Using a Harmonic Balance simulation, the currents and voltages at ports 1 and 2 are computed.

This information is used to calculate the parameters S_{11} and S_{21}. For comparison with the S-parameter simulation, the LSSP simulation takes into account non-linear behaviour, such as gain compression or variations in incident power. It is therefore to be preferred for the simulation of non-linear circuits with highly dependent level behaviour of incidental power, as in the case of the rectennas [120].

e. Momentum simulation

Momentum electromagnetic simulation engine is a planar simulation tool used for the analysis of passive micro-strip circuits. It uses the Momentum Method (MoM) to simulate complex electromagnetic effects including interconnections, couplings and parasitic elements.

The Moment Method is a numerical method for solving linear partial differential equations formulated in integral form [121]. As this method only requires the calculation of values at the edges rather than in the whole space, it is much more efficient in terms of calculation time than 3D numerical methods. The principle is to create a mesh of the characterised surface.

4.4.2 Analysis tools

In the previous chapter, we have shown that the elements of the impedance matching network of energy harvesting systems, i.e. the LC components, are disposed in L, PI and T shapes. In this section, we will present the techniques for transforming these LC component networks into transmission lines of known electrical length and characteristic impedance. The aim of this transformation is the optimization of the circuit, thus making it possible to limit the radiation due to the discrete components in a circuit operating at radio frequencies.

a. Open and short-circuit stubs from lumped components

In general, inductors and capacitors are available and work well at low frequencies meanwhile this is not true at radiofrequencies. It is then convenient to find the equivalences of those components at high frequencies. Richard's transformation and Kudora's identities are consequently used to achieve this goal. The application of these two techniques allows to perform any of the following operations:

- The transformation of capacitors and inductors into open circuit and short circuit transmission line stubs
- The physical separation of transmission line stubs

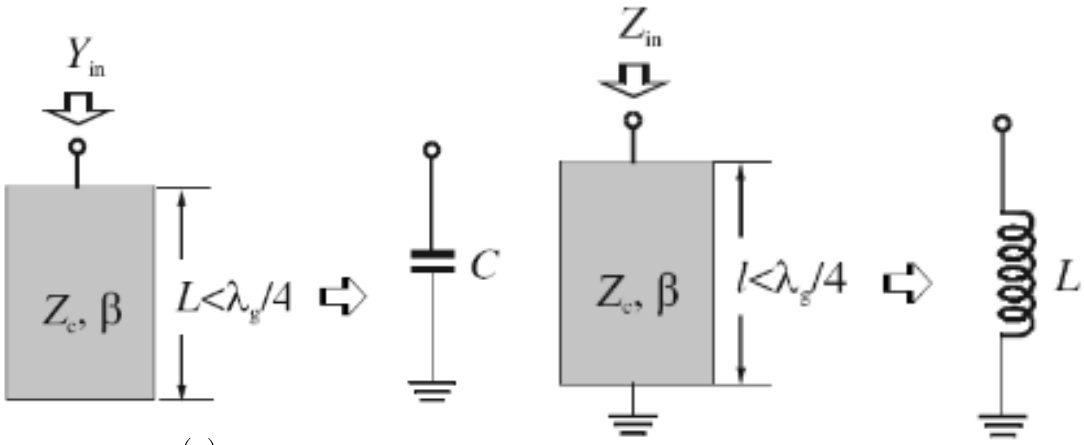

Figure 4.9: Electric model equivalent to: (a) an open stub. (b) a short circuit stub [122]

- The transformation of shunt stubs into series stubs and vice-versa
- The change of impractical characteristic impedances into more realisable values [122].

A lossless open stub microstrip line is equivalent to a parallel-connected capacitor. Similarly, a short-circuit stub is equivalent to a parallel inductor as shown in Figure 4.9.

In this transformation, the phase constant is given by $\beta = \frac{\omega}{V_p}$, where ω is the angular frequency and V_p the phase velocity. Z_C represent the characteristic impedance of the stub line and the electric length is given by $\theta = \frac{\omega}{V_p} l$ with l representing the stub length.

The input impedance of a lossless short-circuit stub is given by [123]:

$$Z_{CC} = jZ_0 \tan\left(\frac{2\pi}{\lambda_g} l\right) \tag{4.22}$$

with:

λ_g: guided wavelength ;

Z_0: characteristic impedance;

l: length of the stub.

This means that if the value of $\tan\left(\frac{2\pi}{\lambda_g}l\right)$ is positive, the stub will behave like an inductance, whereas if this value is negative, it will behave like a capacitance. For $l < \frac{\lambda_g}{4}$, the stub will behave like an inductance. The length l required for a short-circuit stub to behave as an inductance of value L is given by :

$$l = \frac{\lambda_g}{2\pi}\left[n\pi + \arctan\left(\frac{\omega L}{Z_0}\right)\right] \tag{4.23}$$

For a lossless open circuit stub, the input impedance is given by :

$$Z_{OC} = -j.Z_0.\cot\left(\frac{2\pi}{\lambda_g}l\right) \tag{4.24}$$

Consequently, if the value of $\cot\left(\frac{2\pi}{\lambda_g}l\right)$ is positive, the stub will behave as a capacitor, while if it is negative, it will behave as an inductance. For $l < \frac{\lambda_g}{4}$, the stub will behave like an inductance. The length l required for a short-circuit stub to behave as a capacitor of value C is given by :

$$l = \frac{\lambda_g}{2\pi}\left[n\pi + arc\cot\left(\frac{1}{\omega C Z_0}\right)\right] \tag{4.25}$$

Stubs in microstrip technology can also take a radial shape, as in Figure 4.10 The input impedance of such a stub connected in shunt to a transmission line is given by [124]:

$$Z_{radial} = -j.Z_0.\frac{120\pi.h}{r_i.\theta\sqrt{\epsilon_r}}\cot\left(k.r_i, k.r_0\right) \tag{4.26}$$

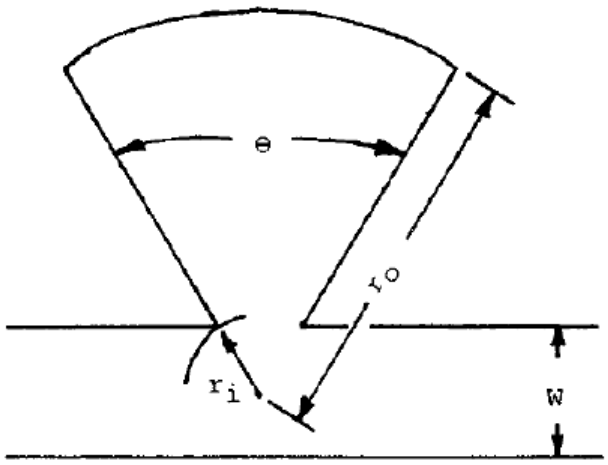

Figure 4.10: Radial stub in microstrip technology [124]

with:

h: substrate thickness;

ϵ_r : relative permittivity of the substrate.

The function $\cot(k.r_i, k.r_0)$ is defined with first and second degree Bessel functions [124].

b. Equivalent model of transmission line

There is a good way to modify the structure of transmission lines so that it can operate on a given frequency. First of all, a microstrip transmission line of characteristic impedance Z_T and electrical length 90 deg ($\lambda/4$) can be represented by an equivalent model as shown in Figure 4.11. The proposed equivalent model consists of a transmission line with impedance Z_A and electrical length θ, to which two transmission lines with admittances denoted by jY are connected in parallel. Using the equations that link the different parameters of a transmission line and that are illustrated in the tables in Appendix 1, we can write the decomposed ABCD matrix of the equivalent model as:

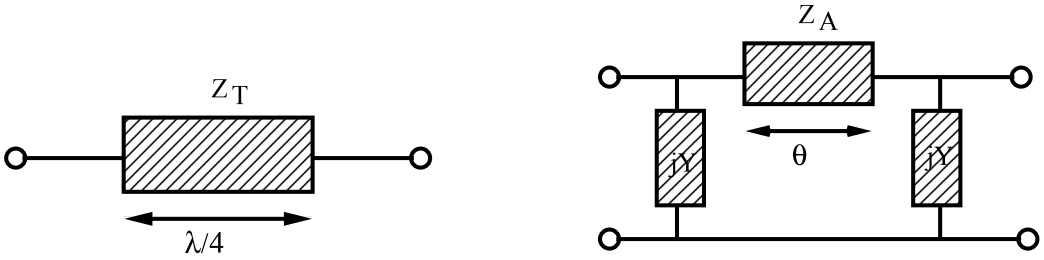

Figure 4.11: Equivalent model of line

$$\begin{bmatrix} 1 & 0 \\ jY & 1 \end{bmatrix} \begin{bmatrix} \cos\theta & jZ_A \sin\theta \\ jZ_A \sin\theta & \cos\theta \end{bmatrix} \begin{bmatrix} 1 & 0 \\ jY & 1 \end{bmatrix} \tag{4.27}$$

After rearrangement, we get

$$\begin{bmatrix} \cos\theta - Z_A Y \sin\theta & jZ_A \sin\theta \\ jY \sin\theta(1 - Z_A^2 Y^2 + 2Z_A Y \cot\theta) & \cos\theta - Z_A Y \sin\theta \end{bmatrix} \tag{4.28}$$

Using equality, we write:

$$Y = \frac{\cot\theta}{Z_A} \tag{4.29}$$

$$Z_A \sin\theta = \pm Z_T \tag{4.30}$$

Equation 4.28 can be rewritten as:

$$\begin{bmatrix} 0 & jZ_A \sin\theta \\ j\frac{1}{Z_A \sin\theta} & 0 \end{bmatrix} = \begin{bmatrix} 0 & \pm jZ_T \\ \frac{1}{\pm jZ_T} & 0 \end{bmatrix} \tag{4.31}$$

It should be noted that the matrix expression in equation (4.31) corresponds to the ABCD matrix of the transmission line with characteristic impedance Z_T and electrical length ± 90 deg in Figure 4.9. Assuming the transmission line in Figure 4.11

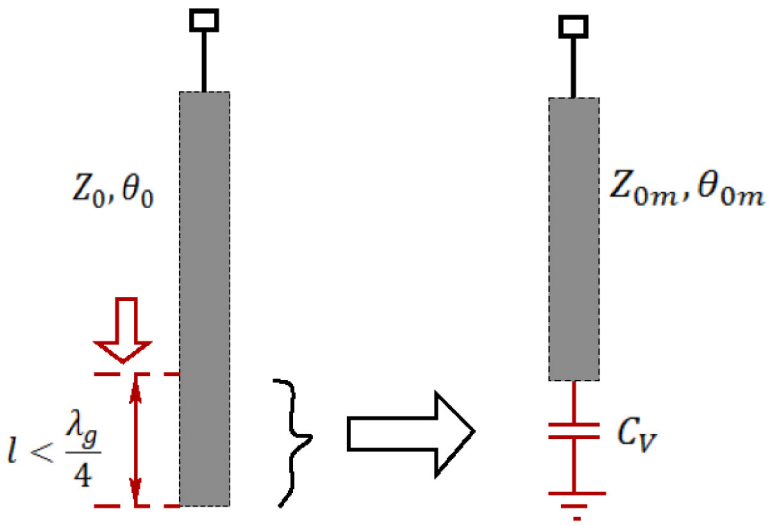

Figure 4.12: Open transmission line and equivalent circuit [djoumessi10]

to be lossless and according to the equations developed in Appendix 1, we obtain the expression of the input admittance Yin of the small portion of open transmission line by [125]:

$$Y_i n = j\left(\frac{1}{Z_0}\right)\tan\left(\frac{2\pi}{\lambda_g}l\right) \tag{4.32}$$

with λ_g being the guided wavelength evaluated at f_0, and l representing the physical length of the small portion of line. We observe from equation (4.32) that, for a line length $l < \lambda_g/4$, the input admittance Y_{in} represents that of a capacitance of the form jX, with $X = \omega C_v$. Accordingly, we can pose the equality :

$$j\left(\frac{1}{Z_0}\right)\tan\left(\frac{2\pi}{\lambda_g}l\right) = \omega C_v \tag{4.33}$$

where $\omega = 2\pi f_0$ is the angular frequency. On the other hand, we can also express the total physical length $\lambda_g/4$, corresponding to the electric length $\theta_0 = \pi/2$, in Figure 4.12.

$$\lambda_g/4 = l + l_{om} \tag{4.34}$$

where l_{0m} is the new physical length associated with the electrical length θ_{0m}. At substituting equation (4.32) in equation (4.34), we obtain the expression of the length l_{om} equal to:

$$l_{om} = \frac{\lambda_g}{4} - \left(\frac{\lambda_g}{2\pi}\right) \arctan(Z_0 \omega C_v) \tag{4.35}$$

In this paragraph, we briefly illustrated how the microwave transmission line concept can be used to modify the structure of a circuit with inductors or capacitors. The telegrapher's equations used in the book [122], show that any lossless microstrip transmission line can be modeled by an infinitesimal succession of LC localized element circuits. C and L represent an equivalent parallel capacitance and series inductance per unit line length. In the same work, it is well demonstrated that the characteristic impedance and guided wavelength of a lossless transmission line, which we denote by Z_C and λ_g, can be expressed as a function of C and L as:

$$Z_C = \sqrt{L/C} \tag{4.36}$$

$$\lambda_g = \frac{1}{f_0\sqrt{LC}} \tag{4.37}$$

We observe from these equations that, when L and C increase with the same ratio so as to keeping an impedance Z_C constant, the guided wavelength λ_g proportional to the physical length of the transmission line decreases.

The techniques of transformation and analysis tools of this section are applied in the following section to design and implement the energy harvesting circuit ap-

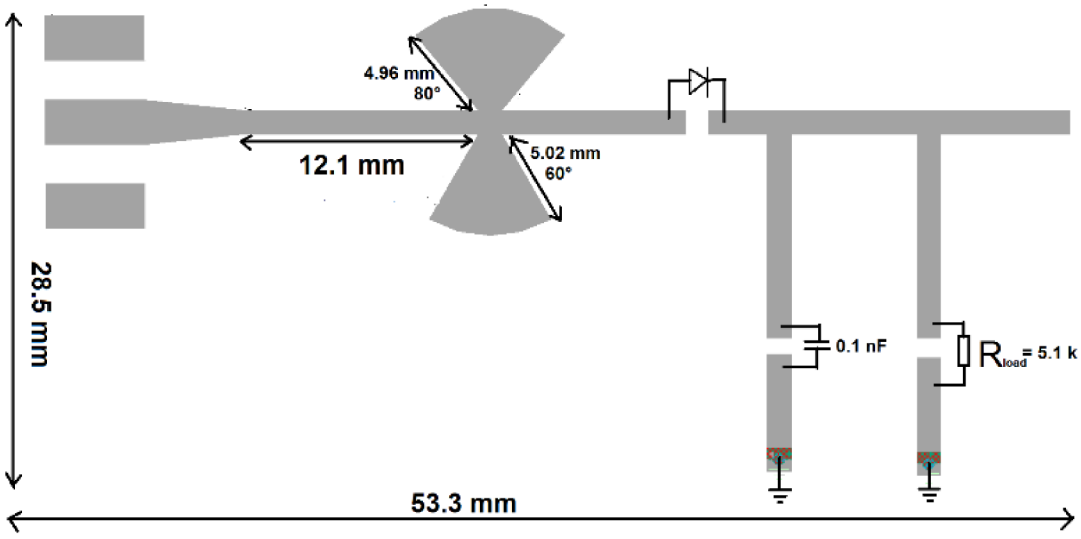

Figure 4.13: Proposed high-efficiency rectifier with a butterfly stub matching circuit and based on SMS7630 diode

plicable to the WuRx.

4.5 Proposed energy harvesting circuit and measurements

Figure 4.13 presents the layout of the proposed harvester based on SMS7630 diode and made up using printed circuit board technology. This technology is used in order to design the impedance matching circuit and is preferred as compared to lumped components because it is less dispersive at high frequency.

The harvesting circuit is made up of butterfly radial stub for large bandwidth providing good impedance matching around the carrier frequency of 2.45 GHz as shown in Figure 4.14.

The rectifier's central frequency was optimized at 2.45 GHz but, due to fabrication constraints, the measured central frequency is shifted down to 2.1 GHz. For

input power levels of -50 dBm, -25 dBm, 0 dBm, the simulated reflection coefficient is presented in Figure 4.14.

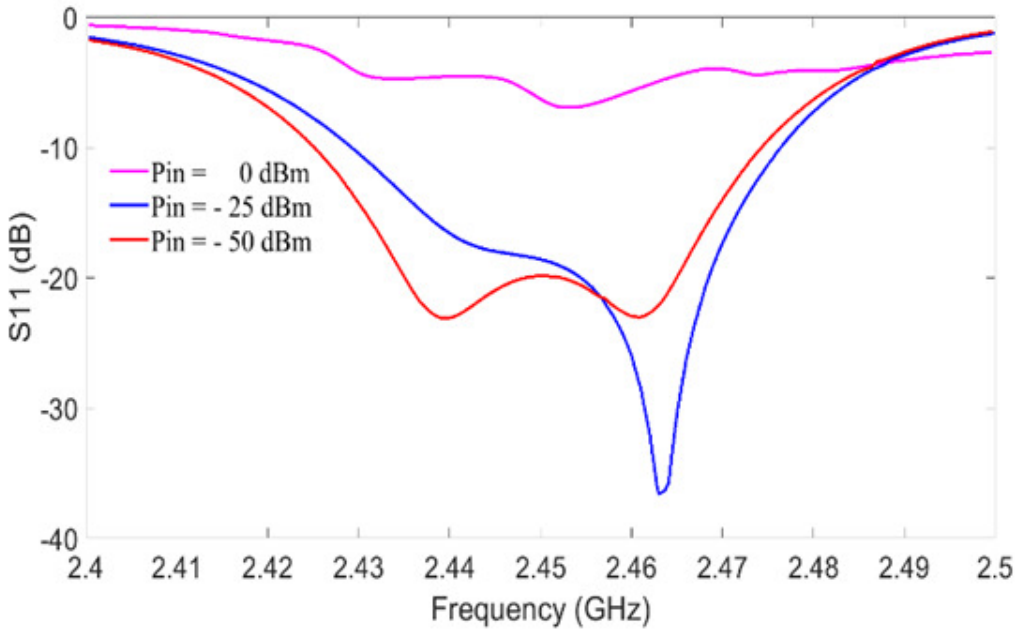

Figure 4.14: S11 (dB) at the input of the circuit for different power levels

At the input power level of -40 dBm the reflection coefficient was measured on the fabricated prototype at a level of – 14 dB as presented in Figure 4.15. The measurements of S_{11} were carried out with a vector network analyzer (VNA) from Rohde and Schwarz.

The capacitor at the output of the rectifier was implemented with a 0.1 nF capacitor in parallel with a 5 kΩ resistor. These specific values have been chosen because they are maximizing the rectifier's efficiency and consequently maximizing the output DC voltage.

Figure 4.16 presents the implementation of proposed high-efficiency harvester optimized and print on a Rogers Duroid (RO4350B) substrate. This hydrocarbon ceramic laminate has a superior high-frequency performance. The dielectric constant is 3.66, it has a dissipation factor of 0.0031, the substrate thickness is 0.51 mm, and

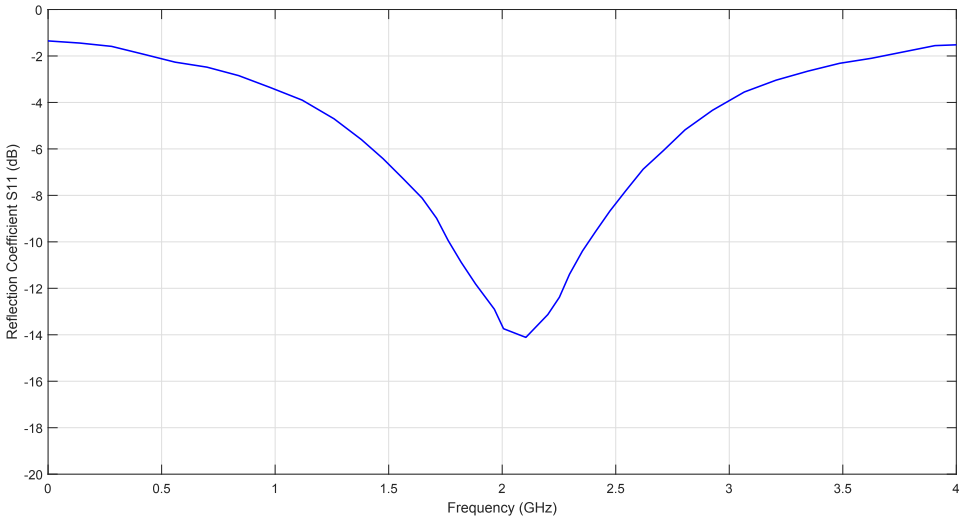

Figure 4.15: Measured reflection coefficient $S11(dB)$ at the rectifier's input

the conductor thickness is 17.5 μm.

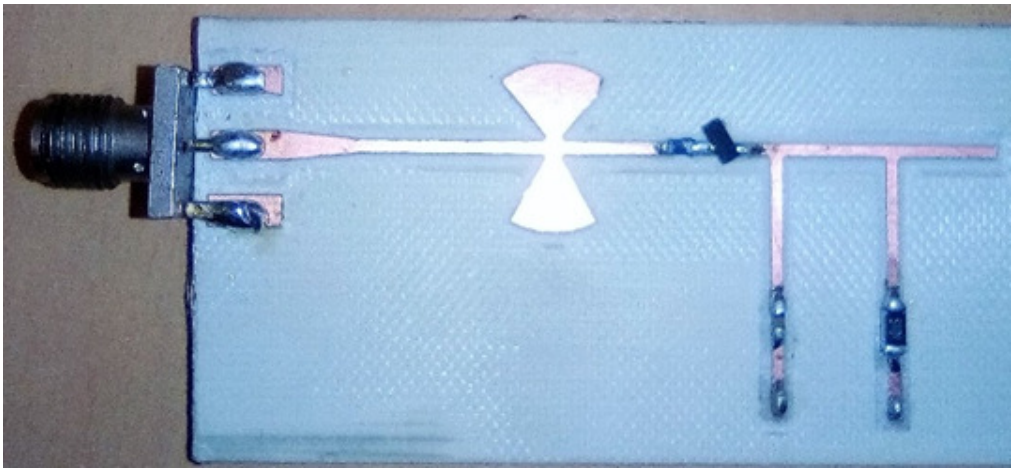

Figure 4.16: Implemented circuit of the energy harvester

In Figure 4.17, the simulated and measured output voltage are presented. From the result, it can be seen that the power harvested is closed to the simulated values.

For the specific case of quasi-passive Wake-Up Radio that it's aimed to supply with this circuit, the 2.025 μW, power corresponding to the output voltage of 3.2 mV for the existing load resistance of 5.1 kOhms. This output voltage is obtained with the input power lower than – 20 dBm according to the measurement.

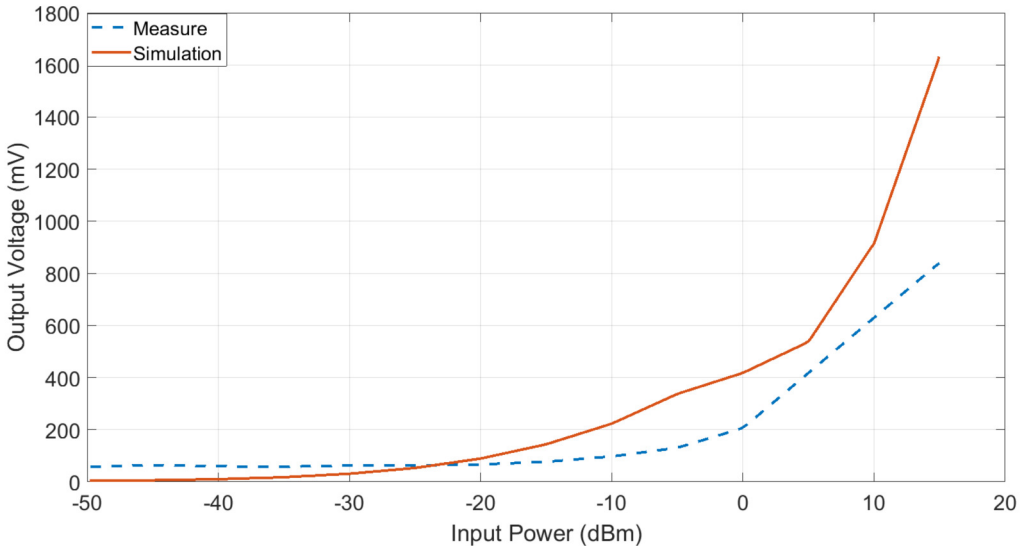

Figure 4.17: The simulated and measured output voltage of the RF energy harvester

Furthermore, if we are to consider two power levels that are 0 dBm and 15 dBm, for which the output voltages are 206.1 mV and 841 mV respectively, the harvested power will then be obtained as 8.3 μW and 138.68 μW. The surveys of WuRx in [27] which one of the most thorough on the subject listed 85 designs, with only 9 designs with power consumption greater than 138.68 μW harvested by this RF energy harvesting circuit. It is important to mention here, that the design did not take into account the storage component which in principle plays the role of energy buffer. We considered that the harvested energy is consumed directly or lost.

4.6 Conclusion

The work presented in this chapter covers RF energy harvesting circuits, more exactly the most employed circuit topologies and three of the main employed diodes in the energy harvesting circuits. After a work done on the state of the art, we proceeded to simulations which allow to establish that the choice of the circuit

as well as the diode to be used depends mainly on the available input power as well as on the topology. We also observe that better results are obtained with one diode compared to the other only for particular power and topology circumstances. In addition, we established that the higher the frequency, the lower the energy harvested. The design and implementation of RF energy harvesting circuit, which is designed to power a wake-up radio and makes it autonomous. Such a combination of the WuRx and the energy harvesting system, as well as the technique used for the implementation, made it possible to harvest a sufficient amount of energy for its supply. The future work should be to focusing on the reduction of the power of WuRx and improvement of RF energy harvesting circuit, by increasing the efficiency, reducing the size of devices and implementation in working environment. It will also be an option to cascade the energy harvesting circuits to maximize the amount of energy to be harvested at the output to meet the demand of any other WuRx.

Chapter 5

General Conclusion

5.1 Conclusion

The main objective of this thesis was to reduce the energy consumption of radio frontends, notably with the duty cycle technique and later with the WuRx. Furthermore, the study was intended to be applied to connected objects.

We stated the operating principle of wake-up radios and showed their advantage over conventional energy saving schemes. We then carried out a taxonomy study of these objects and classified them according to their energy consumption, architecture, implementation technology and identification methods. In addition, a statistical study was carried out to link consumption, technology, sensitivity and communication range.

Based on the study of an existing system developed by the CITI laboratory; an analysis and simulation of each functional block allowed an improvement of the sensitivity and consequently the communication range of the system. For each identifier, we had theoretically an additional gain of about 5 dB, which could improve

the range by approximately 13 meters in free space.

An investigation was done on radio frequency energy harvesting circuits with the aim of making our WuRx autonomous. A state-of-the-art allowed to survey the most recent and important works on the subject. Then, using the hypothesis of influence of the frequency, we validated through the analysis tools that the frequency affects the energy harvesting. For the same architecture, less energy is harvested at higher frequencies. At the same time, this study allowed to identify the circuit corresponding to our case of application. An implementation of this circuit made it possible to harvest the necessary and sufficient energy to power any wake-up radio. We subsequently developed an energy harvesting system capable of supporting its need for electrical energy for operation.

In addition to integrating an energy-saving mechanism, the connected devices of the present and future generations of network must also include a self-powering technique, in other words a remote power supply. For these systems, this will mean both implementing the wake-up radio system for energy saving and also implementing a system for harvesting ambient energy or for reception of the transmitted energy for the purpose of self-supply. It is in this spirit that research must now be carried out to make all the connected devices completely autonomous in terms of energy, as they sometimes require little communication time to share basic information and spend most of their time listening to the radio channel. This represents an enormous waste of energy during the listening periods, in proportion to the energy required.

5.2 Perspectives

For the continuation of this work, we suggest studies to enable an improvement of the wake-up radio with the aim of increasing the range further, but also an incorporation of the energy recovery system to make the two systems one. This will require overcoming the technological difficulties associated with, for instance, the use of different design platforms, as well as the technologies that may be different for the two systems.

In addition, it will be necessary to work on the miniaturization of the resulting system, which may require expertise in the calculation of microstrip lines and the transformation of these lines in the case of the energy harvesting circuit.

Standardization of all forms of future stand-alone WuRx could also be considered, to allow interoperability between products brought to the market by several manufacturers. As it can be reading in chapter 2, WuRx use several architectures and technologies for their implementation. A research effort could be considered to determine a flexible, scalable and low-cost architecture for end-users.

REFERENCES

[1] Eleonora Borgia. The Internet of Things vision: Key features, applications and open issues. *Computer Communications*, pages 1 – 31, December 2014.

[2] D.L. Brock. The Electronic Product Code (epc) – A naming scheme for physical objects. *White Paper*, January 2001.

[3] International Telecommunication Union. ITU Internet Report 2005: The Internet of Things. *International Telecommunication Union*, 2005.

[4] A.K. Jain, Chang-Jin Jeong, L. Hong, and S. Pankanti. Internet of Things - Strategic Research Roadmap. *Tech. rep., Cluster of European Research projects on the Internet of Things*, September 2009.

[5] D. Uckelmann, M. Harrison, and F. Michahelles. Architecting the Internet of Things. *Springer Verlag, Berlin Heidelberg*, 2011.

[6] L. Chettri and R. Bera. A Comprehensive Survey on Internet of Things (IoT) Toward 5 G Wireless Systems. *IEEE Internet of Things Journal*, pages 16 – 32, January 2020.

[7] J. M. Rabaey, M. J. Ammer, J. L. da Silva, D. Patel, and S. Roundy. Picoradio supports ad hoc ultra-low power wireless networking. *Computer*, pages 42 – 48, 2000.

[8] T. Bokareva, W. Hu, S. Kanhere, B. Ristic, N. Gordon, T. Bessell, M. Rutten, and S. Jha. Wireless sensor networksfor battlefield surveillance. *Proceedings of the land war-fare conference*, pages 1 – 8, 2006.

[9] C. R. Baker, K. Armijo, S. Belka, M. Benhabib, V. Bhargava, N. Burkhart, A. D. Minassians, G. Dervisoglu, L. Gut-nik, and M. B. Haick. Wireless sensor networks for home health care. *21st International Conference on Ad-vanced Information Networking and Applications Workshops (AINAW'07)*, pages 832 – 837, 2007.

[10] G. Werner-Allen, K. Lorincz, M. Ruiz, O. Marcillo, J. John-son, J. Lees, and M. Welsh. Deploying a wireless sensor network on an active volcano. *IEEE Internet Computing*, pages 18 – 25, 2006.

[11] B. Rashid and M. H. Rehmani. Applications of wireless sen-sor networks for urban areas: a survey. *Journal of Networkand Computer Applications*, pages 192 – 219, 2016.

[12] M. H. Rehmani. Cognitive Radio Sensor Networks: Applications, Architectures, and Challenges. *IGI Global*, 2014.

[13] J. L. da Silva Jr, J. Shamberger, M. J. Ammer, C. Guo, S. Li, R. Shah, T. Tuan, M. Sheets, J. M. Rabaey, and B. Nikolic et al. Design methodology for picoradio networks. *Proceedings of Conference and Exhibition on Design, Automation and Test in Europe*, pages 314 – 323, 2001.

[14] E. Y. Lin, J. M. Rabaey, and A. Wolisz. Power-efficient rendezvous schemes for dense wireless sensor networks. *IEEE Int. Conf. Communications*, pages 3769 – 3776, 2004.

[15] D. Yoon et al. A New Approach to Low-Power and Low-Latency Wake-Up Receiver System for Wireless Sensor Nodes. *IEEE Journal of Solid-State Circuits*, pages 2405 – 2419, October 2012.

[16] Johannes Blanckenstein, Jirka Klaue, and Holger Karl. A Survey of Low-Power Transceivers and Their Applications. *IEEE Circuits and Systems Magazine*, pages 6 – 17, August 2015.

[17] B. Latré, B. Braem, I. Moerman, C. Blondia, and P. Demeester. A survey on wireless body area networks. *Wireless Networks. New York: Springer*, pages 1 – 18, 2010.

[18] A. Elgani, M. Magno, F. Renzini, L. Perilli, E. F. Scarselli, A. Gnudi, R. Canegallo, G. Ricotti, and L. Benini. Nanowatt wake-up radios: Discrete-components and integrated architectures. *2018 25th IEEE International Conference on Electronics, Circuits and Systems (ICECS)*, pages 793–796, 2018.

[19] Stevan J. Marinkovic and Emanuel M. Popovici. Nano-power wireless wake-up receiver with serial peripheral interface. *IEEE Journal on Selected Areas in Communications*, pages 1641 – 1647, 2011.

[20] M. Zgaren and M. Sawan. A high-sensitivity battery-less wake-up receiver for 915 MHz ISM band applications. *IEEE International Conference on Electronics, Circuits, and Systems (ICECS)*, page 336–339, December 2015.

[21] Chandra Shekhar, Shirshu Varma, and M. Radhakrishna. A 2.4 GHz passive wake-up circuit for power minimization in wireless sensor nodes. *IEEE Region 10 Conf. TENCON*, 2015.

[22] Heinrich Milosiu, Frank Oehler, Markus Ep pel, Dieter Fruehsorger, and Thomas Thoenes. A 7-μW 2.4 GHz wake-up receiver with – 80 dBm sensitivity and high co-channel interferer tolerance. *IEEE Tropical Conf. on Wireless Sensors and Sensor Networks (WiSNet)*, pages 35 – 37, 2015.

[23] Vahid Dabbagh Rezaei, Stephen J. Shellhammer, Mohamed Elkholy, and Kamran Entesari. A fully integrated 320 pj/b OOK super-regenerative receiver with – 87 dBm sensitivity and self-calibration. *IEEE Radio Frequency Integrated Circuits Symposium (RFIC)*, pages 222 – 225, 2016.

[24] J. Im, H.-S. Kim, and D.D. Wentzloff. A 470 μw – 92.5 dbm OOK/FSK receiver for IEEE 802.11 Wifi LP-WUR. *IEEE European Solid-State Circuits Conference*, pages 302 – 305, 2018.

[25] Juha Petäjäjärvi, Konstantin Mikhaylov, Risto Vuohtoniemi, Heikki Karvonen, and Jari Iinatti. On the human body communications: wake-up receiver design and channel characterization. *EURASIP Journal on Wireless Communications and Networking*, August 2016.

[26] H. Milosiu, F. Oehler, and Markus Eppel. Sub – 10 μ A data reception with low latency using a 180 nm CMOS wake-up receiver at 868 MHz. *IEEE Semiconductor Conference*, 2011.

[27] R. Piyare, A. L. Murphy, C. Kiraly, P. Tosato, and D. Brunelli. Ultra Low Power Wake-Up Radios: A Hardware and Networking Survey. *IEEE Communications Surveys and Tutorials*, pages 2117 – 2157, 2017.

[28] Pouya Kamalinejad, Kamyar Keikhosravy, Michele Magno, Shahriar Mirabbasi, Victor C.M. Leung, and Luca Benini. A high-sensitivity fully passive wake-up radio front-end for wireless sensor nodes. *IEEE International Conference on Consumer Electronics (ICCE)*, pages 209 – 210, 2014.

[29] K. W. Choi, L. Ginting, P. A. Rosyady, A. A. Aziz, and D. I. Kim. Wireless-powered sensor networks: How to realize. *IEEE Trans. Wireless Commun.*, pages 221 – 234, January 2017.

[30] C. Salazar, A. Kaiser, A. Cathelin, and J. Rabaey. 13.5 μA -97 dBm sensitivity interferer-resilient 2.4 GHz wake-up receiver using dual- IF multi-N-path architecture in 65 nm CMOS. *Proc. IEEE Int. Solid-State Circuits Conf. (ISSCC)*, pages 1–3, February 2015.

[31] T. Polonelli, T. L. Huy, L. Lizzi, F. Ferrero, and M. Magnod. A wakeup receiver with ad-hoc antenna co-design for wearable applications. *Proc. IEEE Sensors Appl. Symp. (SAS)*, pages 1 – 6, April 2016.

[32] X. Huang, A. Ba, P. Harpe, G. Dolmans, H. de Groot, and J. R. Long. A 915 MHz, ultra-low power 2-tone transceiver with enhanced interference resilience. *IEEE Journal of Solid-State Circuits*, pages 3197 – 3207, Decembre 2012.

[33] T. Wada, M. Ikebe, and E. Sano. 60-GHz, 9-nW wake-up receiver for short-range wireless communications. *Proc. European Solid-State Circuits Conf. (ESSCIRC)*, pages 383 – 386, September 2013.

[34] J. Pandey, J. Shi, and B. Otis. A 120 µW MICS/ISM–band FSK receiver with a 44 µW low-power mode based on injection-locking and 9x frequency multiplication. *Proc. IEEE Int. Solid-State Circuits Conf.*, pages 460 – 462, February 2011.

[35] Han Yan, Jose Gabriel Macias-Montero, Atef Akhnoukh, Leo C. N. de Vreede, John R. Long, John J. Pekarik, and Joachim N. Burghartz. A 120μW fully-integrated BPSK receiver in 90 nm CMOS. *IEEE Radio Frequency Integrated Circuits Symposium*, pages 277 – 280, 2010.

[36] M. Zgaren and M. Sawan. Frequency-to-amplitude converter based FSK receiver for ultra-low power transceivers. *IEEE Conf.*, pages 329 – 332, 2014.

[37] B. Razavi. A study of injection locking and pulling in oscillators. *IEEE Journal of Solid-State Circuits*, September 2004.

[38] F.Xavier Moncunill-Geniz, Pere Palà-Schönwälder, Member, and Orestes Mas-Casals. A generic approach to the theory of super-regenerative reception. *IEEE Transactions on Circuits and Systems*, pages 54 – 70, January 2005.

[39] R. Jurdak, A. G. Ruzzelli, and G. M. P. O'Hare. Radio sleep mode optimization in wireless sensor networks. *IEEE Trans. Mobile Comput.*, pages 955 – 968, July 2010.

[40] V. Mangal and P. R. Kinget. An ultra-low-power wake-up receiver with voltage-multiplying self-mixer and interferer-enhanced sensitivity. *2017 IEEE Custom Integrated Circuits Conference (CICC)*, pages 1–4, 2017.

[41] M. Magno and L. Benini. An ultra low power high sensitivity wake-up radio receiver with addressing capability. *2014 IEEE 10th International Conference on Wireless and Mobile Computing, Networking and Communications (WiMob)*, pages 92–99, 2014.

[42] A. Nikoofard and S. Mandal. An 11.5 nW broadband wake-up RF receiver with - 60 dBm sensitivity at 50 MHz. *2016 IEEE International Symposium on Circuits and Systems (ISCAS)*, pages 2787–2790, 2016.

[43] J. Saez, T. Ungan, L. M. Reindl, and T. Kumberg. Development and characterization of a robust differential wake-up receiver for wireless sensor networks. *2017 13th International Wireless Communications and Mobile Computing Conference (IWCMC)*, pages 1209–1214, 2017.

[44] P. Kolinko and L. E. Larson. Passive RF receiver design for wireless sensor networks. *IEEE International Microwave Symposium*, pages 567–570, 2007.

[45] H. Ba, Ilker Demirkol, and W. Heinzelman. Passive wake-up radios: From devices to applications. *Ad Hoc Netw. Elsevier*, pages 2605 – 2621, 2013.

[46] C. Tzschoppe, R. Kostack, and F. Ellinger. A 2.4 GHz fast settling wake-up receiver frontend. *2014 10th Conference on Ph.D. Research in Microelectronics and Electronics (PRIME)*, pages 1–4, 2014.

[47] L. Chen, J. Warner, W. Heinzelman, and I. Demirkol. Mh-reach-mote: Supporting multi-hop passive radio wake-up for wireless sensor networks. *2015 IEEE International Conference on Communications (ICC)*, pages 6512–6518, 2015.

[48] S. Chen and K. Cheng. A 433 MHz 54 µW OOK/FSK/PSK compatible wake-up receiver with 11 µW low-power mode based on injection-locked oscillator. *ESSCIRC Conference 2016: 42nd European Solid-State Circuits Conference*, pages 137–140, 2016.

[49] H. Fuketa, S. O'uchi, and T. Matsukawa. A 0.3-v 1- μW super-regenerative ultrasound wake-up receiver with power scalability. *IEEE Transactions on Circuits and Systems II: Express Briefs*, 64(9):1027–1031, 2017.

[50] A. Frøytlog and L. R. Cenkeramaddi. Design and implementation of an ultra-low power wake-up radio for wireless iot devices. *2018 IEEE International Conference on Advanced Networks and Telecommunications Systems (ANTS)*, pages 1–4, 2018.

[51] N. Yan, H. Zhang, X. Tan, and H. Min. Analysis and design of a multi-mode wake-up receiver based on direct envelope detection in wireless sensor networks. *IEEE Sensors Journal*, 18(22):9305–9314, 2018.

[52] E. Alpman, A. Khairi, R. Dorrance, M. Park, V. S. Somayazulu, J. R. Foerster, A. Ravi, J. Paramesh, and S. Pellerano. 802.11g/n compliant fully integrated wake-up receiver with -72 dBm sensitivity in 14 nm FinFET CMOS. *IEEE Journal of Solid-State Circuits*, 53(5):1411–1422, 2018.

[53] J. Moody, P. Bassirian, A. Roy, N. Liu, S. Pancrazio, N. S. Barker, B. H. Calhoun, and S. M. Bowers. A -76 dBm 7.4 nW wakeup radio with automatic offset compensation. *2018 IEEE International Solid - State Circuits Conference - (ISSCC)*, pages 452–454, 2018.

[54] M. Del Prete, D. Masotti, A. Costanzo, M. Magno, and L. Benini. A 2.4 GHz– 868 MHz dual-band wake-up radio for wireless sensor network and IoT. *2015 IEEE 11th International Conference on Wireless and Mobile Computing, Networking and Communications (WiMob)*, pages 322–328, 2015.

[55] Sana Ullah, Manar Mohaisen, and Mohamed Alnuem. A review of IEEE 802.15.6 MAC, PHY, and security specifications. *International Journal of Distributed Sensor Networks*, 2013, 04 2013.

[56] S. van Roy, F. Quitin, L. Liu, C. Oestges, F. Horlin, J. Dricot, and P. De Doncker. Dynamic channel modeling for multi-sensor body area networks. *IEEE Transactions on Antennas and Propagation*, 61(4):2200–2208, 2013.

[57] G. U. Gamm and L. M. Reindl. Smart metering using distributed wake-up receivers. *2012 IEEE International Instrumentation and Measurement Technology Conference Proceedings*, pages 2589–2593, 2012.

[58] C. Alippi, R. Ambrosini, V. Longoni, D. Cogliati, and M. Roveri. A lightweight and energy-efficient internet-of-birds tracking system. *2017 IEEE International Conference on Pervasive Computing and Communications (PerCom)*, pages 160–169, 2017.

[59] Gian Picco, Davide Molteni, Amy Murphy, Federico Ossi, Francesca Cagnacci, Michele Corrà, and Sandro Nicoloso. Geo-referenced proximity detection of wildlife with wildscope: Design and characterization. *Proceedings in the 14th International Conference on Information Processing in Sensor Networks*, 04 2015.

[60] V. Jelicic, M. Magno, D. Brunelli, V. Bilas, and L. Benini. Benefits of wake-up radio in energy-efficient multimodal surveillance wireless sensor network. *IEEE Sensors Journal*, 14(9):3210–3220, 2014.

[61] C. Petrioli, D. Spenza, P. Tommasino, and A. Trifiletti. A novel wake-up receiver with addressing capability for wireless sensor nodes. *2014 IEEE International Conference on Distributed Computing in Sensor Systems*, pages 18–25, 2014.

[62] J. Robert, T. Lindner, and H. Milosiu. Sub 10 µW wake-up-receiver based indoor/outdoor asset tracking system. *2015 IEEE 20th Conference on Emerging Technologies Factory Automation (ETFA)*, pages 1–3, 2015.

[63] Johannes Blanckenstein, Javier Garcia-Jimenez, Jirka Klaue, and Holger Karl. A scalable redundant TDMA protocol for high-density WSNs inside an aircraft. *Lecture Notes in Electrical Engineering*, 281:165–177, 01 2014.

[64] DENG D.-J., LIEN S.-Y., LIN C.-C., GAN M., and CHEN H.-C. IEEE 802.11ba Wake-Up Radio: Performance Evaluation and Practical Designs. *IEEE Access*, 8:141547 – 141557, 2020.

[65] F. Hutu, A. Khoumeri, G. Villemaud, and J. M. Gorce. A new wake-up radio architecture for wireless sensor networks. *EURASIP Journal on Wireless Communications and Networking, Special Issue on Green Wireless Communications: Theory and Practice*, October 2014.

[66] G. Sudha, R. Prakash, A. Balaji Ganesh, and Siva V Girish. Network coding based real time wireless sensor network for environmental monitoring. *2016*

International Conference on Wireless Communications, Signal Processing and Networking (WiSPNET), pages 1269–1272, 2016.

[67] Rizky Pratama Hudhajanto, Nurul Fahmi, Eko Prayitno, and Rosmida. Real-time monitoring for environmental through wireless sensor network technology. *2018 International Conference on Applied Engineering (ICAE)*, pages 1–5, 2018.

[68] Sabrine Aroua, Inès El Korbi, Yacine Ghamri-Doudane, and Leila Azouz Saidane. A distributed cooperative spectrum resource allocation in smart home cognitive wireless sensor networks. *2017 IEEE Symposium on Computers and Communications (ISCC)*, pages 754–759, 2017.

[69] Chwan-Lu Tseng, Che-Shen Cheng, Yu-Hsien Hsu, and Bing-Hung Yang. An IoT-based home automation system using Wi-Fi wireless sensor networks. *2018 IEEE International Conference on Systems, Man, and Cybernetics (SMC)*, pages 2430–2435, 2018.

[70] K.S Rekha., A.D. Kulkarni, H.D. Phaneendra, and T. Anantha Padmanabha. Remote monitoring and run-time reconfigurations of an industrial process using wireless sensor networks and IOT. *2018 Fourth International Conference on Research in Computational Intelligence and Communication Networks (ICRCICN)*, pages 193–196, 2018.

[71] Habib Mostafaei, Morshed U. Chowdhury, and Mohammad S. Obaidat. Border surveillance with WSN systems in a distributed manner. *IEEE Systems Journal*, 12(4):3703–3712, 2018.

[72] D. Devi Kala Rathinam, D. Surendran, A. Shilpa, A. Santhiya Grace, and J. Sherin. Modern agriculture using wireless sensor network (WSN). *2019 5th International Conference on Advanced Computing Communication Systems (ICACCS)*, pages 515–519, 2019.

[73] Boubekeur Merabet, Laurent Cirio, Hakim Takhedmit, Francois Costa, Christian Vollaire, Bruno Allard, and Odile Picon. Low-cost converter for harvesting of microwave electromagnetic energy. *2009 IEEE Energy Conversion Congress and Exposition*, pages 2592–2599, 2009.

[74] Simon Hemour, Yangping Zhao, Carlos Henrique Petzl Lorenz, Dimitri Houssameddine, Yongsheng Gui, Can-Ming Hu, and Ke Wu. Towards low-power high-efficiency RF and microwave energy harvesting. *IEEE Transactions on Microwave Theory and Techniques*, 62(4):965–976, 2014.

[75] Tsuyoshi Takahashi, Kenichi Kawaguchi, Masaru Sato, Michihiko Suhara, and Naoya Okamoto. Highly sensitive p-GaAsSb/n-InAs nanowire backward diodes for low-power microwaves. *ESSDERC 2019 - 49th European Solid-State Device Research Conference (ESSDERC)*, pages 214–217, 2019.

[76] David M. Pozar. Microwave engineering. *Third Edition, John Wiley and Sons Inc*, pages 252–257, 2005.

[77] Florin Hutu, David Kibloff, Guillaume Villemaud, and Jean-Marie Gorce. Experimental validation of a wake-up radio architecture. *IEEE Radio and Wireless Symposium (RWS)*, pages 155–158, 2016.

[78] Manuel Piñuela, Paul D. Mitcheson, and Stepan Lucyszyn. Ambient RF energy harvesting in urban and semi-urban environments. *IEEE Transactions on Microwave Theory and Techniques*, 61(7):2715–2726, 2013.

[79] Adnant Jushi, Alain Pegatoquet, and Trong Nhan Le. Wind energy harvesting for autonomous wireless sensor networks. *2016 Euromicro Conference on Digital System Design (DSD)*, pages 301–308, 2016.

[80] Mohammad O. A. Aqel, Ahmed Issa, Eman Qasem, and Wessal El-Khatib. Hydroelectric generation from water pipelines of buildings. *2018 International Conference on Promising Electronic Technologies (ICPET)*, pages 63–68, 2018.

[81] Himanshu Sharma, Ahteshamul Haque, and Zainul Abdin Jaffery. An efficient solar energy harvesting system for wireless sensor nodes. *2018 2nd IEEE International Conference on Power Electronics, Intelligent Control and Energy Systems (ICPEICES)*, pages 461–464, 2018.

[82] Constantinos Psomas and Ioannis Krikidis. Ambient RF energy harvesting with non-linearities in large-scale networks. *2019 IEEE Global Communications Conference (GLOBECOM)*, pages 1–6, 2019.

[83] Rajdevinder Kaur Sidhu, Jagpal Singh Ubhi, and Alpana Aggarwal. A survey study of different RF energy sources for RF energy harvesting. *2019 International Conference on Automation, Computational and Technology Management (ICACTM)*, pages 530–533, 2019.

[84] Yunus Uzun. Design and implementation of RF energy harvesting system for low-power electronic devices. *Journal of Electronic Materials*, 45, 03 2016.

[85] Alanson Sample and Joshua R. Smith. Experimental results with two wireless power transfer systems. *2009 IEEE Radio and Wireless Symposium*, pages 16–18, 2009.

[86] Hiroshi Nishimoto, Yoshihiro Kawahara, and Tohru Asami. Prototype implementation of wireless sensor network using TV broadcast RF energy harvesting. *UbiComp 2010: Ubiquitous Computing, 12th International Conference, UbiComp 2010, Copenhagen, Denmark, September 26-29, 2019, Adjunct Papers Proceedings*, pages 373–374, 2010.

[87] Vamsi Talla, Bryce Kellogg, Benjamin Ransford, Saman Naderiparizi, Joshua Smith, and Shyamnath Gollakota. Powering the next billion devices with Wi-Fi. *Communications of the ACM*, 60:83–91, 02 2015.

[88] Haocheng Hong, Xiuzhang Cai, Xu Shi, and Xinen Zhu. Demonstration of a highly efficient RF energy harvester for Wi-Fi signals. *2012 International Conference on Microwave and Millimeter Wave Technology (ICMMT)*, 5:1–4, 2012.

[89] Ugur Olgun, Chi-Chih Chen, and John L. Volakis. Wireless power harvesting with planar rectennas for 2.45 GHz RFIDs. *2010 URSI International Symposium on Electromagnetic Theory*, pages 329–331, 2010.

[90] Minhong Mi, M.H. Mickle, C. Capelli, and H. Swift. Rf energy harvesting with multiple antennas in the same space. *IEEE Antennas and Propagation Magazine*, 47(5):100–106, 2005.

[91] Thamer S. Almoneef. Design of a rectenna array without a matching network. *IEEE Access*, 8:109071–109079, 2020.

[92] Hamza Tafekirt, Jose Pelegri-Sebastia, Adel Bouajaj, and Britel Mohammed Reda. A sensitive triple-band rectifier for energy harvesting applications. *IEEE Access*, 8:73659–73664, 2020.

[93] Ryan Reed, Fariborz Lohrabi Pour, and Dong Sam Ha. An efficient 2.4 GHz differential rectenna for radio frequency energy harvesting. *2020 IEEE 63rd International Midwest Symposium on Circuits and Systems (MWSCAS)*, pages 208–212, 2020.

[94] Jincheng Zhao, Guru Subramanyam, and Hailing Yue. A dual-band rectifying antenna design for RF energy harvesting. *2020 IEEE 63rd International Midwest Symposium on Circuits and Systems (MWSCAS)*, pages 415–418, 2020.

[95] Si Ce Wang, Min Jun Li, and Mei Song Tong. A miniaturized high-efficiency rectifier with extended input power range for wireless power harvesting. *IEEE Microwave and Wireless Components Letters*, 30(6):617–620, 2020.

[96] Mengfan Wang, Jianing Chen, Xinwang Cui, and Long Li. Design and fabrication of 5.8 GHz RF energy harvesting rectifier. *2019 Cross Strait Quad-Regional Radio Science and Wireless Technology Conference (CSQRWC)*, pages 1–3, 2019.

[97] Mohamed M. Mansour and H. Kanaya. High-efficient broadband CPW RF rectifier for wireless energy harvesting. *IEEE Microwave and Wireless Components Letters*, 29(4):288–290, 2019.

[98] Kapil Bhatt, Sandeep Kumar, Pramod Kumar, and Chandra Charu Tripathi. Highly efficient 2.4 and 5.8 GHz dual-band rectenna for energy harvesting

applications. *IEEE Antennas and Wireless Propagation Letters*, 18(12):2637–2641, 2019.

[99] Shanpu Shen, Yujie Zhang, Chi-Yuk Chiu, and Ross Murch. An ambient RF energy harvesting system where the number of antenna ports is dependent on frequency. *IEEE Transactions on Microwave Theory and Techniques*, 67(9):3821–3832, 2019.

[100] Shunsuke Hatanaka and Haruichi Kanaya. Wireless micro energy harvesting circuit for sensor system. *2019 IEEE 21st Electronics Packaging Technology Conference (EPTC)*, pages 116–119, 2019.

[101] Chih-Hsi Lin, Chien-Wen Chiu, and Jian-Yuan Gong. A wearable rectenna to harvest low-power RF energy for wireless healthcare applications. *2018 11th International Congress on Image and Signal Processing, BioMedical Engineering and Informatics (CISP-BMEI)*, pages 1–5, 2018.

[102] Mohamed M. Mansour and Haruichi Kanaya. Compact and broadband RF rectifier with 1.5 octave bandwidth based on a simple pair of l-section matching network. *IEEE Microwave and Wireless Components Letters*, 28(4):335–337, apr 2018.

[103] Qasim Awais, Yang Jin, Hassan Tariq Chattha, Mohsin Jamil, He Qiang, and Bilal A. Khawaja. A compact rectenna system with high conversion efficiency for wireless energy harvesting. *IEEE Access*, 6:35857–35866, 2018.

[104] Mohamed Aboualalaa, Islam Mansour, Mohamed Mansour, Adel Bedair, Ahmed Allam, Mohammed Abo-Zahhad, Hala Elsadek, Kuniaki Yoshitomi,

and Ramesh K. Pokharel. Dual-band rectenna using voltage doubler rectifier and four-section matching network. *2018 IEEE Wireless Power Transfer Conference (WPTC)*, pages 1–4, 2018.

[105] Alex Mouapi, Nadir Hakem, Nahi Kandil, and Gaelle Vanessa Kamani. A miniature rectifier design for radio frequency energy harvesting applied at 2.45 GHz. *2018 IEEE International Conference on Environment and Electrical Engineering and 2018 IEEE Industrial and Commercial Power Systems Europe (EEEIC / I CPS Europe)*, pages 1–5, 2018.

[106] Arka Biswas, S. Babak Hamidi, Chitralekha Biswas, Palash Roy, Dipankar Mitra, and Debasis Dawn. A novel CMOS RF energy harvester for self-sustainable applications. *2018 IEEE 19th Wireless and Microwave Technology Conference (WAMICON)*, pages 1–5, 2018.

[107] Chun-Hsing Li, Ming-Che Yu, and Hsien-Jia Lin. A compact 0.9-/2.6 GHz dual-band RF energy harvester using SiP technique. *IEEE Microwave and Wireless Components Letters*, 27(7):666–668, 2017.

[108] Mutee ur Rehman, Waleed Ahmad, and Wasif Tanveer Khan. Highly efficient dual band 2.45/5.85 GHz rectifier for RF energy harvesting applications in ISM band. *2017 IEEE Asia Pacific Microwave Conference (APMC)*, pages 150–153, 2017.

[109] A. Eid, J. Costantine, Y. Tawk, A. H. Ramadan, M. Abdallah, R. ElHajj, R. Awad, and I. B. Kasbah. An efficient RF energy harvesting system. *2017 11th European Conference on Antennas and Propagation (EUCAP)*, pages 896–899, 2017.

[110] Mohamed M. Mansour and Haruichi Kanaya. Compact RF rectifier circuit for ambient energy harvesting. *2017 IEEE International Symposium on Radio-Frequency Integration Technology (RFIT)*, pages 220–222, 2017.

[111] J.O. McSpadden, Lu Fan, and Kai Chang. Design and experiments of a high-conversion-efficiency 5.8 GHz rectenna. *IEEE Transactions on Microwave Theory and Techniques*, 46(12):2053–2060, 1998.

[112] Vlad Marian, Christian Vollaire, Jacques Verdier, and Bruno Allard. Potentials of an adaptive rectenna circuit. *IEEE Antennas and Wireless Propagation Letters*, 10:1393–1396, 2011.

[113] Achille Fumtchum, Florin Doru HUTU, Pierre Tsafack, Guillaume Villemaud, and Emmanuel Tanyi. High efficiency rectifier for a quasi-passive wakeup radio. *2019 International Symposium on Signals, Circuits and Systems (ISSCS)*, pages 1–4, 07 2019.

[114] R Keilkowski. Inside SPICE. *McGraw Hill*, 1994.

[115] Hewlett Packard. S parameter techniques for faster, more accurate network design. test and measurement application note 95-1. *http://literature.cdn.keysight.com/litweb/pdf/5989-9273EN.pdf*, pages 1–81, 1996.

[116] R. J. GILMORE and M. B. STEER. Nonlinear circuit analysis using the method of harmonic balance - a review of the art. part i. introductory concepts. *Int. J. Microw. Mill. Wave Comput. -Aided Eng.*, pages 22 – 37, 1991.

[117] V. Rizzoli, C. Cecchetti, A. Lipparini, and F. Mastri. General-purpose harmonic balance analysis of nonlinear microwave circuits under multitone excitation. *IEEE Transactions on Microwave Theory and Techniques*, 36(12):1650–1660, 1988.

[118] Agilent Technologies. Harmonic Balance Simulation. *Tecnical report*, September 2004.

[119] Agilent Technologies. Large-signal s-parameters simulation. *Tecnical report*, September 2004.

[120] Vlad Marian. Transmission d'énergie sans fil : Application au réveil à distance de récepteurs en veille zéro consommation. *https://tel.archives-ouvertes.fr/tel-00787608/file/TH_T2296$_v$marian.pdf*, 2012ECDL0045, PhD Thesis, Nov 2012.

[121] Roger F. Harrington. *Field Computation by Moment Methods.* Wiley-IEEE Press, 1993.

[122] David M. Pozar. Microwave engineering. *Fourth Edition, John Wiley and Sons Inc*, 2012.

[123] *Advanced RF/Microwave Filters*, pages 315–377. John Wiley & Sons, Ltd, 2001.

[124] S.L. March. Analyzing lossy radial-line stubs (short papers). *IEEE Transactions on Microwave Theory and Techniques*, 33(3):269–271, 1985.

[125] Erick E. Djoumessi. Conception de circuits micro-ondes multi-bandes et à fréquences agiles pour la réalisation de systèmes sans fil reconfigurables. *Theses, Université de Monréal*, AOUT 2010.

Appendix

Appendix 1: Transmission and transformation matrices

The S, Y and Z parameters are used to characterise microwave networks regardless of their number of ports. But generally, we have to face systems with two ports cascaded as shown in the figure below.

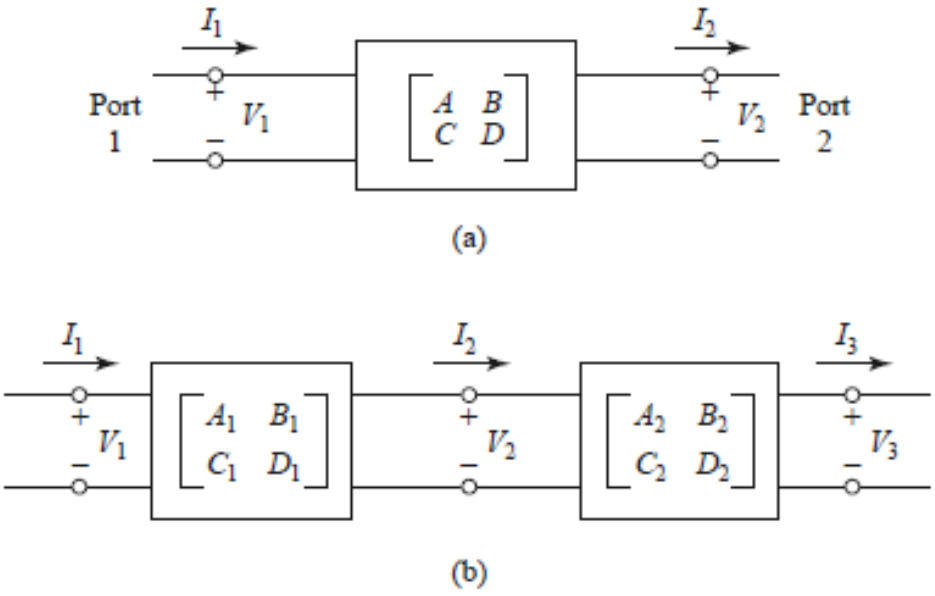

Figure 1: (a) A two-port network; (b) a cascade connection of two-port networks

(a) A two-port network; (b) a cascade connection of two-port networks Tables illustrating the relationships between the different parameters of a transmission line transmission line.

Table 1: S parameters in terms of ABCD, Y, and Z parameters

	ABCD	Y	Z
S_{11}	$\frac{A+\frac{B}{Z_0}-CZ_0-D}{A+\frac{B}{Z_0}+CZ_0+D}$	$\frac{(Y_0-Y_{11})(Y_0+Y_{22})+Y_{12}Y_{21}}{(Y_0+Y_{11})(Y_0+Y_{22})-Y_{12}Y_{21}}$	$\frac{(Z_{11}-Z_0)(Z_{22}+Z_0)-Z_{12}Z_{21}}{(Z_{11}+Z_0)(Z_{22}+Z_0)-Z_{12}Z_{21}}$
S_{12}	$\frac{2(AD-BC)}{A+\frac{B}{Z_0}+CZ_0+D}$	$\frac{-2Y_{12}Y_0}{(Y_0+Y_{11})(Y_0+Y_{22})-Y_{12}Y_{21}}$	$\frac{-2Z_{12}Z_0}{(Z_{11}+Z_0)(Z_{22}+Z_0)-Z_{12}Z_{21}}$
S_{21}	$\frac{2}{A+\frac{B}{Z_0}+CZ_0+D}$	$\frac{-2Y_{21}Y_0}{(Y_0+Y_{11})(Y_0+Y_{22})-Y_{12}Y_{21}}$	$\frac{-2Z_{21}Z_0}{(Z_{11}+Z_0)(Z_{22}+Z_0)-Z_{12}Z_{21}}$
S_{22}	$\frac{-A+\frac{B}{Z_0}-CZ_0+D}{A+\frac{B}{Z_0}+CZ_0+D}$	$\frac{(Y_0+Y_{11})(Y_0-Y_{22})+Y_{12}Y_{21}}{(Y_0+Y_{11})(Y_0+Y_{22})-Y_{12}Y_{21}}$	$\frac{(Z_{11}-Z_0)(Z_{22}+Z_0)-Z_{12}Z_{21}}{(Z_{11}+Z_0)(Z_{22}+Z_0)-Z_{12}Z_{21}}$

Table 2: S parameters in terms of ABCD, Y, and Z parameters

	S	Y	Z
A	$\frac{(1+S_{11})(1-S_{22})+S_{12}S_{21}}{2S_{21}}$	$-\frac{Y_{22}}{Y_{21}}$	$-\frac{Z_{11}}{Z_{21}}$
B	$Z_0\frac{(1+S_{11})(1+S_{22})-S_{12}S_{21}}{2S_{21}}$	$-\frac{1}{Y_{21}}$	$\frac{Z_{11}Z_{22}-Z_{12}Z_{21}}{Z_{21}}$
C	$\frac{1}{Z_0}\frac{(1-S_{11})(1-S_{22})-S_{12}S_{21}}{2S_{21}}$	$-\frac{Y_{11}Y_{22}-Y_{12}Y_{21}}{Y_{21}}$	$-\frac{1}{Z_{21}}$
D	$\frac{(1-S_{11})(1+S_{22})+S_{12}S_{21}}{2S_{21}}$	$-\frac{Y_{11}}{Y_{21}}$	$-\frac{Z_{22}}{Z_{21}}$

Two port network showing the variables of the network

Since $V_2 = -I_2Z_{02}$, the input impedance at port 1 of the above two-port network

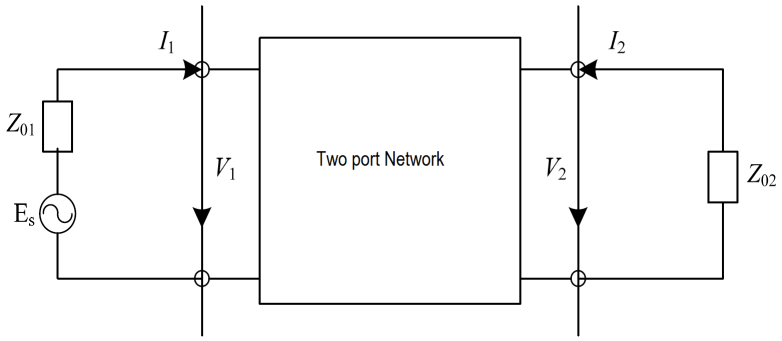

Figure 2: Two port Network

is given by :

$$Z_{in} = \frac{V_1}{I_1} = \frac{Z_{02}A + B}{Z_{02}C + D}$$

Substituting the ABCD parameters for a transmission line network, we obtain the expression :

$$Z_{in1} = Z_C \frac{Z_{02} + Z_C \tanh \gamma l}{Z_C + Z_{02} \tanh \gamma l}$$

with :

Z_C: characteristic impedance

γ : complex propagation constant

l : electrical length of the transmission line

The propagation constant of a lossless transmission line is given by $\gamma = j\beta$, we can thus rewrite the previous expression as :

$$Z_{in1} = Z_C \frac{Z_{02} + jZ_C \tan \beta l}{Z_C + jZ_{02} \tan \beta l}$$

When an open or short circuit is imposed on one of the ports of the transmission

line network, the above equation becomes for open-circuit :

$$Z_{in1} = \frac{Z_C}{j \tan \beta l}$$

and for short-circuit

$$Z_{in1} = j Z_C \tan \beta l$$

List of publications

Journals

Achille Fumtchum, Pierre Tsafack, Florin Hutu, Guillaume Villemaud, Emmanuel Tanyi."'***A survey of RF energy harvesting circuits*** "‘, International Journal of Innovative Technology and Exploring Engineering, Mai 2021, Vol. 10 Issue-7, pp. 99-106, doi: 10.35940/ijitee.G8944.0510721

Fumtchum, C.A.; Hutu, F.D.; Tsafack, P.; Villemaud, G.; Tanyi, E. Towards a Battery-Free Wake-Up Radio. Electronics 2021, 10, 2449. https://doi.org/10.3390/electronics10202449.

Conference

Achille Fumtchum, R. Rousseau, F. Hutu, G. Villemaud, P. Tsafack, Y. Duroc. "‘***State of the art of wake-up radio architectures***,"’ GDR-SEEDS Conference, Nov 2016, INSA Lyon, Poster.

Achille Fumtchum, Florin Hutu, Pierre Tsafack, Guillaume Villemaud, Emmanuel Tanyi. "‘High Efficiency Rectifier for a Quasi-Passive Wake-up Radio."’ ISSCS 2019 - 14-th International Symposium on Signals, Circuits and Systems, Jul

2019, Iasi, Romania. pp.1-4, doi: 10.1109/ISSCS.2019.8801754.